NASA-CR-200746

FINAL
1N-91-CR
OCIT

39324

FINAL REPORT

Pioneer Venus Data Analysis

Prepared under grant NAG 2-687

by Brigham Young University

for

NASA-Ames Research Center

March 1996

Principal Investigator: Douglas E. Jones

Technical Monitor: Larry E. Lasher

Introduction and Work Description

This final report covers the work conducted by Brigham Young University personnel in the analysis and interpretation of data obtained by the Orbiter Retarding Potential Analyzer (ORPA) during the funding period of October 1, 1990 through September 30, 1994. During this 4 year period $46,130 was received, of which $12,000 was spent on faculty wages and $18,400 on student wages. The students working on this were Steven McNeil, Laralee Gordon, Dawn Gifford and Noe Yamaguchi. Steven and Laralee (1991, 1992) were graduate students who focused their efforts primarily on the data reduction, - specifically writing programs used to prepare the data (.TAB) files for plotting and analysis. Dawn Gifford (1993) and Noe Yamaguchi (1994) were honors students who used analyses of the ORPA suprathermal electron data as the focus of their honors theses.

Much of the early period of this grant was spent reanalyzing the ORPA data in response to the three revisions of the primary reduction program, LSFK, that were received approximately one year apart. The first revision of this program (7273 lines of code) was received from NASA-Ames on 11 September, 1991. The second revision was received 12 Aug 1992 (7653 lines of code) and the third on 3 September 1993 (7827 lines of code). Between revisions 1 and 2 there were two changes sent via e-mail in subroutine EPS (27 Nov, 1991 and 6 Dec 1991), and one change each to subroutines IONPK and SPLREA. The major difference between the 2nd and 3rd revisions was the extension of the analysis interval of the ORPA data to full orbits. We were informed in the Spring of 1993 that this expanded orbit analysis version was coming, but fortunately, for the specific program we had settled on it was not necessary to wait for revision 3; i.e., we could still proceed with a first order determination of the extent to which the sprathermal electron densities derived from the ORPA instrument tracked the OPA proton densities in the region of the orbit beyond the Venus ionopause.

During the Spring-Summer terms (typically April 20 thru August 20) of 1993, Dawn Gifford used the second revised version of LSFK to determine the extent and under what conditions the ORPA and OPA densities tracked. Since the electrons in the solar wind are

derived from ionization of Hydrogen, Helium and other atoms in the solar atmosphere, it was expected that if, beyond the ionopause, the suprathermal electrons were in fact solar wind electrons, then the two densities should agree within something approachihg 5-10%. Dawn found that during the times that the spacecraft potential was greater than 3.0 volts the two densities tracked very well. There is a second order effect observed at voltages above 3.0 volts, and with the extended orbit analysis available with the final version of LSFK it will be possible to determine more accurately what the form of the expression describing the relationship actually is (preliminary results suggest a simple linear relationship between the orbserved ORPA suprathermal electron/OPA density ratio and the spacecraft potential). She interrupted her studies Fall term 1993 through Spring 1995 (LDS Mission). Although most of the work on her thesis was completed prior to the date she left (September, 1993), she just finished her thesis defense corresponding to the date of this report. Although dated later than that of the student who followed her in this project, her thesis is found at the end of this report as Appendix A.

The second student, Noe Yamaguchi, used Dawn Gifford's results and studied 366 plots of the suprathermal electron density and temperature. She used the shock jump ratios to determine the equivalent upstream, mass-loaded mach number of the solar wind, and the corresponding charge exchange pickup of O+ ions from Venus necesarry to explain the decrease in the mach from its defined value on the basis of the solar wind flow speed and magnetosonic velocity. A copy of her undergraduate honors thesis is included as Appendix B

The BYU principle investigator (D. Jones) was away from the university from September 1994 through August 1995. As of January 1 1996, the work on this analysis has been started up again. A student is becoming familiar with the reduction and analysis programs and the data in anticipation of their graduate studies that will start this coming Fall. By that time, William Knudsen, the Principal Investigator of the ORPA instrument will have moved to Utah Valley and will be an adjunct professor in the Physics Department at BYU specifically helping in the analysis and

interpretation of the ORPA data. Hence, although the several modifications that occurred to the principal computer program used to reduce the ORPA data occurred in such a way as to essentially set the analysis effort back several times, as a minimum we intend to complete the determination of the electron density, temperature and velocity behind the bow shock to the point where a major paper can be submitted to the JGR, and,- more specifically,- to provide these results to theorists who need them to complete their modelling of the Venus bow shock and magnetosheath (see, e.g., Murawski and Steinolfson, 1996). A cooperative shock analysis involving both the ORPA suprathermal electron and magnetometer data (Chris Russell and Khrishan Khurana) will also begin shortly. Hence, although the continual modification of the ORPA computer programs basically prevented us from getting the analysis to the point of being able to submit any papers to the JGR, nevertheless the funding has provided the necessary "seed money" to set an important analysis program in place here at BYU.

Summary

        As a result of this analysis program it has been found that the ORPA suprathermal electron densities corresponding to spacecraft potentials of under 3.0 volts basically tracked the OPA densities fairly well although frequently the ORPA data appeared quite noisy. On the other hand, the ORPA data corresponding to spacecraft potentials of greater than 3.0 volts tracked very well and was considerably less noisy (see Figures 6,7, and 8 of Appendix A). Hence, using spacecraft potential dependent proportionality constant (near unity), the ORPA suprathermal electron densities basically represent solar wind electron densities, thus allowing the high resolution study of Venus bow shocks using both magnetic field and solar wind electron data. A preliminary analysis of 366 bow shock penetrations was completed using the the solar wind electron data as determined from the ORPA suprathermal electron densities and temperatures, resulting in an estimate of the extent to which mass loading pickup of O^+ (UV ionized O atoms flowing out of the Venus atmosphere) upstream of the Venus obstacle occurred (pickup of O^+

averaged 9.95%, ranging from 0.78% to 23.63%). The seed money provided for this research effort will result in detailed, high resolution solar wind electron density and temperature data that, when combined with the UCLA magnetometer, will provide excellent data needed to constrain models presently being developed for the solar wind-Venus ionosphere interaction.

Two papers have been given during the period of this research grant:

D. Gifford, D. E. Jones, N. Yamaguchi, W. C. Knudsen, J. D. Mihalov, "Pioneer Venus Orbiter Retarding Potential Analyzer Observatins of the Electron Component of the Solar Wind and Observations of Venus Bow Shock Crossings and the Magnetosheath Region", EOS, 74, 493, 1993. (Abstract of paper given at the Fall, 1993 Meeting of the American Geophysical Union, San Francisco, California, December 1993)

N. Yamaguchi, D. E. Jones, and W. C. Knudsen, "Pioneer Venus Orbiter Retarding Potential Analyzer Observations of the Electron Component of the Solar Wind, and of the Venus Bow Shock and Magnetosheath", (paper presented at the Spring, 1994 Meeting of the Utah Academy of Sciences, Arts, and Letters, Ogden, Utah)

References:
Murawski, K., and R.S. Steinolfson, Numerical Simulations of Mass Loading in the Solar Wind Interaction with Venus, JGR, 101, 2547, 1996.

Comparison of ORPA Suprathermal Electron and OPA Solar Wind Proton Data from the Pioneer Venus Orbiter
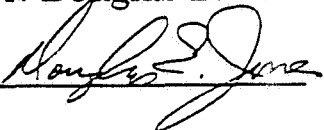
by

Dawn K. Gifford

submitted to Brigham Young University in partial fulfillment

of graduation requirements for University Honors

March 15, 1996

Advisor: Dr. Douglas E. Jones   Honors Dean: Dr. Paul Cox

Signature:_____   Signature:_____

CONTENTS

LIST OF FIGURES

Abstract

In this study, we compared the data from two instruments on the Pioneer Venus Orbiter (PVO). The two data sets are the suprathermal electron data from the retarding potential analyzer (ORPA) and the proton data from the plasma analyzer (OPA). This study was designed to determine if the ORPA suprathermal electron data obtained outside of Venus' ionopause represented solar wind electrons and could be used to increase the time resolution of the solar wind data from PVO. To discover whether or not this was the case, we compared the ORPA suprathermal electron data with the OPA solar wind proton data. We determined that the two sets correlate well. This indicates that the ORPA suprathermal electron measurements outside of the Venusian ionopause are in fact measurements of solar wind electrons. With this data, it will now be possible to conduct high time resolution studies of the bow shock and the region between the ionopause and the bow shock. These data will provide constraints on the several models currently being developed to represent the interaction of the mass loaded solar wind with Venus' ionosphere.

Introduction

A bow shock is a paraboloid-shaped shockwave that forms around a planet similar to one that forms around an airplane traveling faster than the speed of sound. In the airplane's case, the plane is flying at supersonic velocities in the air's reference frame; the air has to move around the plane and forms a shockwave. In the case of a planet, the planet is traveling faster than the speed of sound in the solar wind's reference frame (actually the solar wind is supersonic, not the planet, but the effect is the same), so the solar wind-planet interaction forms the bow shock. In the interplanetary medium, the speed of sound is typically around 30 km/s and the solar wind speed is about 500 km/s. A rough diagram of a bow shock around Venus is shown in Figure 1.

The bow shock can be detected by measuring several quantities, such as solar wind proton and electron densities, temperatures and velocities and the interplanetary magnetic field upstream (in front of the planet on the sunward side, see Fig. 1) of the planet. To get a full understanding of the bow shock, all of these measurements are vital. When the spacecraft taking the measurements passes through the bow shock, the values of the measured quantities will change drastically. Taking several measurements of these changes while passing through the bow shock at different places helps map the structure of the bow shock, which can change with varying conditions in the solar wind, planetary ionosphere, planetary magnetic field, and interplanetary magnetic field. The time resolution of the measurements must, however, be high enough to reliably measure the jumps in each quantity.

Figure 1. Diagram of Bow Shock, Ionosphere, Ionopause, Ionotail of Venus and Sample PVO Orbit.

IONOTAIL

IONOSPHERE

VENUS

IONOPAUSE

BOW SHOCK

SAMPLE PVO ORBIT

UPSTREAM

TO SUN
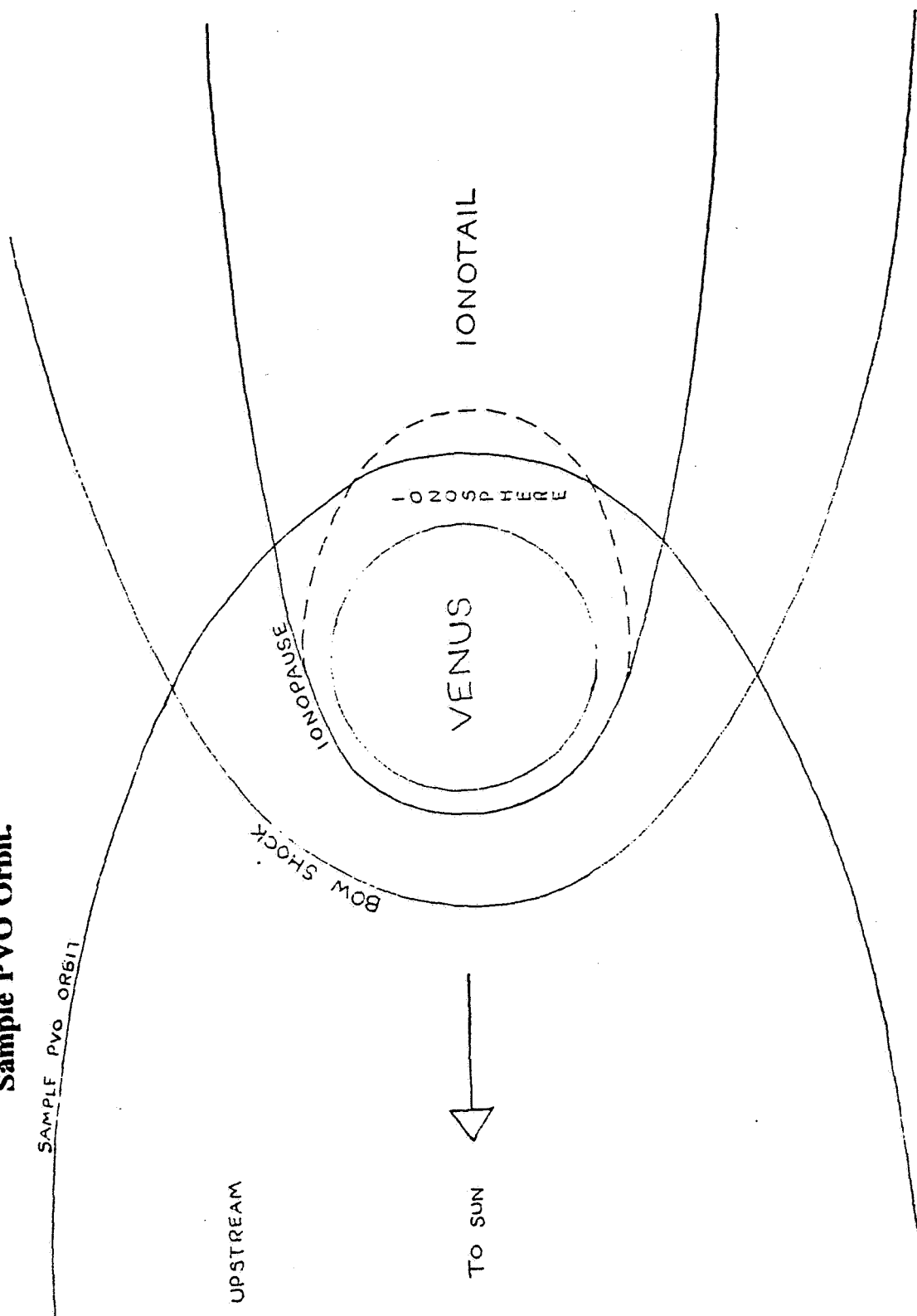
In May 1978, NASA launched the Pioneer Venus Orbiter (PVO). PVO orbited Venus every twenty-four hours until Fall of 1992, taking measurements with a number of instruments designed to study the planet and its environment[1]. One of the questions PVO was devised to answer was: what is the structure of Venus' bow shock and how does it respond to solar activity? Up to now only the magnometer could be used to study the bow shock. High time resolution plasma data taken while passing through the bow shock are needed to further understand the shock's structure. One of the instruments on the orbiter, the plasma analyzer (OPA), was designed to take measurements of the solar wind[2]. Because the instrument was designed primarily to sample the upstream solar wind, the measurements closer to the planet were not taken often enough to adequately study the bow shock. In addition, OPA only took good measurements of the solar wind protons and not of the other quantities necessary for a complete study of the bow shock.

Another instrument, the retarding potential analyzer (ORPA), was designed to take measurements of the ionosphere, including the densities, temperatures and velocities of ions, thermal electrons, and suprathermal, or high energy, electrons[3]. Because this instrument was designed to measure

---

[1]More information about PVO is contained in "Pioneer Venus Orbiter - Ten years of Discovery."

[2]For a detailed description of the OPA instrument, read "The Pioneer Venus Orbiter Plasma Analyzer Experiment" by Intriligator, Wolfe, and Mihalov.

[3]A complete description of the ORPA instrument is contained in the papers by Knudsen et al. and the "Detailed instrument Description of the Pioneer-Venus Orbiter Retarding Potential Analyzer" prepared by Knudsen.

near the planet, the measurements were taken much more frequently than those taken by the OPA instrument.

Dr. William Knudsen, the principle investigator of the ORPA instrument, has proposed that the suprathermal electrons ORPA measured when the orbiter was outside the Venusian ionosphere were actually solar wind electrons. If Dr. Knudsen's idea is correct, when PVO was outside the Venusian ionopause, the outer boundary of the ionosphere (see Fig. 1), ORPA became a solar wind electron measuring device when operating in the suprathermal electron mode (Knudsen Private Communication with Dr. Jones). If this is the case, because the OPA instrument measured only proton data and these only with low time resolution, the high time resolution ORPA suprathermal electron measurements are critical for a better understanding of the region at and behind the Venusian bow shock and its dependence on solar activity. The main question is then: can the ORPA suprathermal electron measurements be used as reliable high time resolution solar wind electron data?

Background

As stated above, one of the factors PVO was designed to investigate was the structure of the bow shock around Venus. As different supersonic speeds of an airplane form different shapes and structures of shockwaves, changing solar wind speed, changes in solar activity, different conditions in the ionosphere, differences in the planetary magnetic field, and changes in the interplanetary magnetic field also modify the characteristics of a planetary bow shock. Venus' bow shock is particularly important to study because Venus, unlike the Earth, has no magnetic field of its own. Earth's bow shock has been widely studied and as a result is relatively well understood. The lack of a Venusian magnetic field and differing conditions in the Venusian ionosphere form a very different bow shock around Venus, one that is not well understood.

Earth's strong magnetic field causes the Terrestrial bow shock to form much farther from the planet than Venus' does (typically around ten Earth radii from the earth compared to a little more than one Venus radius from Venus), keeping the solar wind well away from the Earth's ionosphere where particles could otherwise be picked up by the solar wind. Venus has no magnetic field, so the solar wind interacts with particles, particularly heavy ions, from the Venusian ionosphere. The solar wind picks up these heavy ions, causing mass loading which reduces the solar wind's Mach number, the ratio of solar wind velocity to sound speed in the medium, by a factor of three to five. The amount of mass loading that occurs, and in turn the amount of solar wind slowing, depends upon solar activity and the resulting conditions in the Venusian ionosphere.

All of these factors form a very different bow shock around Venus than around the Earth. Study of this bow shock would greatly enhance our understanding of the structure of this and other bow shocks around non-magnetic planets and satellites. In addition, the process of bow shock formation around a planet occurs only under collisionless (relatively few collisions in the solar wind in transit from the sun to Venus) conditions, which are unattainable in the laboratory. Any increase in information regarding this process will greatly add to our understanding of the physics of collisionless plasmas.

Measurements like those taken of the solar wind by OPA could contribute significantly to the study of Venus bow shock and its associated physics if they were of high enough time resolution. The highest time resolution of the OPA data is, however, only about eight minute intervals. Since the time during which the orbiter passes through the bow shock is only a few minutes or less, the spacecraft would pass through the bow shock before OPA could measure any details.

The ORPA instrument, however, can yield several suprathermal electron measurements per minute while crossing through the bow shock. According to Dr. Knudsen's suggestion, the suprathermal electron measurements outside of the ionopause actually represent solar wind electrons. If so, the ORPA suprathermal electron data would be solar wind data of sufficient time resolution with which to study the bow shock.

To test Dr. Knudsen's idea, we can compare the OPA proton densities with the ORPA suprathermal electron densities. In the solar wind, the electron and proton densities are almost identical, differing only by a small amount. In

the sun, where the solar wind originates, the extreme temperatures ionize all elements. The vast majority of atoms in the sun are hydrogen, which is only a proton when ionized. Helium forms the next largest fraction of the mass in the sun and other elements only a tiny portion. When the elements other than hydrogen are ionized by the heat of the sun, like hydrogen they form electrons, but the resulting ions are not single protons. Thus the electron density in the solar wind will be greater than the proton density by the amount of non-hydrogen ions formed in the sun (about 4%). It is simple, however, to compensate for this difference by accounting for the amount of helium ions likely to be in the solar wind. The fraction of other ions is negligible. Because the difference in densities is so small, the ratio of proton density to electron density in the solar wind is close to one. Thus, if the ratio of OPA proton density to ORPA suprathermal electron density is close to one, this indicates that Dr. Knudsen's ideas are correct: outside of the ionopause the suprathermal electrons ORPA measured are indeed solar wind electrons.
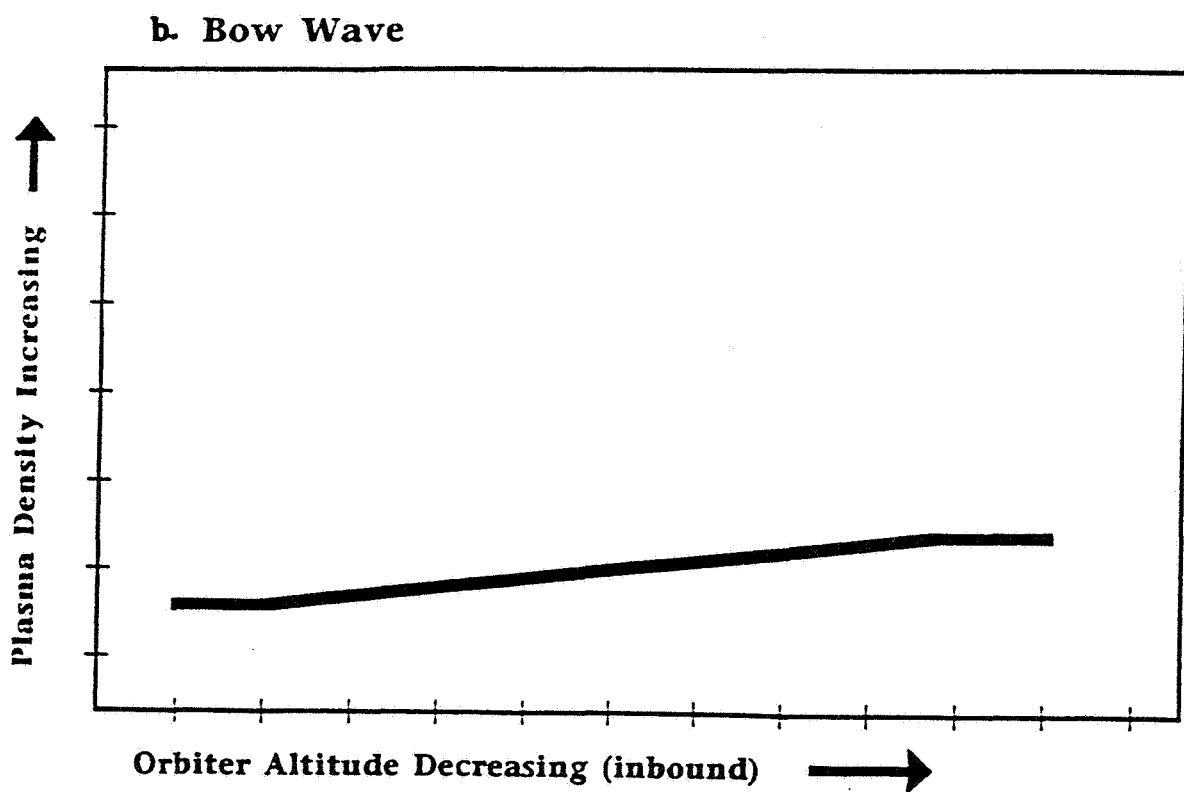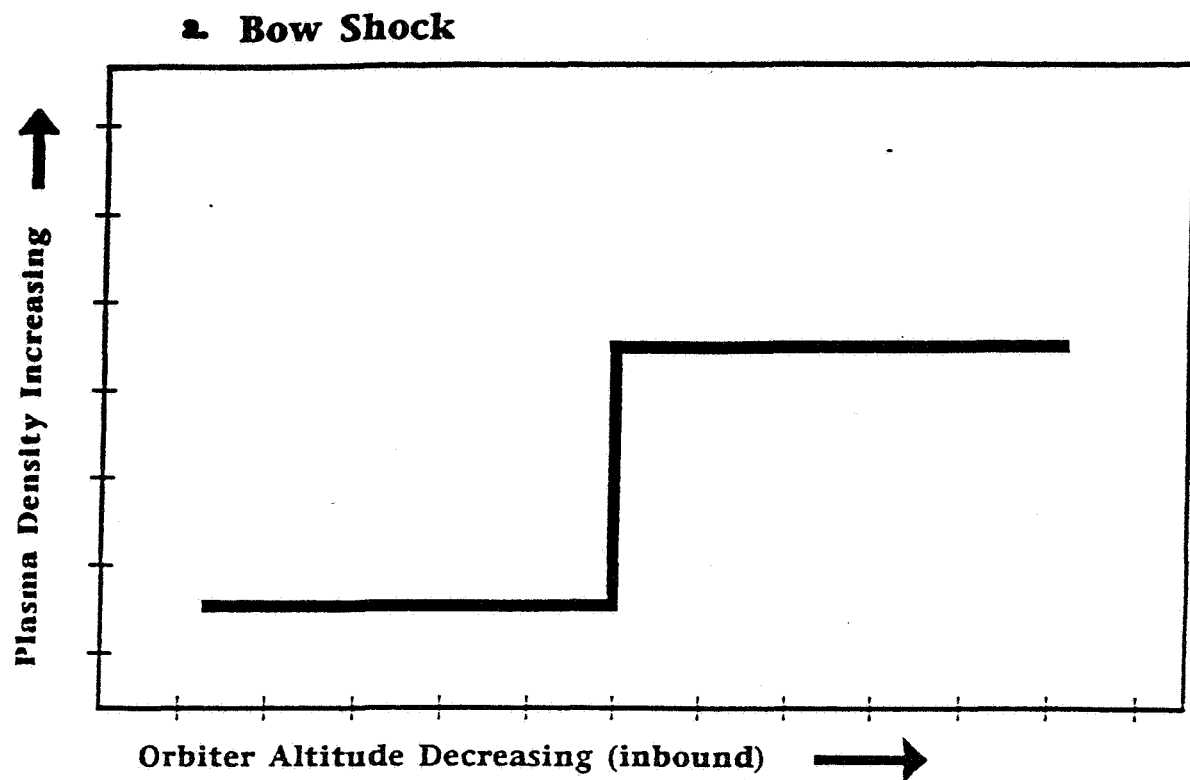
Yet another prospective benefit of this study is bow wave measurements. A bow wave is similar to a bow shock, but the changes in plasma parameters when passing through it are not as dramatic. It is formed when the mass loading upstream of an obstacle is slow enough and over a long enough distance that it does not produce the abrupt changes in solar wind speed and other quantities that indicate a bow shock. This occurs mostly upstream of comets, where the low gravity allows the neutral particles to boil off out to great distances upstream of the comet's nucleus. Here they are ionized and interact with the solar wind, causing mass loading to occur over a very large distance.

On a graph, a bow shock looks like a near-vertical cliff connecting two very different levels of flat ground. In contrast, a bow wave looks like a relatively gentle incline connecting two more similar heights. Figure 2 shows rough models of density changes when passing through a bow shock and a bow wave. The slope of the incline depends on the speed of the solar wind, which in turn depends on how many heavy ions it has picked up.

Because of Venus' unique environment, particularly the high amount of mass loading that occurs, the shockwave may occasionally not be abrupt enough to be a bow shock, but only a bow wave. Currently the locations of the bow shock have been determined by magnetic field data. These counted only abrupt changes as any form of shock: in essence, they have been used to detect only bow shocks, not bow waves. High time resolution data obtained from the ORPA instrument would make it possible to locate and study a combined total of between 5,000 to 10,000 bow wave and bow shock crossings. This would contribute to a much more accurate picture of the solar wind-Venus interaction and ultimately to our understanding of collisionless shock formation under varying conditions.

The purpose of this study was to analyze and compare the OPA proton and ORPA suprathermal electron data to determine if the two sets correlate well enough to indicate that ORPA suprathermal electron data can be used as solar wind data.

Figure 2. Sample Density vs. Altitude Curves Passing Through Bow Shock (a) and Bow Wave (b).

a. Bow Shock

Plasma Density Increasing →

Orbiter Altitude Decreasing (inbound) →

b. Bow Wave

Plasma Density Increasing →

Orbiter Altitude Decreasing (inbound) →

Methodology

Analyzing the data involved a long and cumbersome process to get the data into useable form. Figure 3 shows a flow chart of the process. The ORPA data comes from NASA-Ames Research Center on large tape reels in reduced data records or "RDR" files for each orbit. We first loaded these files onto a VAX system and used a program produced by Ames to put the data into useable form. We then ran a program to tabulate the data into readable tables. Next we used a simple program to divide these files into separate files for each ORPA mode, i.e. thermal electron, ion, and suprathermal electron, and stripped the labels from the tables to make the data plottable.

The suprathermal electron data files then needed to be rearranged into a format compatible with the OPA data, which we received from UCLA. First we modified the ORPA date/time tag to match the OPA tag. The OPA data files have a year-month-day-hour-minute-second date/time tag. Since the ORPA data comes as individual orbit data files, the files have no date tag. In addition, the time tag is a single number combining the hour, minute, and second. For example, the data for the tenth hour, twelfth minute, and 59.2 second would be tagged 101259.2. These incompatibilities, however, are easy to correct. We wrote a simple program to input the date, which we obtained from a table of periapsis dates for each orbit, and convert the time tag to hour-minute-second format for each ORPA file.

Another difference between the OPA and ORPA data is that the OPA data comes in one-hour averages. In order to compare the two data sets, we developed another simple program to calculate hourly averages from the ORPA

Figure 3. Flow Chart of Programs to Process Data.
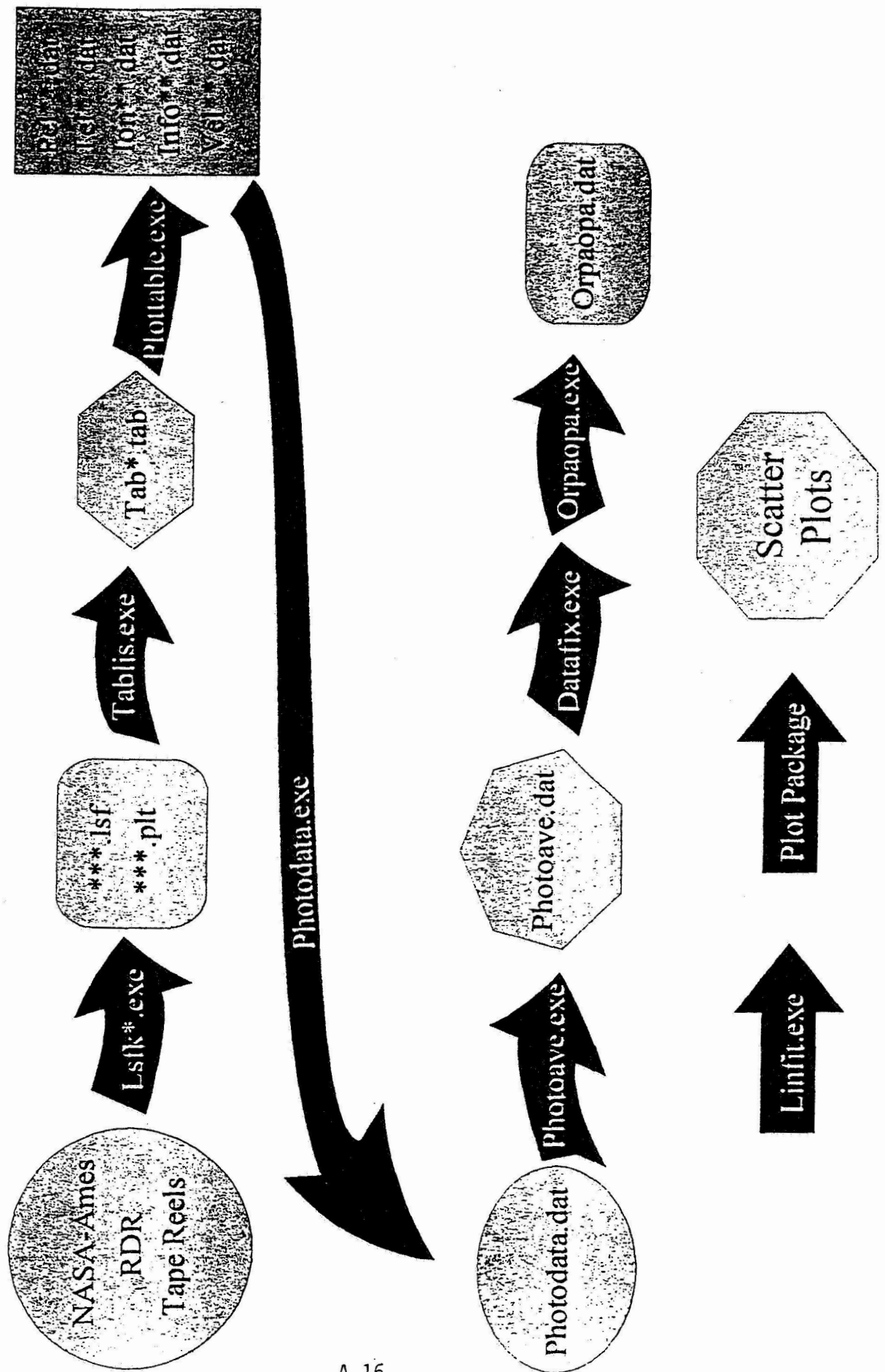
data, using the same start and stop times for each average that were used to obtain the OPA averages. Once the ORPA data was in one-hour averages, the average files, which were still in individual files for each orbit, needed to be appended into one long file and combined with the OPA data, synchronizing each ORPA average with the corresponding OPA average.

To determine if the data sets match well enough, we made scatter plots of the OPA-ORPA data file, plotting OPA proton density versus ORPA suprathermal electron density. If they were exactly the same, this would produce a straight line with a slope of one and a y-intercept of zero. This, however, would not occur since the densities are necessarily not identical because of the extra ions in the solar wind. A plot of a good match would roughly outline a straight line with a slope close to one and an intercept close to zero.

As well as giving a general idea of how well the data match, the plots indicated what data might be inaccurate. Any data well outside of the main group could be questionable. We used the plots to find the data points which fell significantly outside the main group and then analyzed the points to determine why they were anomalous.

After eliminating questionable data, we ran a linear least squares fitter on the data file, which fits a line to the data, giving the slope and intercept of this line as well as the correlation coefficient, which tells how well the data fit the line. The slope of the line determines the proportionality constant that relates the two data sets. A high correlation coefficient, a slope close to one, and an intercept close to zero indicate that the data match well and essentially that Knudsen's ideas are correct; the ORPA suprathermal electrons are solar wind electrons.

A-17

Analysis and Results

We processed the ORPA suprathermal electron data for orbits 1-120. A scatter plot of these versus the OPA proton data produced the predicted straight line with a slope close to one and a y-intercept relatively close to zero. Figure 4 shows the plot of these data and the best linear fit. The linear fit indicated that this line had a slope of .740, an intercept of 5.598, and a correlation coefficient of .631. Though the slope was relatively close to one, the correlation coefficient and the intercept were not good enough to represent a good match.

There were, as can be seen in the figure, several data points that were well outside the main group. Searching through the data, we tried to determine the reason these points were anomalous. Any ORPA averages in which the variance divided by the average value was over .15 had already been eliminated, removing much of the data that was very far from the norm. In addition, any data which was taken below an altitude of 2700 km had been removed. This should exclude any data taken inside the ionopause (only on the sunward side, not in the ionotail), which would be invalid for this study. Any OPA averages with less than four measurements per average and any ORPA data where the value for the thermal electron density was zero were also excluded.

Examination of the data determined that the points well outside the main group were probably not good data. Statistics alone indicates that any data far from the dominant group are probably questionable and should be discarded. We first tried eliminating any ORPA averages that had been

Figure 4. OPA Proton Density vs. ORPA Suprathermal Electron Density (#/cm³). Straight line shows best linear curve fit. ORPA data taken below 2700 km and OPA data with less than four samples per average are excluded.
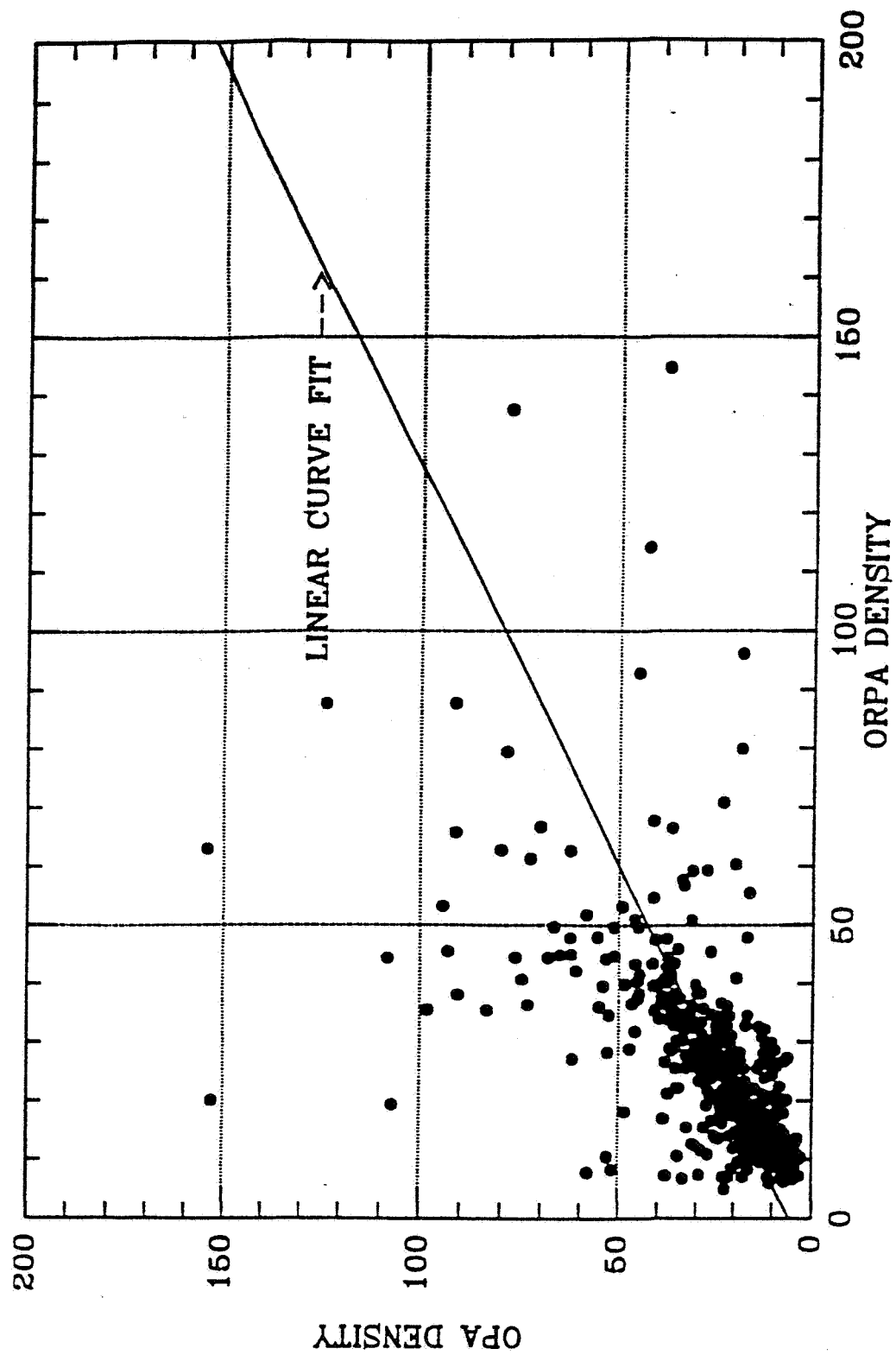
computed from data that were not spread uniformly throughout the hour interval, removing all averages in which any two measurements in the hour were over ten minutes apart. This made certain that there were at least five measurements per average and that these spanned the entire hour. Figure 5 shows the scatter plot of the improved data set. This plot looked considerably cleaner than the last, though it still had some points away from the group. The linear fit produced a line with a slope of .999, a y-intercept of 1.175, and a correlation coefficient of .665. These figures were much better than those from the last data set. There were still, however, some stray data points.

Subsequent conversations between Dr. Jones and Dr. Knudsen and a closer examinations of some of the data files indicated that these questionable data points were related to the effect of spacecraft potential on the ORPA instrument. Plotting the ORPA suprathermal electron density versus the orbiter potential for several orbits indicated a definite trend. Figure 6 shows such a plot for orbit 9. Above a potential of 3, the densities are relatively closely spaced, but at a potential of 2.64 the densities scatter. Figures 7 & 8 show suprathermal electron pressures throughout orbits 22 and 40. There are distinct lines representing different vehicle potentials. The upper trace corresponds to 2.64 volts, the middle to 3.74 and the lower to 5.02 and 6.48 volts. Clearly, an algorithm can be developed to relate the spacecraft potential to density and eliminate the discrepancies. In any case, in the shock equations, it is the ratio of densities before and after the shock that matters and this ratio would be the same as long as we use the data corresponding to one vehicle potential.

Figure 5. OPA Proton Density vs. ORPA Suprathermal Electron Density (#/cm³). Straight line shows best linear curve fit. ORPA data with over ten minute intervals between samples, OPA data with less than four samples per average, and ORPA data taken below 2700 km are excluded.
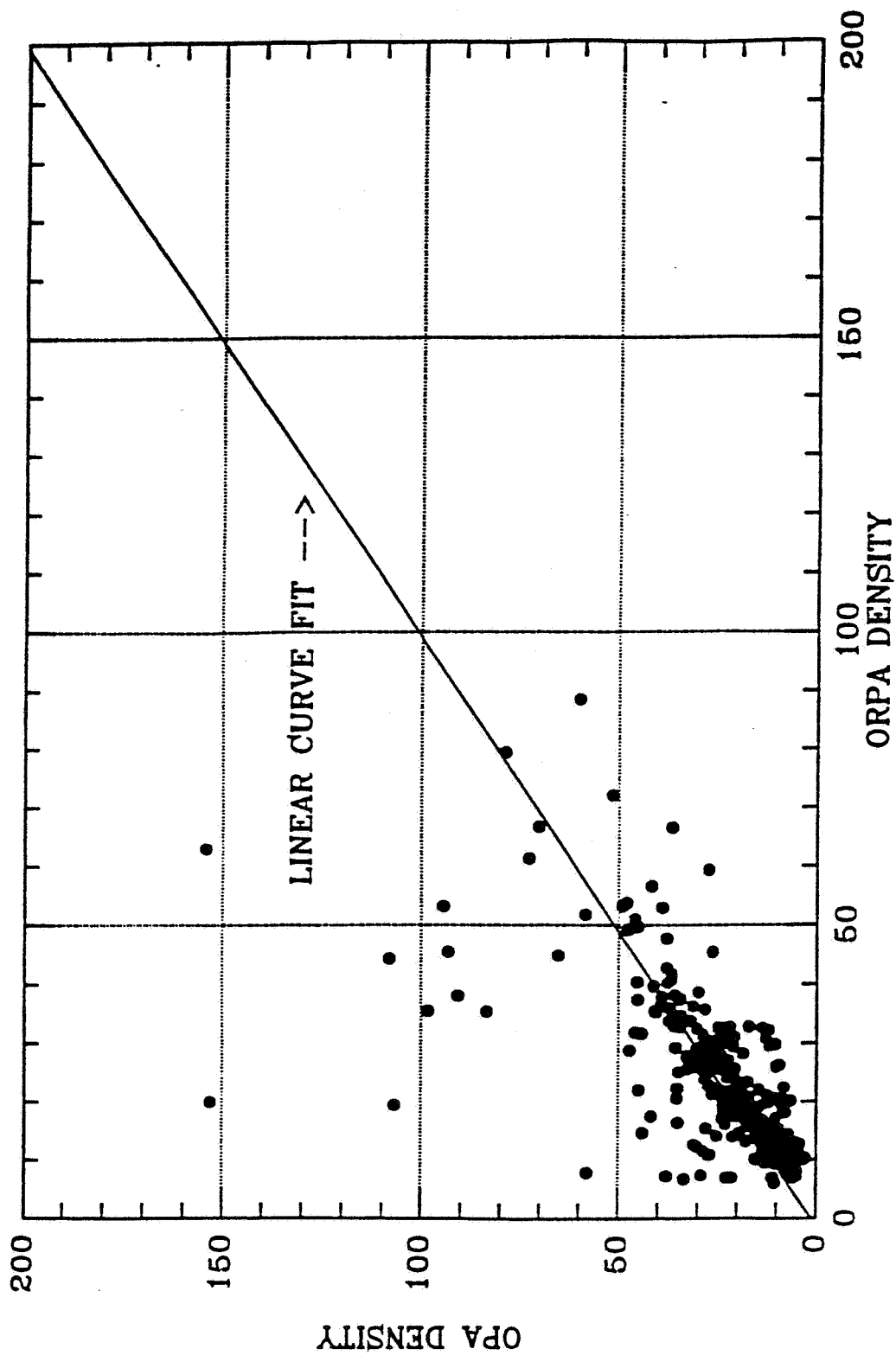
Figure 6. ORPA Suprathermal Electron Density vs. Spacecraft Potential, Orbit 9.
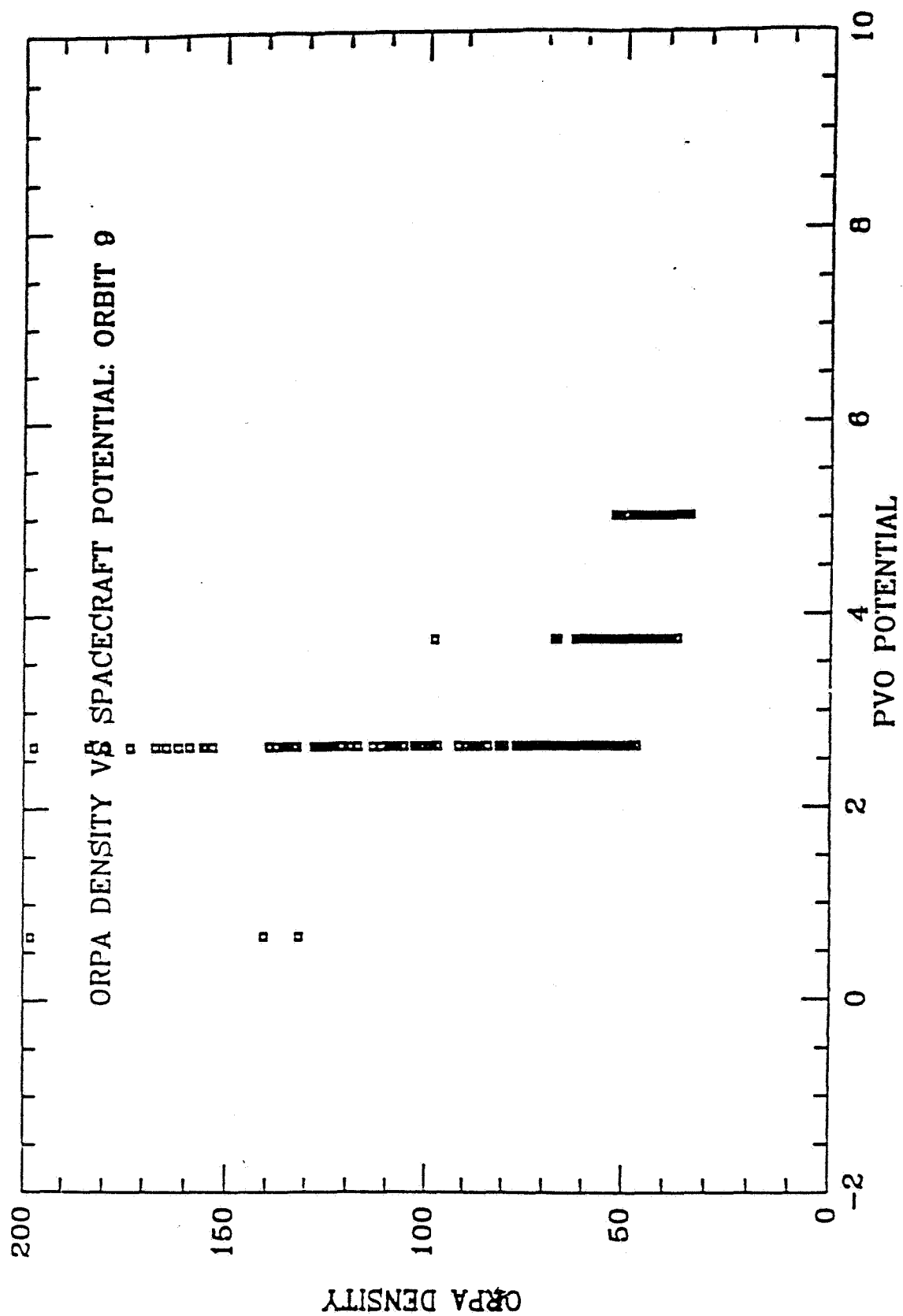
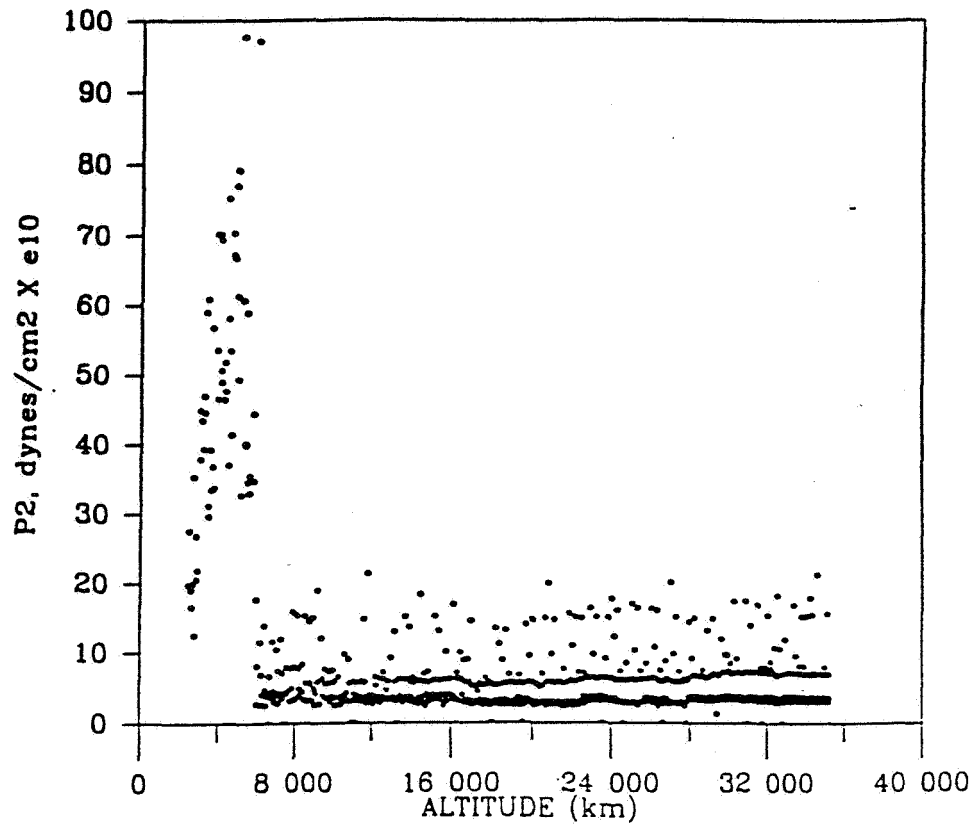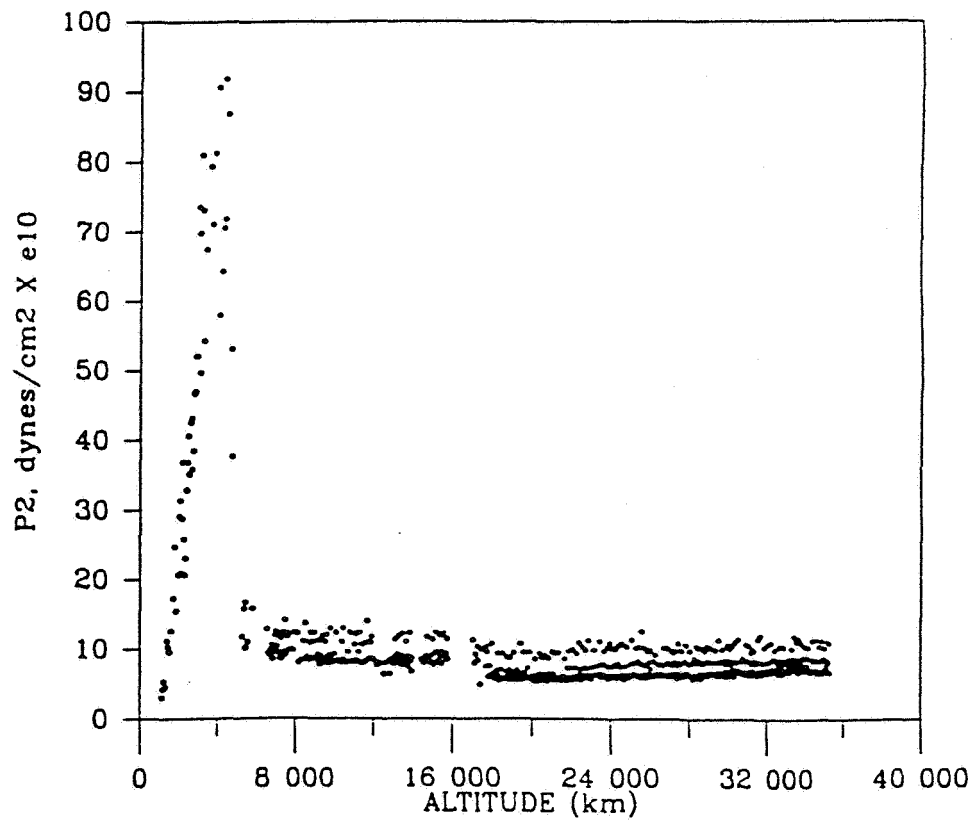**Figure 7. ORPA Suprathermal Electron Pressure vs. Altitude, Orbit 22.**

Figure 8. ORPA Suprathermal Electron Pressure vs. Altitude, Orbit 40.

To investigate the effect of vehicle potential on the data. we plotted three different graphs of the data in orbits 1-79, one with all data points included regardless of potential, one with only those with potential greater than 2.0 volts included, and one with only those with potential greater than 3.0 volts included. The only restrictions on these data sets were: altitude greater than 2700 km, suprathermal electron density greater than zero, number of OPA samples per average greater than three. and the given spacecraft potential limits. Those with potentials of under 3.0 volts included had a large amount of data points clustered at the bottom of the plot (see Fig 9 & 10). The one with only potentials greater than 3.0 volts looked much better (see Fig. 11). As noted previously, this indicated that vehicle potentials of less than 3.0 volts adversely affected the data.

The plot of the data with spacecraft potential greater than 3.0 volts still had some problem points. however. and suggested that elimination of potentials less than 3.0 volts would not take care of all the orbits. More examination of the data showed a cyclic effect in some of the orbits where the ORPA and OPA data didn't match. The potential would alternate (not in a periodic cycle. but still visibly cyclic) between two or three different potential levels. and the density values would change dramatically with the potential. During a visit to BYU. Dr. Knudsen indicated to Dr. Jones that this could be because of the orientation of the ORPA sensor. When the sensor axis vector has any component towards the sun the solar extreme ultraviolet radiation (EUV) on the sensor produces extra suprathermal electrons and thus affects the density readings. This means any data where the sensor axis vector has

Figure 9. OPA Proton Density vs. ORPA Suprathermal Electron Density (#/cm³). Straight line shows best linear curve fit. OPA data with less than four samples per average and data taken below 2700 km are excluded. All potentials are included.
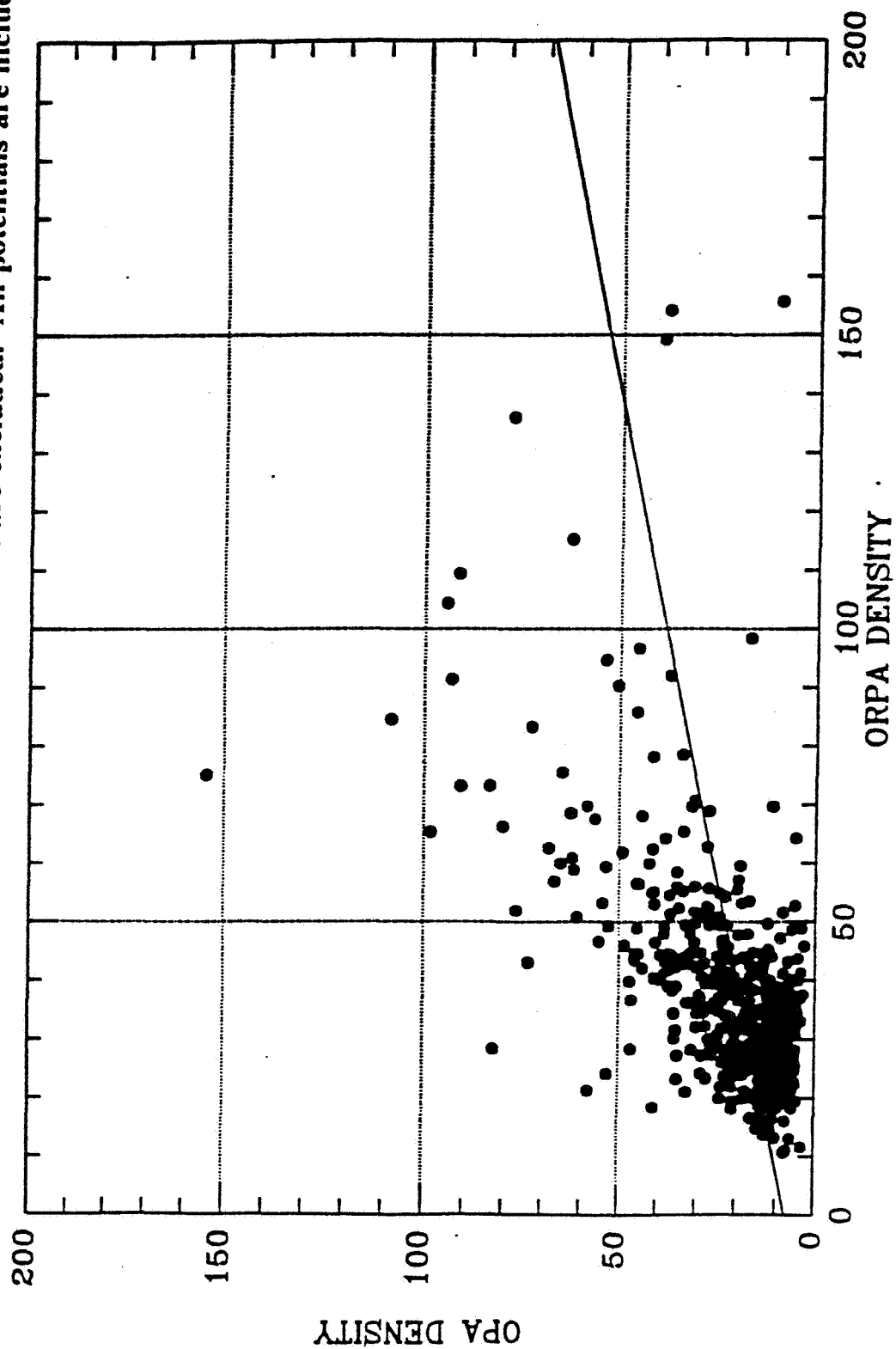
A-25

Figure 10. OPA Proton Density vs. ORPA Suprathermal Electron Density (#/cm³). Straight line shows best linear curve fit. OPA data with less than four samples per average and data taken below 2700 km., and ORPA data with potential less than two are excluded.
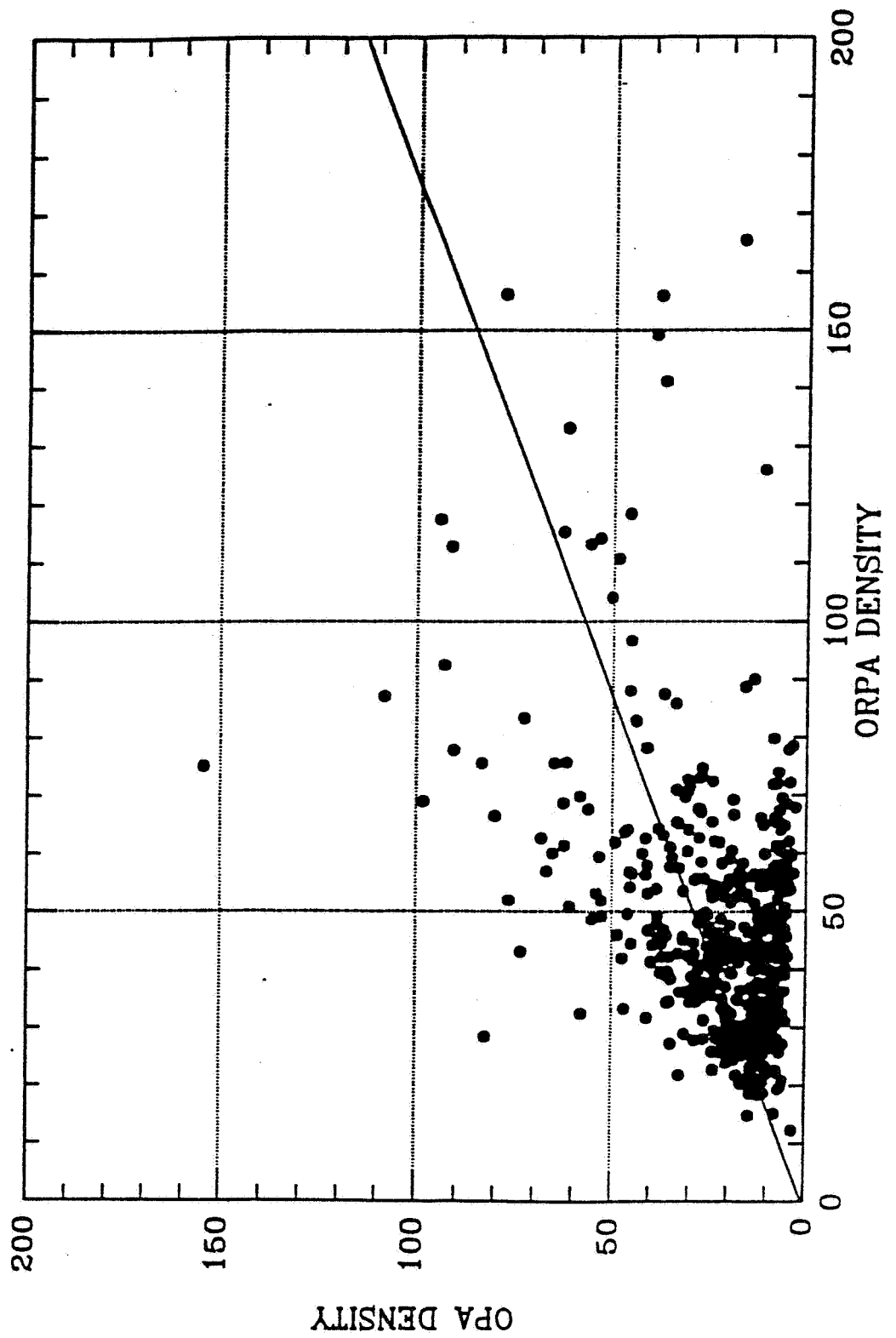
Figure 12. OPA Proton Density vs. ORPA Suprathermal Electron Density (#/cm³). Straight line shows best linear curve fit. OPA data with less than four samples per average, data taken below 2700 km, ORPA data with potential less than three, and ORPA data in orbits 13,14, and 25 are excluded.

A-27
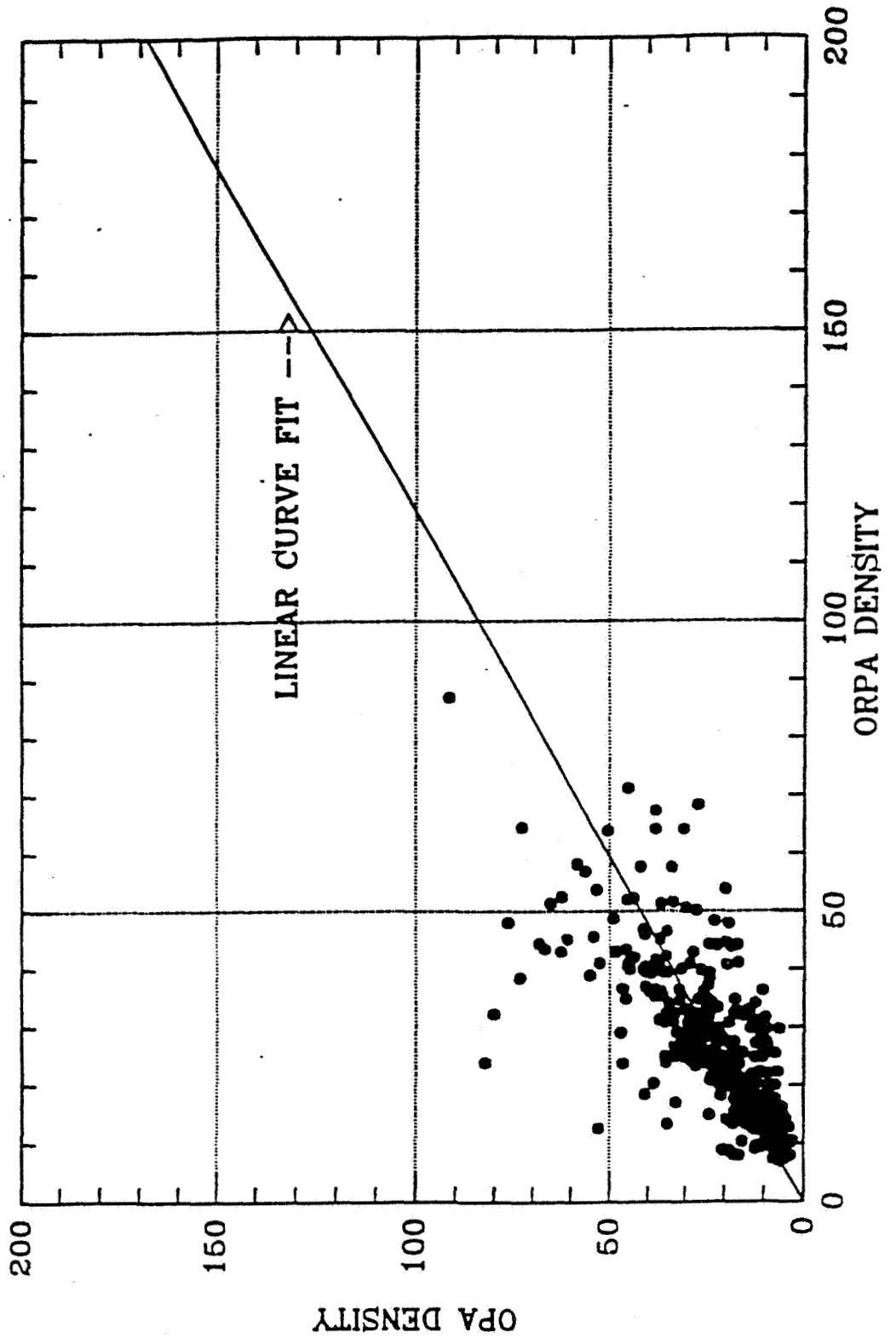
any component towards the sun needs to be eliminated in a further study. This could clean up the data well enough to get an accurate proportionality constant.

For the purpose of this study, however, we simply eliminated all data points in the most questionable orbits: 13, 14 and 25. The scatter plot of this data, Figure 12, looked much cleaner. The data clearly outlined a straight line with a slope close to one and an intercept close to zero. The linear least squares fit showed that this line had a slope of .842, an intercept of -.036, and a correlation coefficient of .756. The correlation coefficient was significantly higher than the previous fits and the intercept was very nearly zero. There were still some data points away from the main group, but they were on both sides of the curve fit, balancing each other out well enough to produce a relatively accurate preliminary proportionality constant.

This result strongly supports Dr. Knudsen's idea that the ORPA suprathermal electron data outside of the ionopause does indeed represent solar wind electron data. The preliminary proportionality constant relating the OPA proton data and the ORPA suprathermal electron data is .842, the slope of the line. Multiplying the ORPA suprathermal electron density data by this number would produce high resolution solar wind electron densities with which to study the Venusian bow shock region.

Figure 11. OPA Proton Density vs. ORPA Suprathermal Electron Density (#/cm³). Straight line shows best linear curve fit. OPA data with less than four samples per average, data taken below 2700 km, and ORPA data with potential less than three are excluded.
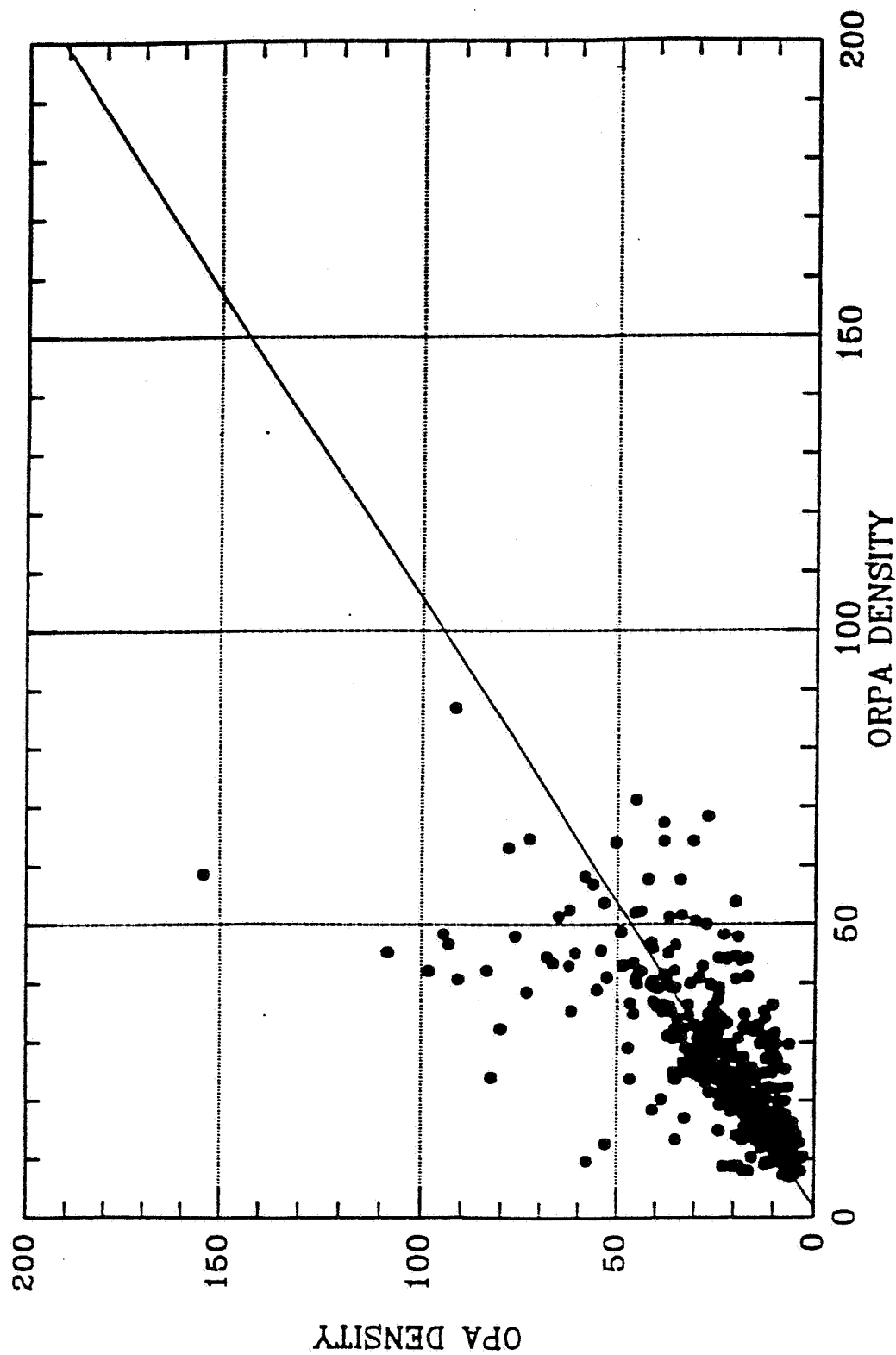
Representative Bow Shock Crossings

To illustrate the high resolution bow shock data which ORPA gives, we plotted some bow shock crossings from different orbits. Figure 13 shows an inbound bow shock crossing during the first orbit. In this plot, the step up in suprathermal electron density as the vehicle passes through the bow shock is clearly depicted. Figure 14 shows an outbound crossing during orbit 61. The step is also clear in this figure, but the density decreases closer to the planet. Figure 15 is a plot of an outbound crossing during orbit 78. This shock is much more dramatic than the last two, with density increasing to about 150 per cubic centimeter as opposed to around 40 per cubic centimeter in the last two. Orbit 78's inbound crossing (Fig. 16) shows an even higher density jump, up to about 170 per cubic centimeter.

Both Figures 14 and 15 show multiple density levels in the shock jumps caused by varying spacecraft potential. This indicates that much of the scatter remaining in Figure 12 is probably due to the vehicle potential. At a fixed potential, the suprathermal electron densities will undoubtably track the solar wind proton densities exceptionally well.

Figure 17 illustrates the difference in sampling rate between the OPA and the ORPA data. The dotted vertical lines show approximately where the eight-minute OPA measurements would occur during orbit 78's inbound bow shock crossing. It is clear that the OPA time resolution is much less than the ORPA, and is not high enough to obtain an accurate picture of the jump in plasma parameters at the bow shock which occurs typically in a fraction of a

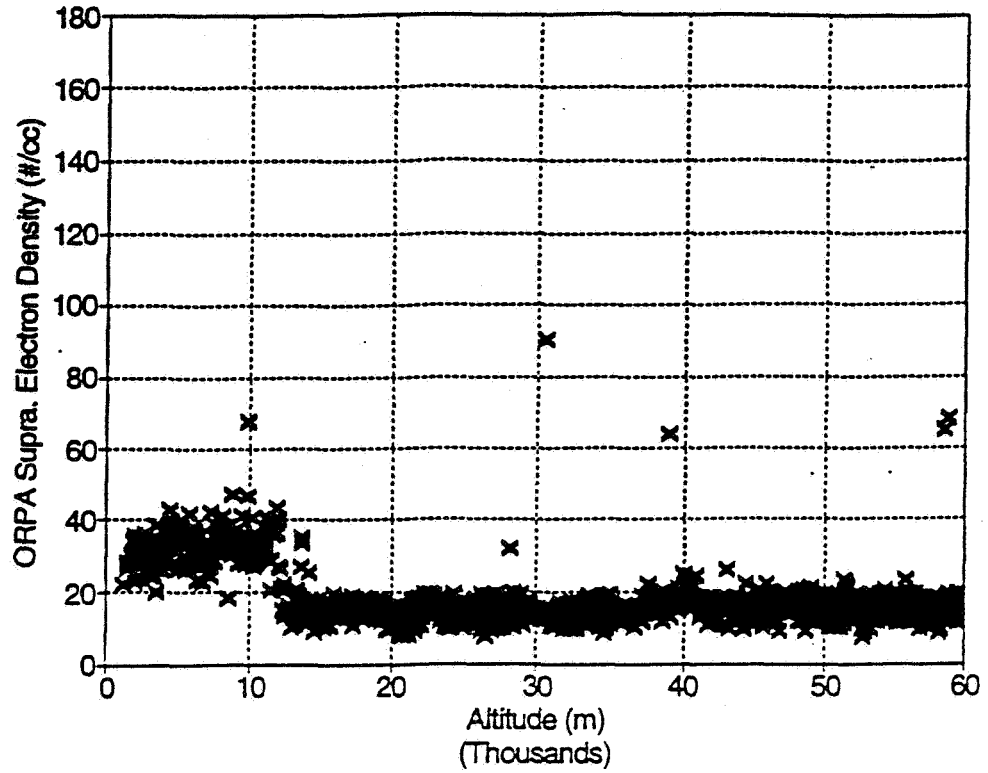**Figure 13. Bow Shock Crossing Orbit 1 Inbound**

Figure 14. Bow Shock Crossing Orbit 61 Outbound

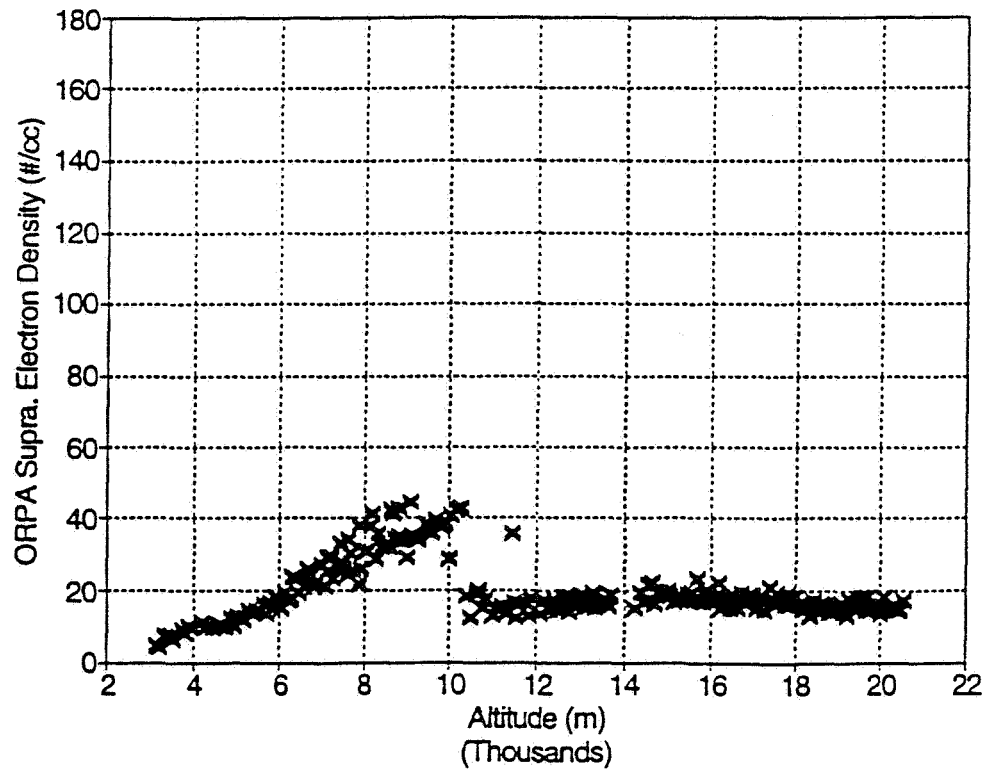## Figure 15. Bow Shock Crossing Orbit 78 Outbound
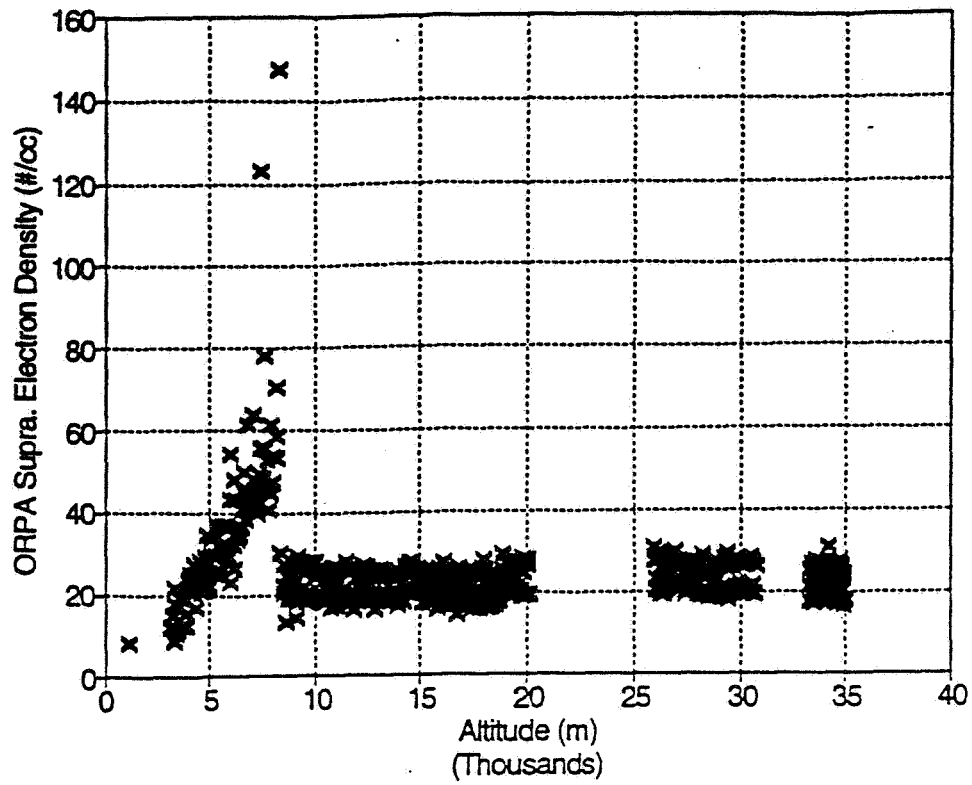

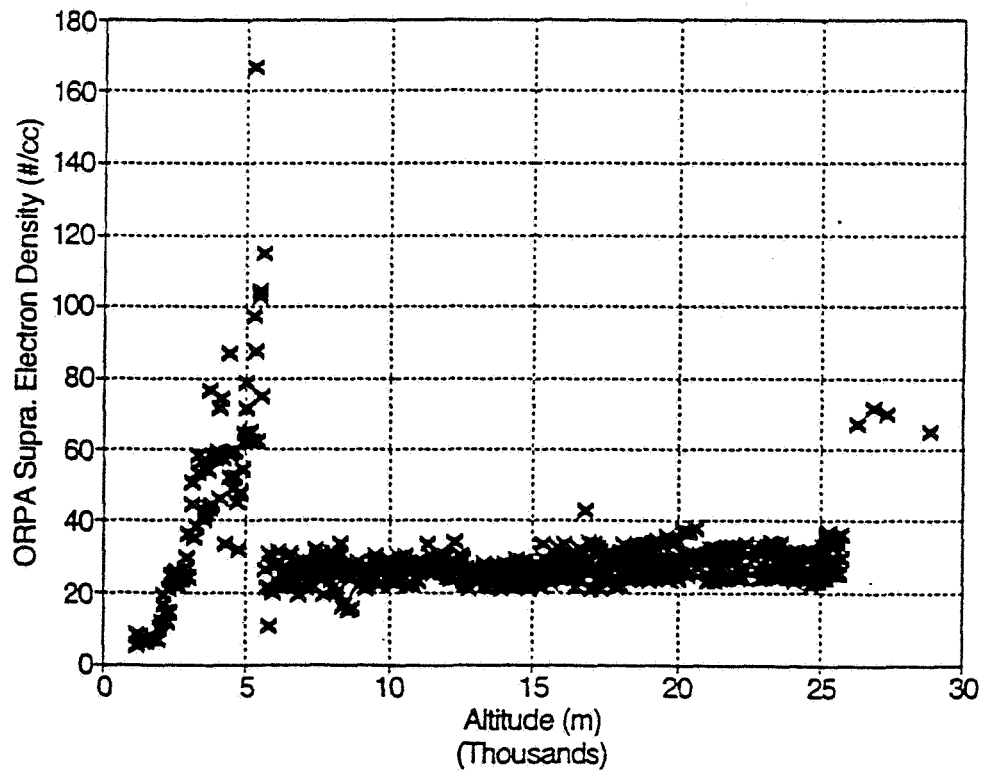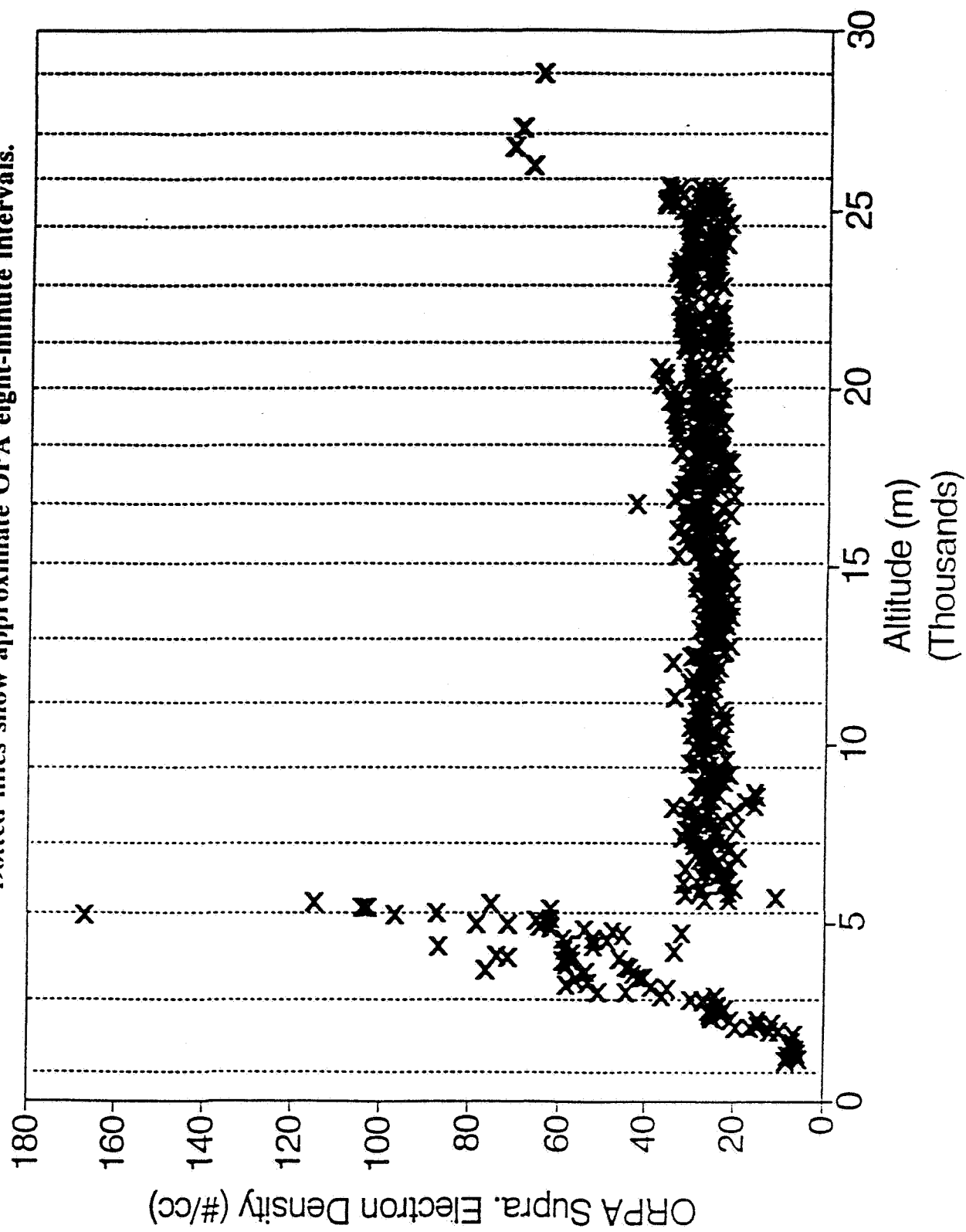## Figure 16. Bow Shock Crossing Orbit 78 Inbound

Figure 17. Bow Shock Crossing Orbit 78 Inbound
Dotted lines show approximate OPA eight-minute intervals.

minute. These plots illustrate the high resolution data which the ORPA instrument produces and that this data is a great improvement over the OPA data for studying the bow shock.

Conclusions

This study strongly indicates that the ORPA suprathermal electron data taken outside of the Venusian ionopause represents solar wind electron data. Our analysis showed that the ORPA suprathermal electron density data matches the OPA proton density data very well. The preliminary proportionality constant relating the two data sets is .842. The data produced using this constant would be high time resolution solar wind electron density data with which to study the Venusian bow shocks and bow waves. This is not possible with the low time resolution solar wind proton data currently available from the OPA instrument.

A future study is needed to determine a more accurate proportionality constant by eliminating any densities which may have been effected by solar EUV, accounting for the relationship between density and vehicle potential, plotting more orbits (probably up to orbit 1500), and comparing the ORPA data with the OPA eight minute measurements, not just the hour averages. Though this further work is clearly needed, the present study strongly supports Dr. Knudsen's suggestion that when outside the ionopause, ORPA suprathermal electron data represents solar wind electron data. With this high time resolution solar wind data, potentially over 5,000 bow shock penetrations can now be studied under a full cycle of solar EUV variations, leading to the most comprehensive study of the interaction of the supersonic solar wind with a nonmagnetic planet that has ever been attempted and thus dramatically increasing our understanding of the physics of shock formation in a collisionless medium.

Works Cited

Colin, Lawrence, ed. "Pioneer Venus Orbiter - Ten Years of Discovery." Unpublished Report, 1989.

Intriligator, D. S., J. H. Wolfe, and J. D. Mihalov. "The Pioneer Venus Orbiter Plasma Analyzer Experiment." IEEE Transactions on Geoscience and Remote Sensing. GE-18, No. 1. Jan. 1980: 39-43.

Knudsen, W. C. Private Communication with Dr. Doug Jones. June 1993.

Knudsen, William C. "Detailed Instrument Description of the Pioneer-Venus Orbiting Retarding Potential Analyzer (ORPA)." Contract NAS 2-8811. Lockheed Palo Alto Research Laboratory. Oct. 1977.

Knudsen, W. C., J. Bakke, K. Spenner, and V. Novak. "Pioneer Venus Orbiter Planar Retarding Potential Analyzer." IEEE Transactions on Geoscience and Remote Sensing. GE-18, No. 1. Jan. 1980: 54-59.

Knudsen, W. C., K. Spenner, J. Bakke, an V. Novak. "Retarding Potential Analyzer for the Pioneer-Venus Orbiter Mission." Space Science Instrumentation 4 (1979): 351-372.

Appendix of Programs

(Note: This appendix does not contain all of the

programs used. just some of the shorter ones we developed.)

PHOTODATA.FOR

This program asks the user to input the year, month, and day of the orbit file to be processed. It then adds this date tag onto the data, converts the ORPA time tag to the OPA hour-minute-second format, and writes the newly formatted data to a new file. To run this program, the user must assign the data file to be processed as FOR001 and the name of the new file as FOR002.

```fortran
      DIMENSION XA(30000),D1(30000),T1(30000),SZA(30000),EP1(30000),
     *D2(30000),T2(30000),EP2(30000)
      CHARACTER TITLE*35
      TYPE 888
  888 FORMAT(1X,'ENTER YEAR, IYR (I4)')
      ACCEPT 889, IYR
  889 FORMAT(I4)
      TYPE 890
  890 FORMAT(1X,'ENTER MONTH, MON (I2)')
      ACCEPT 891, IMON
  891 FORMAT(I2)
      TYPE 892
  892 FORMAT(1X,'ENTER DAY OF MONTH, NDAY (I2)')
      ACCEPT 893, IDAY
  893 FORMAT(I2)
      IM=1
C        ELECTRON PRESSURE WILL BE IN UNITS OF DYNES/CM2 TIME E10.
      ALPHA=1.6E-02
   11 READ(1,333,END=7734)N1,P2,P3,P4,P5,P6,P7,P8,P9,P10,P11,P12,P13
  333 FORMAT(I5,2F9.1,F8.1,F10.2,2F11.3,6F10.3)
      IF(P6 .LE. 0.0) GO TO 11
      IF(P8 .LE. 0.0) GO TO 11
      IF(P10 .LE. 0.0) GO TO 11
      IM=IM+1
      TT=P2
      IHR=INT(TT/10000.)
      DELT=TT-10000.*REAL(IHR)
      IMIN=INT(DELT/100.0)
      SEC=TT-(10000.*REAL(IHR)+100.*REAL(IMIN))
      XA(IM)=P3
      SZA(IM)=P4
      D1(IM)=P6
      T1(IM)=P8
      D2(IM)=P10
      T2(IM)=P12
      EP1(IM)=ALPHA*D1(IM)*T1(IM)
      EP2(IM)=ALPHA*D2(IM)*T2(IM)
      WRITE(2,3434) IYR,IMON,IDAY,IHR,IMIN,SEC,XA(IM),SZA(IM),
     *D1(IM),T1(IM),EP1(IM),D2(IM),T2(IM),EP2(IM)
 3434 FORMAT(I5,4I3,F5.1,1X,F8.1,F6.1,F11.2,5F11.3)
      GO TO 11
 7734 CONTINUE
      CLOSE(UNIT=1)
   12 CALL EXIT
      END
```

PHOTOAVE1.FOR

This program takes one-hour averages of the data file assigned FOR001 and writes them to the file assigned FOR002. It puts high junk numbers in as the data for any averages with less than three measurements per average and removes any data taken below 2700 km.

```fortran
C
C     THIS PROGRAM REQUIRES PHOTODATA.DAT ASSIGNED AS FOR001 AND
C     PHOTOAVE.DAT ASSIGNED AS FOR002
C
      DIMENSION DENS(9000),TEMP(9000),NT(9000)
C     TYPE 80
C  80 FORMAT(1X,'TAILBX POLARITY : P = BX > 0,N = BX < 0,A=ALL')
C     ACCEPT 81, SIGN
C  81 FORMAT(A1)
 1003 CONTINUE
      KK=1
 1002 READ(1,3434,END=900) IYR,IMON,IDAY,IHR,IMIN,SEC,XA,SZA,
     *D1,T1,EP1,D2,T2,EP2
 3434 FORMAT(I5,4I3,F5.1,1X,F8.1,F6.1,F11.2,5F11.3)
      IF(XA .LT. 2700.0) GO TO 1002
      NT(KK)=IHR
      IF(IHR .GT. NT(1)) GO TO 1004
      IF(IHR .LT. NT(1)) GO TO 1004
      DENS(KK)=REAL(D2)
      TEMP(KK)=REAL(T2)
      KK=KK+1
   10 GO TO 1002
 1004 CONTINUE
      KPTS=KK-1
      IF(KPTS .LE. 2) GO TO 18
      CALL XFIT(DENS,KPTS,0,DENAVE,SIGDN,SIGD)
      CALL XFIT(TEMP,KPTS,0,TEMAVE,SIGTN,SIGT)
      GO TO 19
   18 DENAVE=0.0
      SIGDN=999.9
      SIGD=999.9
      TEMAVE=0.0
      SIGTN=999.9
      SIGT=999.9
   19 CONTINUE
      WRITE(2,3800) IYR,IMON,IDAY,NT(1),KPTS,DENAVE,SIGDN,SIGD,
     *TEMAVE,SIGTN,SIGT
 3800 FORMAT(1X,I4,4I3,6F10.2)
      SDENS=REAL(D2)
      STEMP=REAL(T2)
      NT(1)=NT(KK)
      KK=1
      DENS(KK)=SDENS
      TEMP(KK)=STEMP
      KK=KK+1
      GO TO 1002
  900 CONTINUE
      KPTS=KK-1
      IF(KPTS .LE. 2) GO TO 28
      CALL XFIT(DENS,KPTS,0,DENAVE,SIGDN,SIGD)
      CALL XFIT(TEMP,KPTS,0,TEMAVE,SIGTN,SIGT)
      GO TO 29
   28 DENAVE=0.0
      SIGDN=999.9
      SIGD=999.9
      TEMAVE=0.0
      SIGTN=999.9
      SIGT=999.9
   29 CONTINUE
      WRITE(2,3800) IYR,IMON,IDAY,NT(1),KPTS,DENAVE,SIGDN,SIGD,
```

```
      *TEMAVE,SIGTN,SIGT
       CLOSE(UNIT=1)
       CALL EXIT
       END



C*************************************************************
C
*********************************
       SUBROUTINE XFIT(X,NPTS,MODE,XMEAN,SIGMAM,SIGMA)
       DOUBLE PRECISION SUM,SUMX,WEIGHT,FREE
       DIMENSION X(1)
C
C          ACCUMULATE WEIGHTED SUMS
C
       IF(NPTS .LE. 2) GO TO 888
    11 SUM = 0.
       SUMX = 0.
       SIGMA = 0.
       SIGMAM = 0.
    20 DO 32 I = 1, NPTS
    21 IF (MODE) 22, 22, 24
    22 WEIGHT = 1.
       GO TO 31
    24 WEIGHT = 1.
    31 SUM = SUM + WEIGHT
    32 SUMX = SUMX + WEIGHT*X(I)
C
C          EVALUATE MEAN AND STANDARD DEVIATIONS
C
    41 XMEAN = SUMX/SUM
    51 DO 52 I=1,NPTS
    52 SIGMA = SIGMA + (X(I)-XMEAN)**2
       FREE = NPTS - 1
    54 SIGMA = DSQRT(SIGMA/FREE)
    61 IF (MODE) 62, 64, 66
    62 SIGMAM = DSQRT(XMEAN/SUM)
       GO TO 70
    64 SIGMAM = SIGMA / DSQRT(SUM)
       GO TO 70
    66 SIGMA = DSQRT(1./SUM)
       GO TO 889
   888 WRITE(4,9033)
  9033 FORMAT(1X,'NOT ENOUGH DATA')
   889 CONTINUE
    70 RETURN
       END
```

PHOTOAVE2.FOR

This program is the same as Photoave1.for, but it excludes any averages with time jumps of over ten minutes between any two measurements.

```
C
C     THIS PROGRAM REQUIRES PHOTODATA.DAT ASSIGNED AS FOR001 AND
C     PHOTOAVE.DAT ASSIGNED AS FOR002
C
      DIMENSION DENS(9000),TEMP(9000),NT(9000),MDIFF(9000)
C     TYPE 80
C  80 FORMAT(1X,'TAILBX POLARITY : P = BX > 0,N = BX < 0,A=ALL')
C     ACCEPT 81, SIGN
C  81 FORMAT(A1)
 1003 CONTINUE
      KK=1
      KD=1
      MD=0
 1002 READ(1,3434,END=900) IYR,IMON,IDAY,IHR,IMIN,SEC,XA,SZA,
     *D1,T1,EP1,D2,T2,EP2
 3434 FORMAT(I5,4I3,F5.1,1X,F8.1,F6.1,F11.2,5F11.3)
      IF(XA .LT. 2700.0) GO TO 1002
      NT(KK)=IHR
      IF(IHR .GT. NT(1)) GO TO 1004
      IF(IHR .LT. NT(1)) GO TO 1004
      MDIFF(KD)=IMIN-MD
      MD=IMIN
      KD=KD+1
      DENS(KK)=REAL(D2)
      TEMP(KK)=REAL(T2)
      KK=KK+1
   10 GO TO 1002
 1004 CONTINUE
      MDIFF(KD)=59-MD
      KPTS=KK-1
      MCOUNT=KD-KPTS
  111 IF(MDIFF(MCOUNT) .GT. 10) GO TO 222
      MCOUNT=MCOUNT+1
      IF(MCOUNT .GT. KD) GO TO 112
      GO TO 111
  112 IF(KPTS .LE. 2) GO TO 18
      CALL XFIT(DENS,KPTS,0,DENAVE,SIGDN,SIGD)
      CALL XFIT(TEMP,KPTS,0,TEMAVE,SIGTN,SIGT)
      GO TO 19
   18 DENAVE=0.0
      SIGDN=999.9
      SIGD=999.9
      TEMAVE=0.0
      SIGTN=999.9
      SIGT=999.9
   19 CONTINUE
      WRITE(2,3800) IYR,IMON,IDAY,NT(1),KPTS,DENAVE,SIGDN,SIGD,
     *TEMAVE,SIGTN,SIGT
 3800 FORMAT(1X,I4,4I3,6F10.2)
  222 SDENS=REAL(D2)
      STEMP=REAL(T2)
      NT(1)=NT(KK)
      KK=1
      DENS(KK)=SDENS
      TEMP(KK)=STEMP
      KK=KK+1
      KD=KD+1
      MD=0
      MDIFF(KD)=IMIN-MD
      MD=IMIN
```

A-44

```
                KD=KD+1
                GO TO 1002
        900 CONTINUE
                MDIFF(KD)=59-MD
                KPTS=KK-1
                MCOUNT=KD-KPTS
        211 IF(MDIFF(MCOUNT) .GT. 10) GO TO 322
                MCOUNT=MCOUNT+1
                IF(MCOUNT .GT. KD) GO TO 212
                GO TO 211
        212 IF(KPTS .LE. 2) GO TO 28
                CALL XFIT(DENS,KPTS,0,DENAVE,SIGDN,SIGD)
                CALL XFIT(TEMP,KPTS,0,TEMAVE,SIGTN,SIGT)
                GO TO 29
         28 DENAVE=0.0
                SIGDN=999.9
                SIGD=999.9
                TEMAVE=0.0
                SIGTN=999.9
                SIGT=999.9
         29 CONTINUE
                WRITE(2,3800) IYR,IMON,IDAY,NT(1),KPTS,DENAVE,SIGDN,SIGD,
             *TEMAVE,SIGTN,SIGT
        322 CLOSE(UNIT=1)
                CALL EXIT
                END




C*******************************************************
C
***********************************
                SUBROUTINE XFIT(X,NPTS,MODE,XMEAN,SIGMAM,SIGMA)
                DOUBLE PRECISION SUM,SUMX,WEIGHT,FREE
                DIMENSION X(1)
C
C            ACCUMULATE WEIGHTED SUMS
C
                IF(NPTS .LE. 2) GO TO 888
         11 SUM = 0.
                SUMX = 0.
                SIGMA = 0.
                SIGMAM = 0.
         20 DO 32 I = 1, NPTS
         21 IF (MODE) 22, 22, 24
         22 WEIGHT = 1.
                GO TO 31
         24 WEIGHT = 1.
         31 SUM = SUM + WEIGHT
         32 SUMX = SUMX + WEIGHT*X(I)
C
C            EVALUATE MEAN AND STANDARD DEVIATIONS
C
         41 XMEAN = SUMX/SUM
         51 DO 52 I=1,NPTS
         52 SIGMA = SIGMA + (X(I)-XMEAN)**2
                FREE = NPTS - 1
         54 SIGMA = DSQRT(SIGMA/FREE)
         61 IF (MODE) 62, 64, 66
         62 SIGMAM = DSQRT(XMEAN/SUM)
```

```
         GO TO 70
      64 SIGMAM = SIGMA / DSQRT(SUM)
         GO TO 70
      66 SIGMA = DSQRT(1./SUM)
         GO TO 889
     888 WRITE(4,9033)
    9033 FORMAT(1X,'NOT ENOUGH DATA')
     889 CONTINUE
      70 RETURN
         END
```

ORPAOPA.FOR

This program correlates the OPA proton data and the ORPA suprathermal electron one-hour averages, matching the data by date/time tags. It also removes any ORPA data where the variance divided by the average value is greater than .15. It can also remove any data where the OPA density is over 60 or the ORPA temperature average is over 250000, but these lines are commented out in this version. The program requires the OPA data file assigned as FOR001, the ORPA averages data file assigned as FOR002, and the output file name assigned as FOR003.

```
      REAL NREC
 1002 OPEN(UNIT=2,STATUS='OLD',FORM='FORMATTED',RECL=11,
     *RECORDTYPE='FIXED',IOSTAT=ISTAT,READONLY)
   12 READ(1,302,END=900)NYR,NMON,NDAY,NHR,NMIN,SEC,NREC,TEMP,
     *DENS,VEL,AZ,POL
  302 FORMAT(I5,4I3,F7.3,F8.0,F12.0,F9.3,F7.1,2F9.3)
      IF(NREC .LT. 5) GO TO 12
   11 READ(2,3800,END=800) IYR,IMON,IDAY,IHR,KPTS,DENAVE,SIGDN,SIGD,
     *TEMAVE,SIGTN,SIGT
 3800 FORMAT(I4,4I3,6F10.2)
C     IF(DENS :GT. 60.0) GO TO 800
    . TEMAVE=TEMAVE*11594.2
      IF(DENAVE .EQ. 0.00) GO TO 11
      IF(SIGDN/DENAVE .GT. 0.15) GO TO 11
C     IF(TEMAVE .GT. 250000.0) GO TO 11
      IF(IYR.EQ.NYR.AND.IMON.EQ.NMON.AND.IDAY.EQ.NDAY.AND.IHR.EQ.NHR)
     *GO TO 10
      IF(IYR.NE.NYR.OR.IMON.NE.NMON.OR.IDAY.NE.NDAY.OR.IHR.NE.NHR)
     *GO TO 11
   10 WRITE(3,3010) NYR,NMON,NDAY,NHR,DENS,DENAVE,TEMP,TEMAVE
 3010 FORMAT(I5,3I3,4F10.2)
  800 CONTINUE
      CLOSE(UNIT=2)
      GO TO 1002
  900 CONTINUE
      CLOSE(UNIT=1)
      CALL EXIT
      END
```

DATAFIX.FOR

This program removes any data from the correlated ORPA/OPA data file in which the OPA density divided by the ORPA density is greater than 1.70 or less than .30. This is the program I used to eliminate any questionable data far from the main group. It requires the ORPA/OPA data file assigned as FOR001 and the output file name assigned as FOR002.

```
   12 READ(1,111,END=77)NYR,NMON,NDAY,NHR,DENS,DENAVE,TEMP,TEMAVE
  111 FORMAT(I5,3I3,4F10.2)
      IF(DENS/DENAVE .LT. 0.30) GO TO 12
      IF(DENS/DENAVE .GT. 1.70) GO TO 12
      WRITE(2,222)NYR,NMON,NDAY,NHR,DENS,DENAVE,TEMP,TEMAVE
  222 FORMAT(I5,3I3,4F10.2)
      GO TO 12
   77 CLOSE(UNIT=1)
      CALL EXIT
      END
```

LINFITPVO.FOR

This is the linear least squares fitter we used to fit the ORPA density vs. OPA density lines. It requires the ORPA/OPA file assigned FOR001 and the output file name assigned FOR002. It writes the number of data points, the y intercept, the variance on the intercept, the slope, the variance on the slope, the correlation coefficient, the average ORPA density, and the average OPA density to the output file.

```
C THIS IS THE PROGRAM "LINFITPVO.FOR"
C
      DIMENSION AA(10000),BB(10000)
      NN=0
    1 READ(1,100,END=900) OPADENS,ORPADENS
  100 FORMAT(14X,2F10.2)
      NN=NN+1
      AA(NN)=ORPADENS
      BB(NN)=OPADENS
      GO TO 1
  900 CLOSE(UNIT=1)
      KPTS=NN
      IF(KPTS .EQ. 0) GO TO 302
      CALL LINFIT(AA,BB,KPTS,YNT,SGYNT,YSLP,SGYSLP,YY,AVA,AVB)
      WRITE(2,300) KPTS,YNT,SGYNT,YSLP,SGYSLP,YY,AVA,AVB
  300 FORMAT(I7,7F9.3)
  302 CALL EXIT
      END
C
C****************************************************************
C
      SUBROUTINE LINFIT(X,Y,NPTS,A,SIGMAA,B,SIGMAB,R,AVX,AVY)
      DOUBLE PRECISION SUM,SUMX,SUMY,SUMX2,SUMXY,SUMY2
      DOUBLE PRECISION XI,YI,WEIGHT,DELTA,VARNCE
      DIMENSION X(1),Y(1)
C
C     ACCUMULATE WEIGHTED SUMS
C
      IF(NPTS .LE. 2) GO TO 500
   11 SUM=0.
      SUMX=0.
      SUMY=0.
      SUMX2=0.
      SUMXY=0.
      SUMY2=0.
   21 DO 50 I=1,NPTS
      XI =  X(I)
      YI = Y(I)
      WEIGHT = 1.
   41 SUM  = SUM - WEIGHT
      SUMX = SUMX - WEIGHT*XI
      SUMY = SUMY - WEIGHT*YI
      SUMX2= SUMX2- WEIGHT*XI*XI
      SUMXY= SUMXY- WEIGHT*XI*YI
      SUMY2= SUMY2- WEIGHT*YI*YI
   50 CONTINUE
C
C     CALCULATE COEFFICIEINTS AND STANDARD DEVIATIONS
C
      AVX=SUMX/NPTS
      AVY=SUMY/NPTS
   51 DELTA = SUM*SUMX2 - SUMX*SUMX
      IF(DELTA .EQ. 0.) GO TO 500
      A = (SUMX2*SUMY - SUMX*SUMXY) / DELTA
   53 B = (SUMXY*SUM - SUMX*SUMY ) / DELTA
      C = REAL(NPTS-2)
      VARNCE = (SUMY2+ A*A*SUM + B*B*SUMX2
     *-2.*(A*SUMY + B*SUMXY - A*B*SUMX))/ C
   67 SIGMAA = DSQRT(VARNCE*SUMX2 / DELTA)
```

```
68 SIGMAB = DSQRT(VARNCE*SUM / DELTA)
71 R = (SUM*SUMXY - SUMX*SUMY) /
   *DSQRT(DELTA*(SUM*SUMY2 - SUMY*SUMY))
500 CONTINUE
   RETURN
   END
```

PHOTORUN.COM

This is a sample of a command file which can be used to process the data. It takes the data from the plottable data files to the correlated GRPA/OPA data files. To use it, simply change the file names and the date entered to fit the orbit(s) to be processed.

```
$ASSIGN PEL0001.DAT FOR001
$ASSIGN PHOTODATA01.DAT FOR002
$RUN PHOTODATA
1978
12
4
$ASSIGN PHOTODATA01.DAT FOR001
$ASSIGN PHOTOAVE01.DAT FOR002
$RUN PHOTOAVE
$ASSIGN PEL0002.DAT FOR001
$ASSIGN PHOTODATA02.DAT FOR002
$RUN PHOTODATA
1978
12
5
$ASSIGN PHOTODATA02.DAT FOR001
$ASSIGN PHOTOAVE02.DAT FOR002
$RUN PHOTOAVE
$APPEND PHOTOAVE02.DAT PHOTOAVE01.DAT
$RENAME PHOTOAVE01.DAT PHOTOAVE.DAT
$ASSIGN OPA.DAT FOR001
$ASSIGN PHOTOAVE.DAT FOR002
$ASSIGN ORPAOPA.DAT FOR003
$RUN ORPAOPA
```
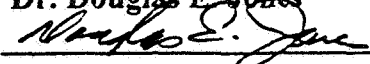
Pioneer Venus Orbiter Retarding Potential Analyzer
Observations of the Electron Component
of the Solar Wind, and of the Venus Bow Shock and Magnetosheath

by

Noe Yamaguchi

Submitted to Brigham Young University in partial fulfillment

of graduation requirements for University Honors

March 1, 1995

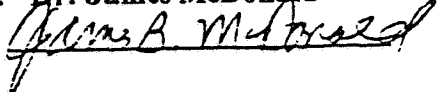Advisor: Dr. Douglas E. Jones
Signature: _____

Honors Dean: Dr. James McDonald
Signature: _____

TABLE OF CONTENTS

LIST OF FIGURES

1. Abstract

We have used the supra thermal electron data obtained by the Pioneer Venus Orbiter ORPA (Retarding Potential Analyzer) instrument to study the bow shock of Venus. The supra thermal electron density component of ORPA data was found by Gifford (1993) to track the solar wind proton density under certain spacecraft potential conditions. Using the Spreiter (1966) gas dynamic equations, we have estimated the Mach number that can be calculated from the change in plasma parameters that results from the interaction of the solar wind with the upper ionosphere of Venus. Using the Mach number calculated from Spreiter's equations and employing the mass loading equations developed for the solar wind interaction with comets, we have been able to estimate the fractional number of solar wind protons that have been replaced by atomic oxygen ions through charge exchange.

The Mach number calculated had its average of 2.71 and ranged from 1.14 to 4.27 (excluding two abnormal events). The fraction of the picked up solar wind protons that were replaced by 16 m_p ions (oxygen ions) had an average of 9.95% and ranged from 0.78% to 23.63%. This result takes only charge exchange and the resulting mass loading into account, neglecting the effect of interplanetary magnetic field pile up in the day-side ionosphere of Venus. At times it is clear that such is needed in order to more accurately estimate the amount of charge exchange pick up of O+.

2. Introduction

2.1 PVO Mission

The Pioneer Venus Orbiter (PVO) was launched by NASA on May 20, 1978, and injected into Venus orbit on December 4, 1978. PVO orbited Venus every twenty-four hours until the Fall of 1992, taking measurements with a number of instruments designed to study the planet and its environment (See Figure 2.1.1). Two of the instruments on PVO designed to study plasma properties around Venus were the plasma analyzer (OPA) and the retarding potential analyzer (ORPA). These two instruments were a part of the complement of six in-situ[1] experiments during the mission. The data were made available to us by NASA-Ames Research Center and fills a vital role in the study of the plasma environment of Venus.

Before the arrival of the PVO at Venus on December 4, 1978, no spacecraft had entered that planet's ionosphere to study it as described in Tatrallyay and his coworkers' report (1983):

"The first spacecraft to visit Venus were either flyby, bus, or entry probe vehicles that provided only one or two samples of the bow shock, hence limiting the ability to perform statistical investigations of the physical conditions around the earth's nearest neighbor. . . . in December 1978, the Pioneer Venus orbiter (PVO) was placed into a 24-hour Venus orbit and has been transmitting data almost continually since that time. One of the first studies to be made with the resulting data concerned the location of the Venus bow shock. While the identification of most crossings of the bow shock is straight

---

[1] "In-situ experiments measure quantities at the spacecraft's location, either by ingesting particles into the instruments or by measuring local, non-propagating fields, as opposed to the remote sensing experiments where they measure electromagnetic fields (optical, infrared, ultraviolet. X-ray, and radio) propagating from a reflecting or emitting source on the planet or within its atmosphere." (*Ten Years of Discovery*)

Figure 2.1.1 Diagram of the Pioneer Venus Orbiter spacecraft identifying the main components.
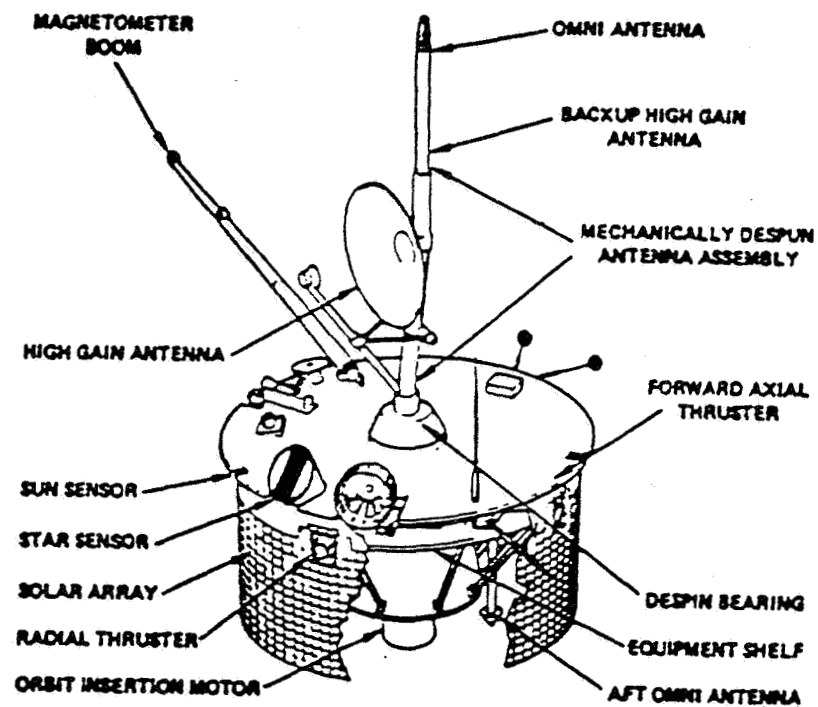
Source: Colin (1989)

forward in almost any of the plasma and field measurements, the subject of the location of the bow shock has been one of the most controversial topics of Venus studies because, in part, the location of the bow shock is sensitive to the physics of the interaction, and the physics of that interaction is at best poorly understood."

Numerous studies have been completed since the time PVO started receiving data on the near environment of Venus beginning near the end of 1978. Some of these studies involve the vigorous modeling of various characteristics of the bow shock. Our research follows and, at the same time, makes an attempt to expand these earlier investigators' works on the Venus' bow shock formation. We utilize the electron component of the PVO ORPA data, which has not been reported up to this point.

2.2 Bow Shock Formation

A bow shock is a paraboloid-shaped shockwave that forms around the planet as the solar wind interacts with the planet (See Figure 2.2.1). The process of planetary bow shock formation is similar to that which forms when a supersonic airplane passes through the upper atmosphere at speeds greater than that of sound. This interaction between the aircraft and the air produces a shock that is caused by the phenomena called steepening. Steepening occurs because the passage of either a fast or slow wave alters the previously undisturbed air condition and thus allows the trailing wave to travel faster and catch up with the first wave.

The shock formation from the aircraft-air interaction faces much more simplified physical phenomena compared to what takes place when the bow shock forms from the solar wind-planet

Figure 2.2.1 Bow Shock Formation — Sketch of the principal regions of the terrestrial magnetosphere and its connections to the solar wind magnetic field (not in scale).
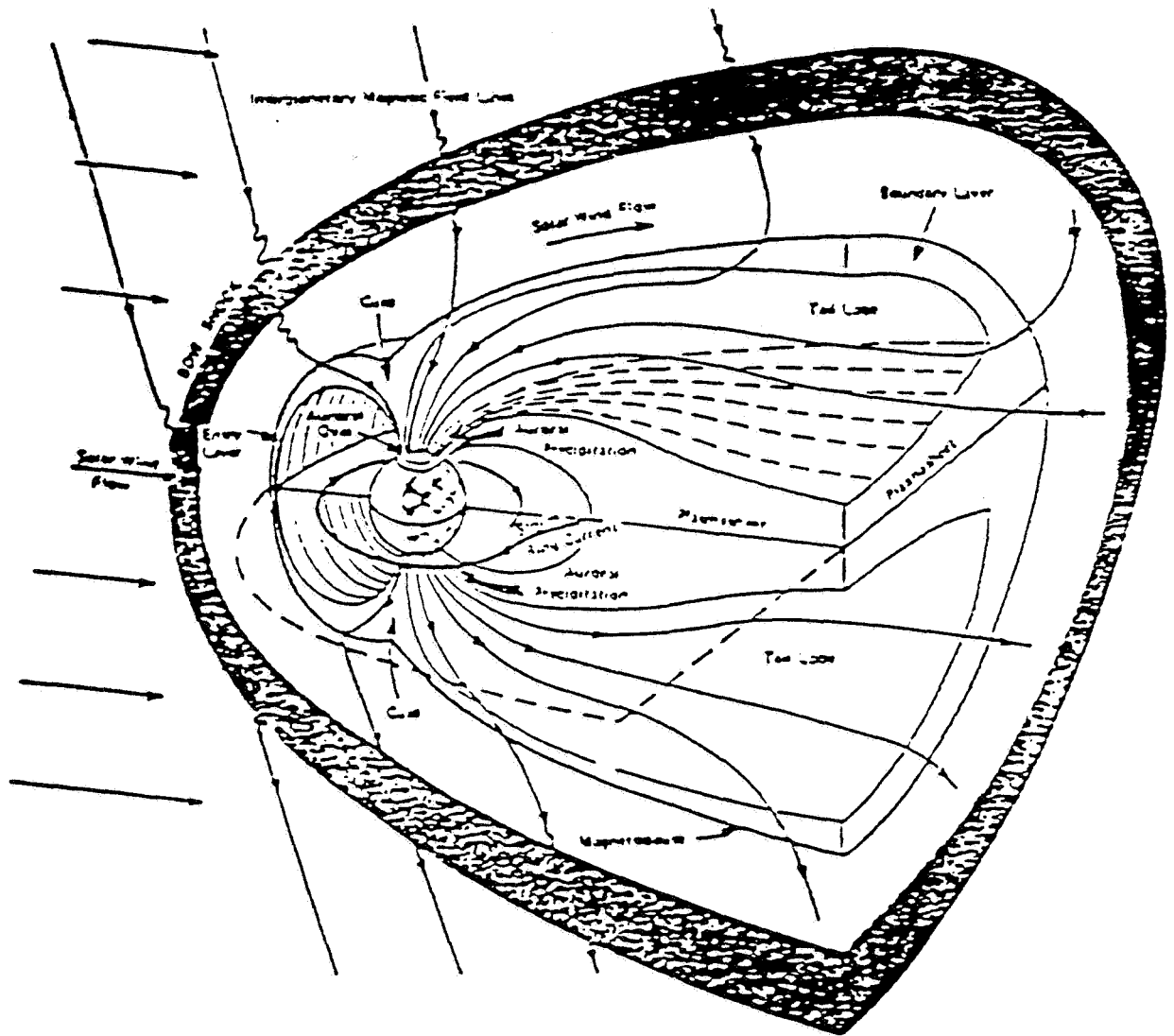
Source: Lui (1987)

interaction. The latter case must deal with magneto hydrodymanic (MHD[2]) effects which include the interplanetary magnetic field influences, and the complex plasma behavior of the solar wind. However, the basic shock formation process from the solar wind-planet interaction still shares the similar effects also faced by the aircraft-air interaction. When the solar wind traveling through space reaches the planet, it compresses both the planet's plasma and the planet's magnetic field. As the various waves of solar wind arrive at the planet, they appear to have similar effects as the steepening, if the amplitude of those waves are sufficient. A bow shock wave may be described as a thin discontinuity where the normal solar wind wave conditions are altered causing irreversible changes in the plasma. Such a discontinuance occurs at the bow shock where the plasma parameters show abrupt changes.

We can locate the position of the interplanetary bow shock and study its characteristics by measuring the change of solar wind plasma[3] parameters, such as density, temperature and pressure. Shifts in these parameters take place during any kind of shock formations. For example, the bow shock formation from the aircraft-air interaction is detected by the human ear drum since the abrupt pressure change before and after the bow shock is large enough for the ear drum to sense. However, for the MHD dependent parameters, such as magnetic field, the discontinuance is observed only in the case of bow shock formation within the interplanetary medium.

---

[2] MHD requires use of physical laws, such as Maxwell equations, Ohm's law, and the conservation of mass and momentum, to describe the characteristics of the fluid plasma -- Plasmas in the solar system often find themselves in unstable situations in which the MHD equations would predict a rapid change of configuration.

[3] Plasma is gas of charged particles in which the potential energy of a particle due to its nearest neighbor is much smaller than its kinetic energy

3. Background

3.1 Venus-Earth Comparison

Venus has been described as the earth's twin because of its numerous similar characteristics to the earth. Some of the characteristics include its mass (0.81 earth masses), radius (0.95 earth radii), mean density (95% that of earth), and gravity (90% that of earth). However, in terms of atmospheric structure and chemical composition, "Venus is anything but a twin of earth" (Levine 1992). Some of the notable atmospheric structural differences are: the mean planetary surface temperature of Venus being 750°K, compared to about 300 °K for earth; and the surface pressure on Venus being about 90 atm, while it is 1 atm for earth. Also, the most apparent atmospheric chemical composition difference is that ". . .carbon dioxide at 96 % by volume, is the overwhelming constituent in the atmosphere of Venus, while it is only a trace constituent in the earth's atmosphere (0.034% by volume)" (Levine 1992).

The most important difference between the two planets for our study lies in the characteristics of their planetary magnetic fields. Earth's magnetic field is strong enough to stand off the solar wind pressure at about 10 earth radii. Since there is no intervention between the solar wind and the terrestrial atmosphere, the interaction is very "clean." On the other hand, there is zero or undetectably small planetary magnetic field for the case of Venus, so that the solar wind can interact directly with the Venus atmosphere and ionosphere (Tatrallyay 1983). This contrasting magnetic nature between these two planets, which are similar in many other ways, urges us to perform a comparison study to further our understanding of the physics of plasma behavior.

3.2 Solar Wind Interaction with Venus

As discussed previously, the bow shock formation in the interplanetary medium differs greatly from the case in the earth's atmosphere. The two cases share the similarity only in the context of the pressure jump occurring due to the density increase and temperature increase (p = nkT) at the obstacle interaction point. The formation of the bow shock of Venus involves considerably greater complexities, resulting from the fact that the solar wind is collisionless[4] and is permeated by a magnetic field.
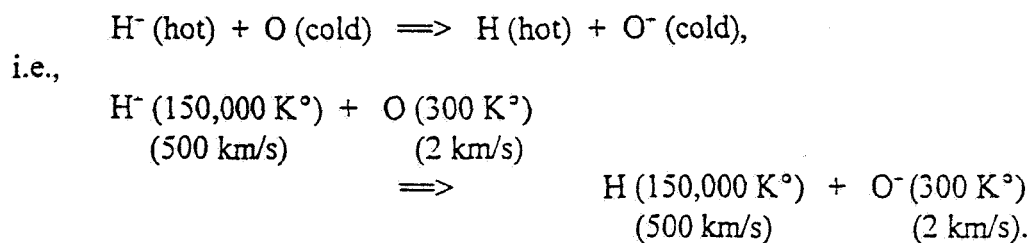
The solar wind is a fully ionized plasma that flows continuously outward from the solar corona, dragging the "frozen-in" remnant of the solar magnetic field through the solar system. Solar wind plasma is composed almost entirely of electrons and protons, with small numbers (few percent) of He^-. As a result of the strong outward pressure in the solar corona, the solar wind becomes supersonic at a few solar radii (1 solar radius = 6.97×10^5 km) above the visible surface of the Sun (the photosphere). It attains speeds in the range 250 - 750 km/s in interplanetary space and is believed to remain supersonic out to a distance from the Sun of 50-100 astronomical units (AU). Although the solar wind eventually loses its high speed as it encounters the interstellar gas and magnetic field, the relatively collisionless space in which they travel through (only 2-3 collisions between sun and earth orbit) allows them to retain their high speed for a long time (Levine 1992).

Due to the absence of a planetary magnetic field in the space around Venus, the solar

---

[4] Although interplanetary space is generally perceived as a vacuum, it contains continuously changing low density plasma. Also, the solar wind is so tenuous that collisions between the charged particles of the plasma occur only several times on average during the entire travel from the sun to earth orbit (distance of 1.5×10^8 km). Hence, the plasma is termed collisionless.

wind is able to interact directly with the upper atmosphere of the planet. When the supersonic

solar wind interacts with the upper atmosphere of Venus, it produces a number of complex

surfaces in this region such as a bow shock, an ionosheath, and an ionopause (Figure 3.2.1). As

the solar wind approaches the Venus ionosphere, neutral particles from the planet move upstream

and become subject to the interaction with the solar wind ionized particles. This interaction

between solar wind plasma and outflowing neutral oxygen atoms from Venus results in the

conversion of the latter into oxygen ions through charge exchange, which are then picked up by

the solar wind. (The pick up results from any events that can cause the ionization of the particles

in the solar wind.) Charge exchange and ionization by ultraviolet radiation from the sun are the

two major sources of the ionization and subsequent pick up of O^- during the solar wind-Venus

interaction.

Specifically, as the high speed hydrogen ions in the solar wind approach the ionosphere

of the planet, they encounter the neutral oxygen atoms from the planet that are moving upstream.

As the hydrogen ion and the neutral atoms collide with each other, charge exchange occurs as

follows:

$$H^- \text{(hot)} + O \text{(cold)} \implies H \text{(hot)} + O^- \text{(cold)},$$

i.e.,

$$H^- (150,000 \text{ K}°) + O (300 \text{ K}°)$$
$$(500 \text{ km/s}) \qquad (2 \text{ km/s})$$
$$\implies \qquad H (150,000 \text{ K}°) + O^- (300 \text{ K}°)$$
$$(500 \text{ km/s}) \qquad (2 \text{ km/s}).$$

Each O^- formed takes the place of an H^-, or a proton, of the solar wind and gets picked up

(dragged along) by the motional electric field ($E = -v \times B$) produced by the moving solar wind.

This reaction is significant because the neutral oxygen atom that is flowing away from Venus at

Figure 3.2.1 Diagram of Bow Shock. Ionosheath and Ionopause
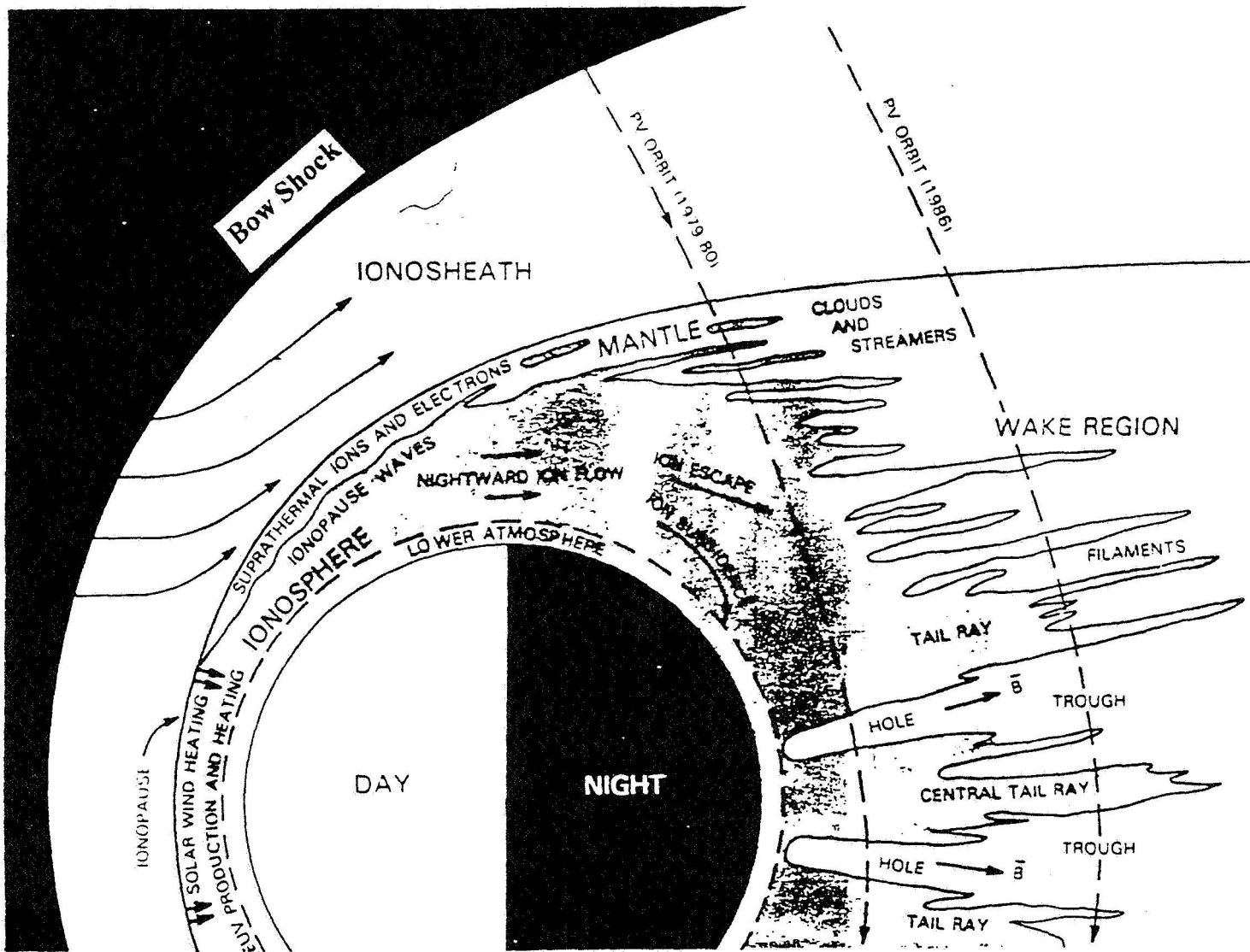
Source: Colin (1989)

only several kilometers per second is brought up to several hundred times the original speed when ionized. Because the ionized oxygen weighs sixteen times more than the ionized hydrogen, conservation of momentum causes the slow-down of the solar wind.

As noted above, another ionization source is the solar ultraviolet radiation. If the neutral oxygen atom is in the solar UV long enough, it becomes ionized by means of the reaction:

$$O + h\nu ==> O^+ + e^-.$$

Both the ionized oxygen and the electron are picked up by the solar wind flow since they are now subject to the magnetic field induced by the solar wind. The slow down process of the solar wind due to the UV radiation is the same as with the charge exchange effect. However, it is considered much less significant than that of the charge exchange because the ionization time by this mechanism is too long for the Venus case.

The solar wind slows as it approaches the upper ionosphere of the planet. This slow down of the solar wind is caused by the phenomenon called *mass loading*. The concept of mass loading is similar to that of the traffic congestion. As more vehicles come into the highway, they all have to slow down. Unaware of the solar wind slow down taking place at the upper ionosphere of the planet, the in-coming solar wind continues to send its plasma into the area, creating the congestion of particles at the interaction point. If the rate of mass loading of the solar wind is great enough, it can lead to the formation of a bow shock. This forefront section of the mass loading field is the bow shock. At the bow shock, the plasma parameters of the solar wind change abruptly. The solar wind velocity drops behind the bow shock because a large part of the plasma gets thermalized. As a result, the 400 km/sec purely rectilinear velocity (outward

from sun) becomes randomized. This shows up as a much higher plasma temperature behind the shock (of the order of a million degrees or so). Since the particle congestion takes place, the density of solar wind should also be greater. The increase in both the density and the temperature in the formation of the shock occur under adiabatic conditions. Consequently, more active interactions among particles arise, thus resulting also in a higher temperature, and therefore a higher pressure.

4. Methodology and Analysis

4.1 Observation of the Bow Shock from the ORPA Data

4.1.1 ORPA-OPA Data Correlation

The measuring instrument on PVO designed primarily to study the upstream solar wind, the Orbiter Plasma Analyzer (OPA), was sampled so infrequently that the measurements closer to the planet were not taken often enough to adequately study the bow shock. In addition, the OPA solar wind ion temperature and electron density measurements, which would be necessary for a complete study of the bow shock, are not reliable. Another instrument, the retarding potential analyzer (ORPA), was designed to take measurements of the ionosphere, including the densities and temperatures of ions, thermal electrons and supra thermal (high energy) electrons. Because this instrument was designed to measure near the planet, the measurements were taken much more frequently than those taken by the OPA instrument. The time resolution of the ORPA data is high and the electron data is reliable. However, it was not clear how the ORPA supra thermal electron data related to solar wind electrons.

In the fall of 1993, another BYU undergraduate physics student, Dawn Gifford, completed a study which indicates that the tracking of the ORPA and OPA density data is quite good most of the time if certain simple spacecraft voltage constraints are satisfied as shown in Figure 4.1.1.1. As a result, because of the higher sampling rate of the ORPA compared to that of the OPA (comparison shown on Figure 4.1.1.2), the former will allow a reasonably precise study of the location and nature of the bow shock that forms upstream of Venus in terms of the upstream and shocked solar wind electrons. Hence, upon carefully examining her study

Figure 4.1.1.1

OPA Proton Density vs. ORPA Suprathermal Electron Density (#/cm³).
Straight line shows best linear curve fit. OPA data with less than four samples per
average and data taken below 2700 km., ORPA data with potential less than three,
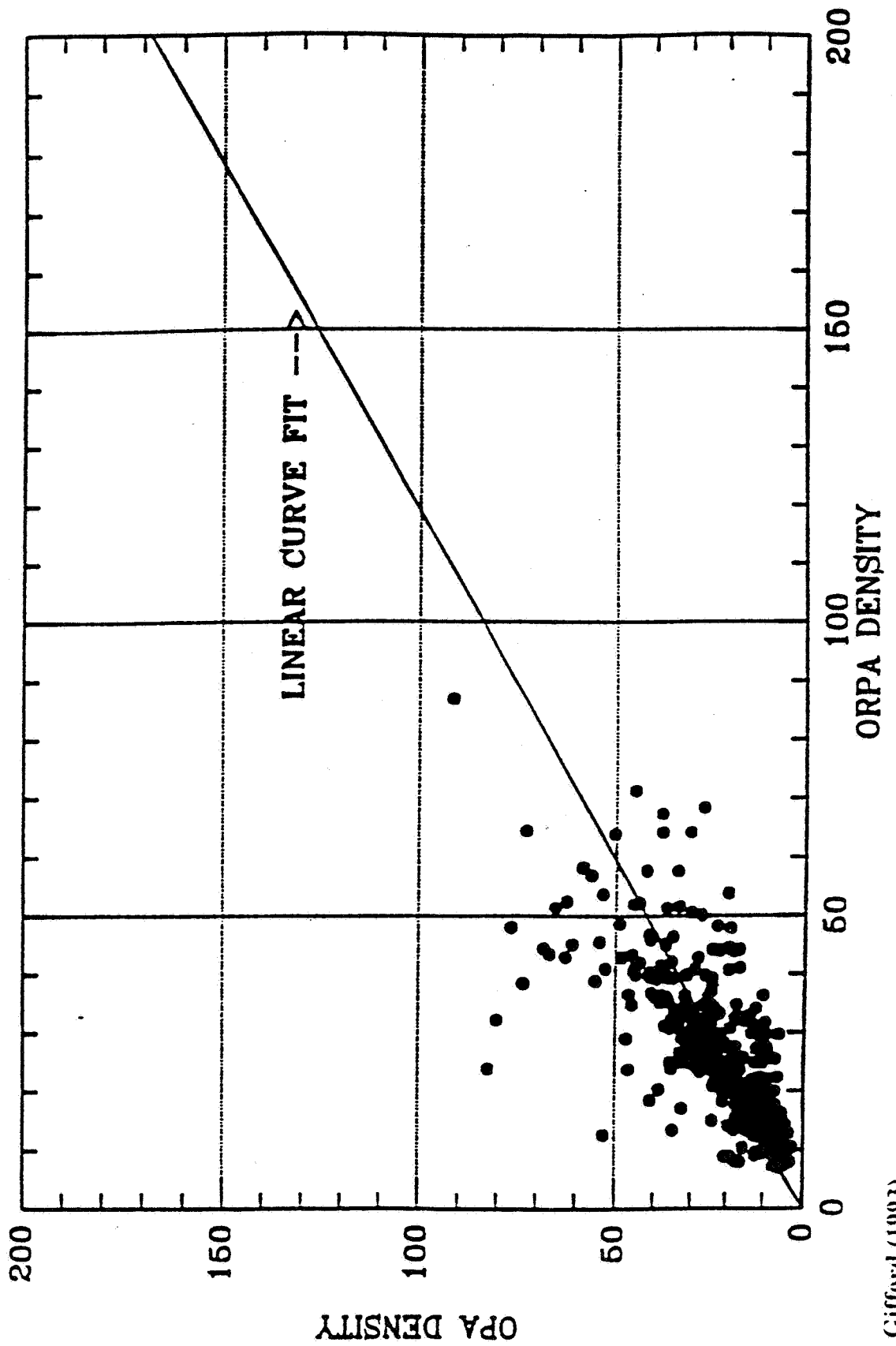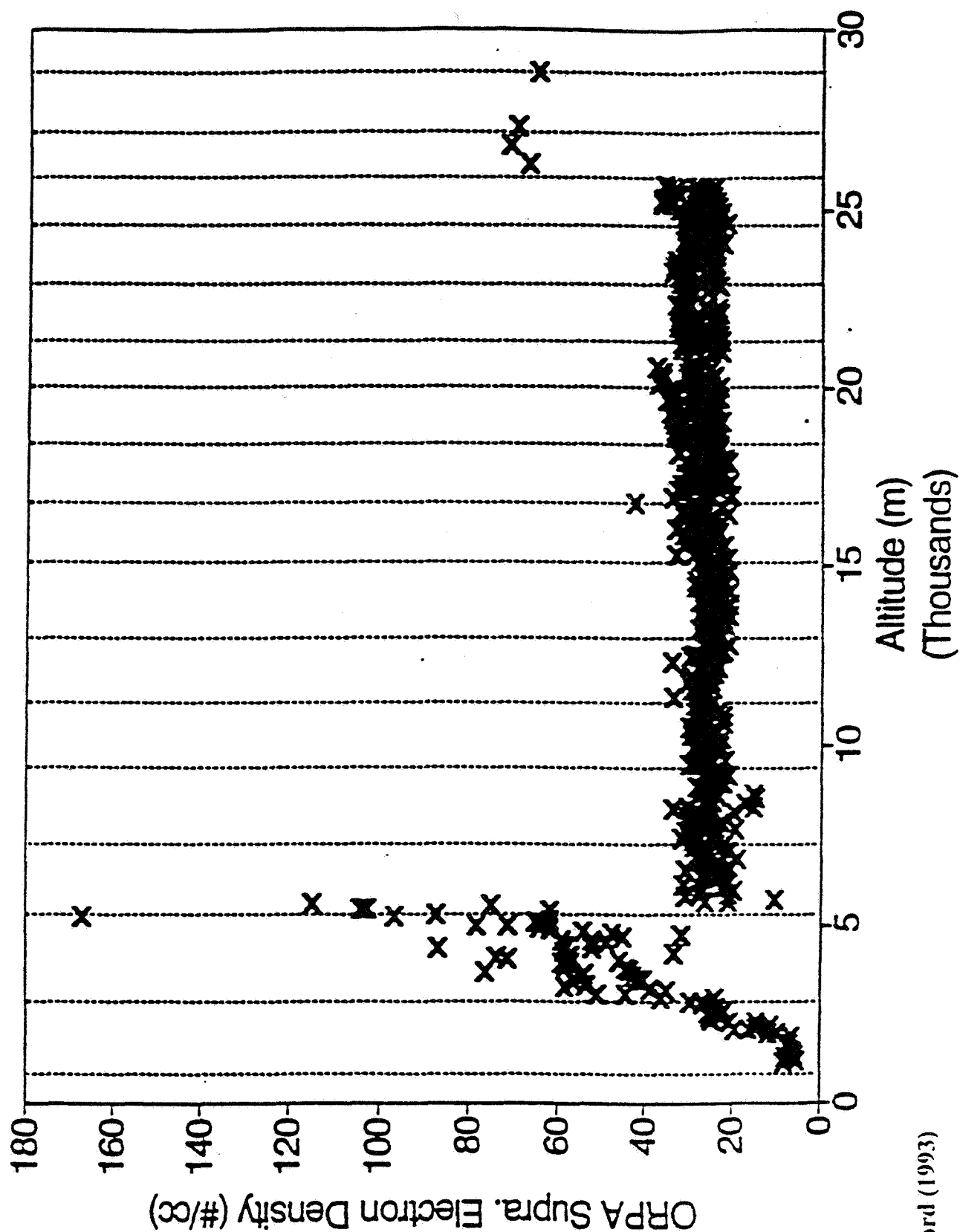and ORPA data in orbits 13,14, and 25 are excluded.

Figure 4.1.1.2

Bow Shock Crossing Orbit 78 Inbound
Dotted lines show approximate OPA eight-minute intervals.

ORPA Supra. Electron Density (#/cc)

Altitude (m)
(Thousands)

of the OPA-ORPA data compatibility, we find it feasible to employ the ORPA data for our analysis of the bow shock. We will utilize the data available to us from the PVO mission. The computing programs, developed by the principle investigator of the OPA and ORPA instrument, have been employed to process the raw information from the PVO into supra thermal electron densities and temperatures. Additional computer programs have been developed to utilize only the supra thermal electron data for which the spacecraft potential constraints determined by Gifford (1993) have been satisfied.

4.1.2 Plot ORPA Plasma Parameter Data

Approximately 825 orbits of the ORPA density, temperature and pressure data have been plotted against the altitude of the spacecraft in each of the PVO orbits of Venus. By examining these plots, we have been able to closely study the nature of the Venus bow shock using the electron component of the solar wind as measured by the ORPA instrument.
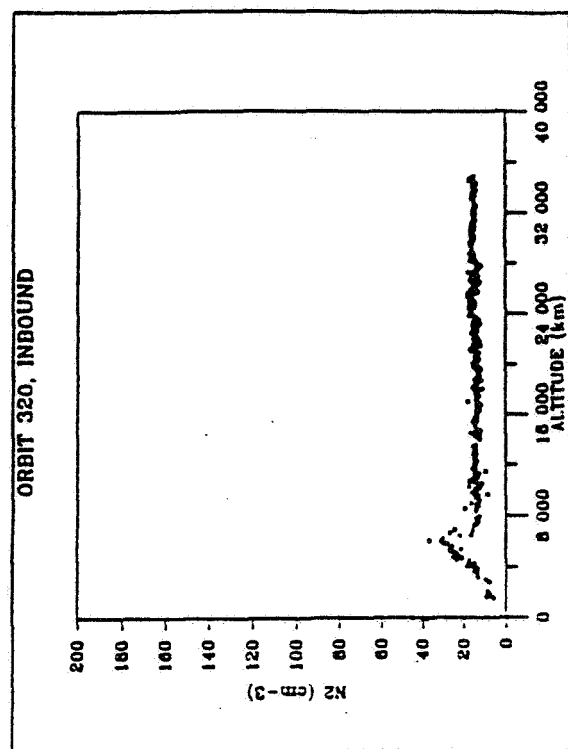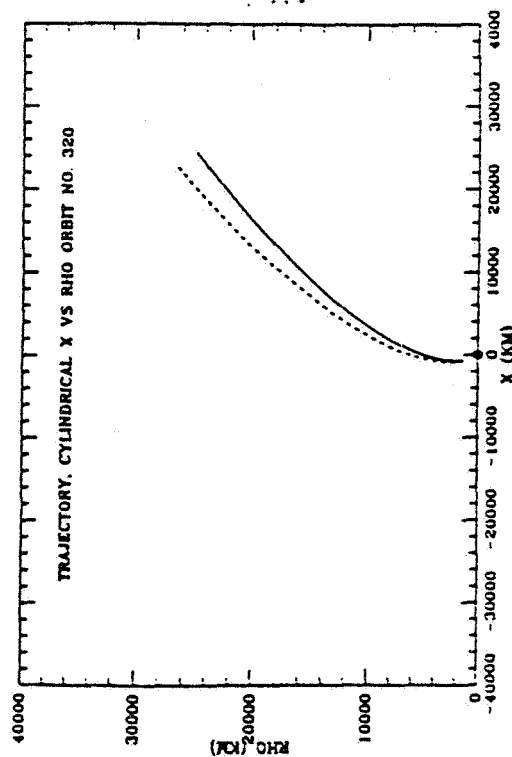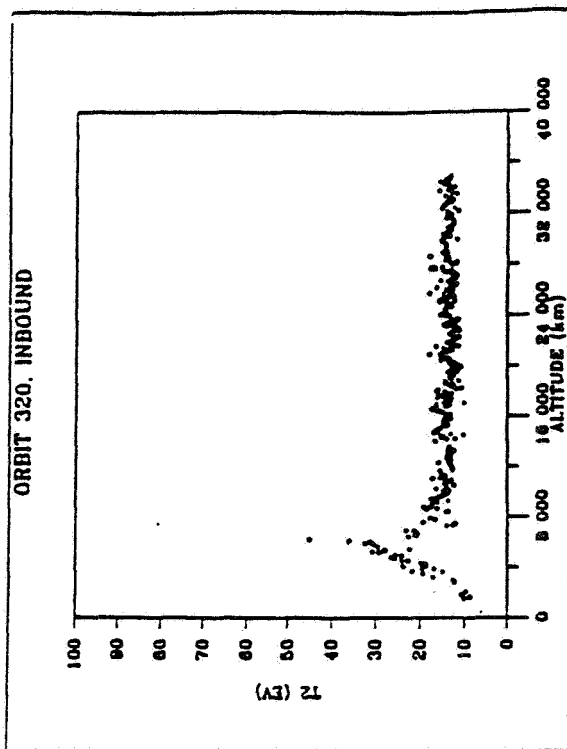
The Figures 4.1.2.1 - 4.1.2.4 shows the abrupt shock jumps in all of the three plasma parameters -- density, temperature and pressure -- as the spacecraft crosses the bow shock. The spacecraft passes through the bow shock twice in one orbit interval: at both the inbound and outbound portions of each trajectories near the planet (Figure 4.1.2.5). In both portions of the trajectory, all of the three solar wind plasma parameters generally remained steady at a certain value when the spacecraft was at a high altitude. The high altitude data suggests that the measurement has been taken outside the range where the solar wind-planetary ionosphere interaction takes place. As the spacecraft altitude decreases, we see the sudden jump in the plasma parameter values. We observed the bow shock formation from these jumps which

indicated the instant increase of each of the parameters. After the parameter values reach their maximum, the values gradually decrease back to, and occasionally becomes lower than, the initial values. This shows that the plasma contents beyond the bow shock have less direct contacts with the solar wind as the altitude continues to decrease toward the surface of the Venus. At such low altitude, relative to the bow shock location, many of the solar wind ions must have already deflected away toward the night-side of the Venus ionosphere or have become absorbed and neutralized in the upper atmosphere.

Most of the plots from the 825 orbits showed a similar result, i.e. the plot showed the abrupt jump of the parameter values. The inbound plot showed such a jump after a steady initial high altitude value and the outbound showed the jump first and the steady high altitude value afterward (See Figure 4.1.2.1). However, there were some abnormal cases as shown in Figures 4.1.2.2 - 4.1.2.4. Figure 4.1.2.2 shows the unusual scattering of the parameter values after entering the bow shock. The shock shown in Figure 4.1.2.3 is so small that it is almost non-measurable. Furthermore, some of the shock jumps were unrealistically high as seen in Figure 4.1.2.4. We suspect that the reason behind these abnormal cases are related to the considerable complexity of the solar wind-ionosphere interaction. Other important factor that must be considered include the direction and magnitude of the interplanetary magnetic field, the varying solar activity, and the direction of the ORPA instrument's gates for sample collecting relative to the solar wind flow direction. Also the position at which the spacecraft crosses the bow shock relative to the planet-sun direction influences the magnitude of the jump shock (Figure 4.1.2.6). For example, if the measurements are taken at the center of the day-side hemisphere of the planet, the direction in which the interaction between the solar wind and the

Venus ionopause is almost perpendicular. Thus, the interaction there produces a stronger shock than that produced near the terminator.

Figure 4.1.2.1 ORPA Plot of Bow Shock Crossing Orbit 320 Inbound

ORBIT 320, INBOUND

T2 (EV)

ALTITUDE (km)

ORBIT 320, INBOUND

N2 (CM-3)

ALTITUDE (km)

ORBIT 320, INBOUND

P2, dynes/cm2 x e10

ALTITUDE (km)

TRAJECTORY, CYLINDRICAL X VS RHO ORBIT NO. 320

X (KM)

RHO (KM)
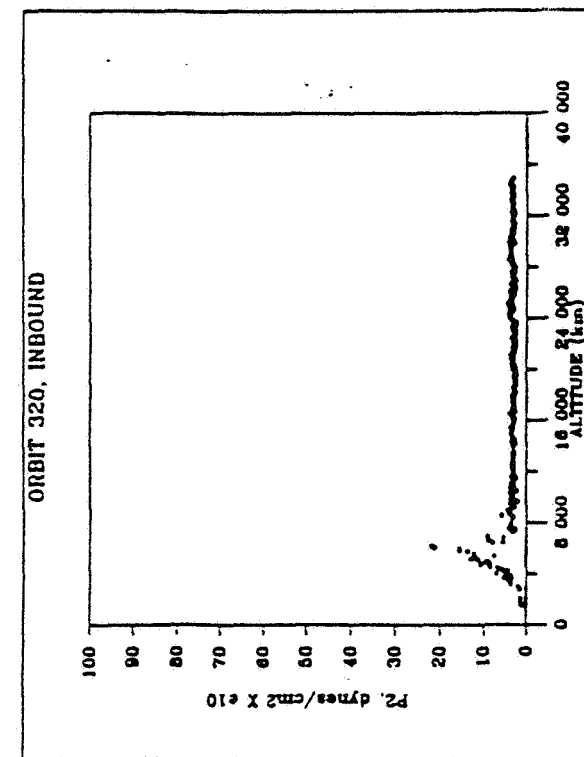
* Dashed line indicates the Inbound.
  Solid line indicates the Outbound.
** Coordinate system fixed to Venus.

Figure 4.1.2.2 ORPA Plot of Bow Shock Crossing Orbit 355 Inbound
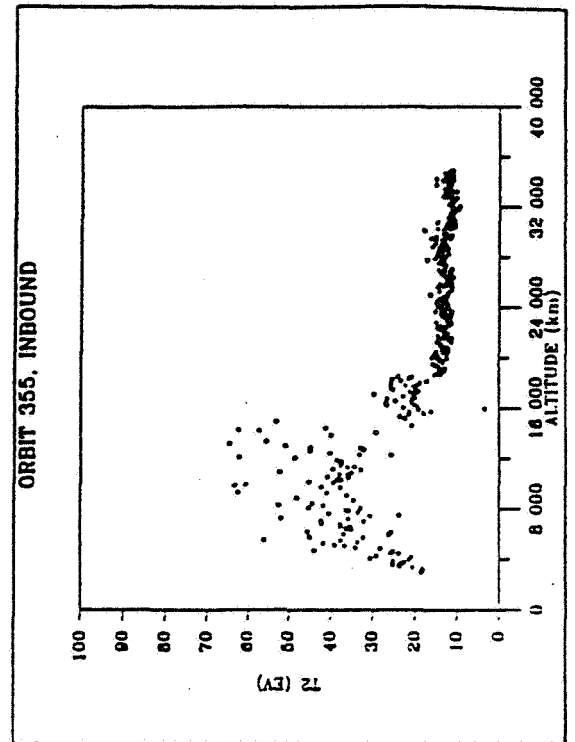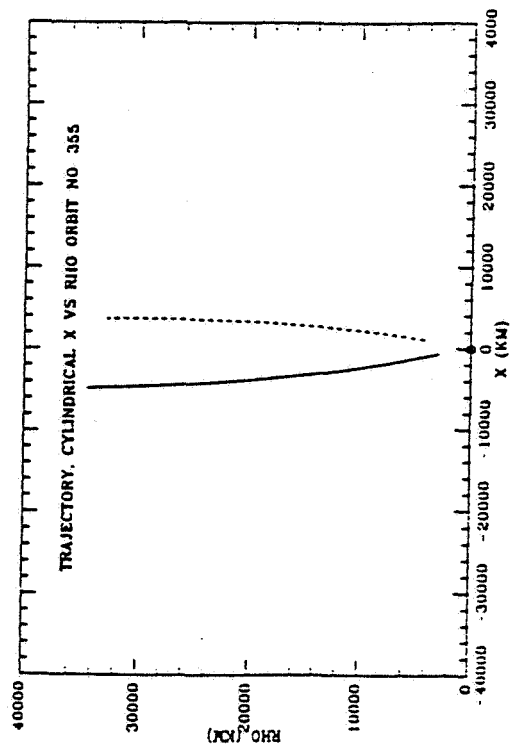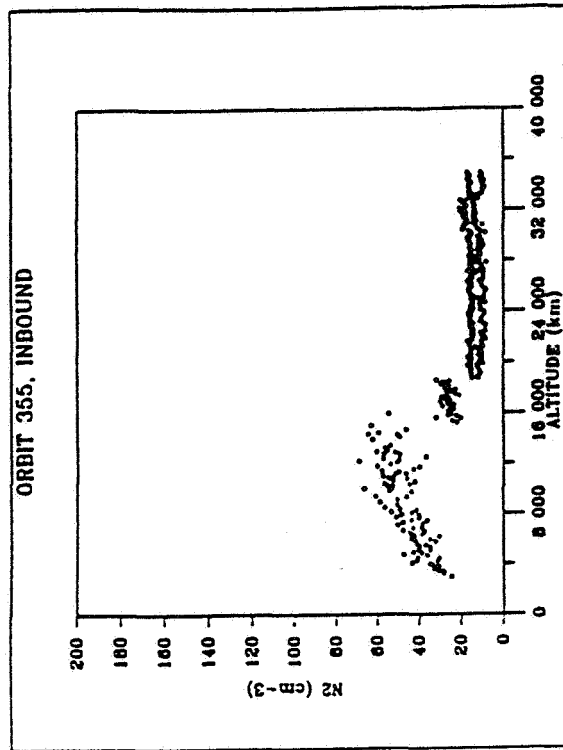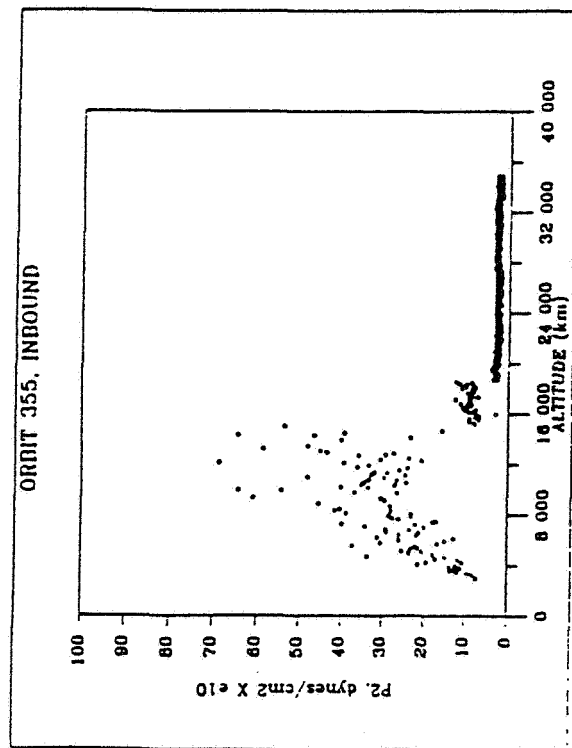
Figure 4.1.2.3   ORPA Plot of Bow Shock Crossing Orbit 365 Inbound
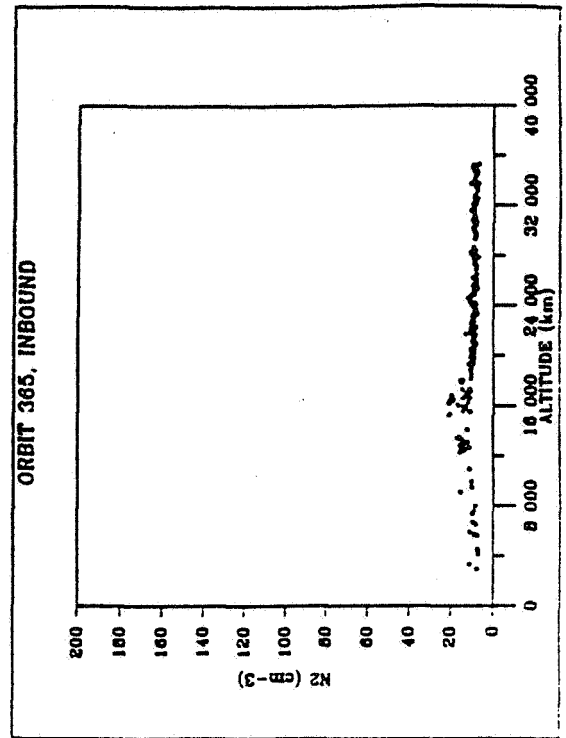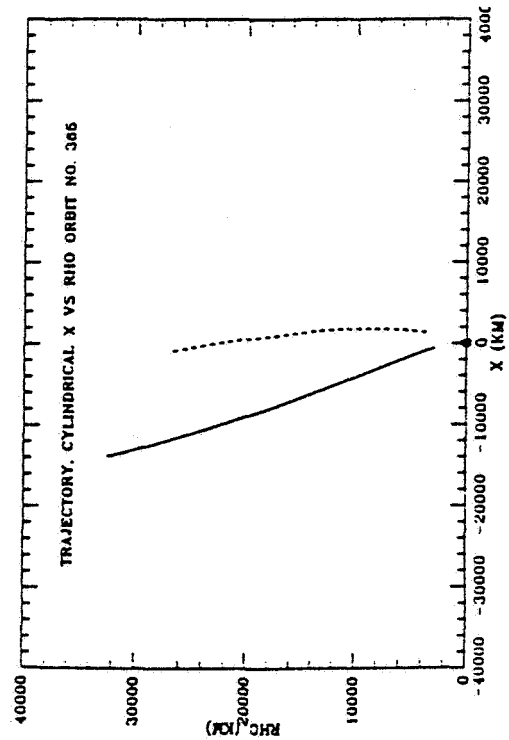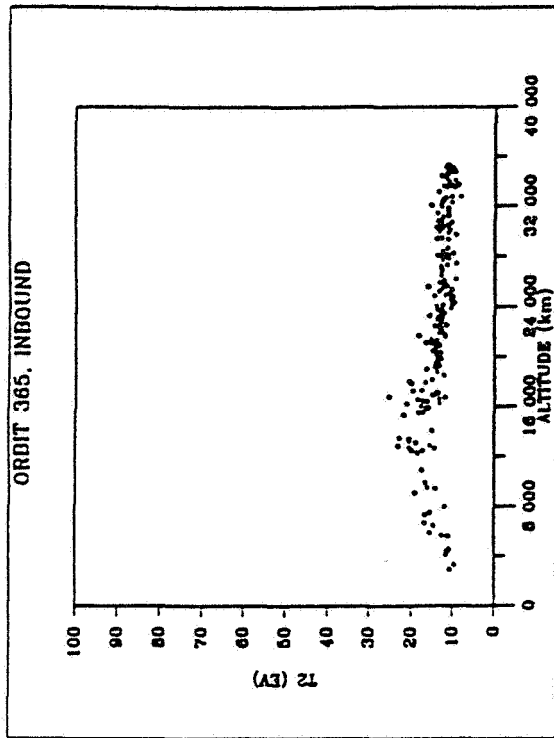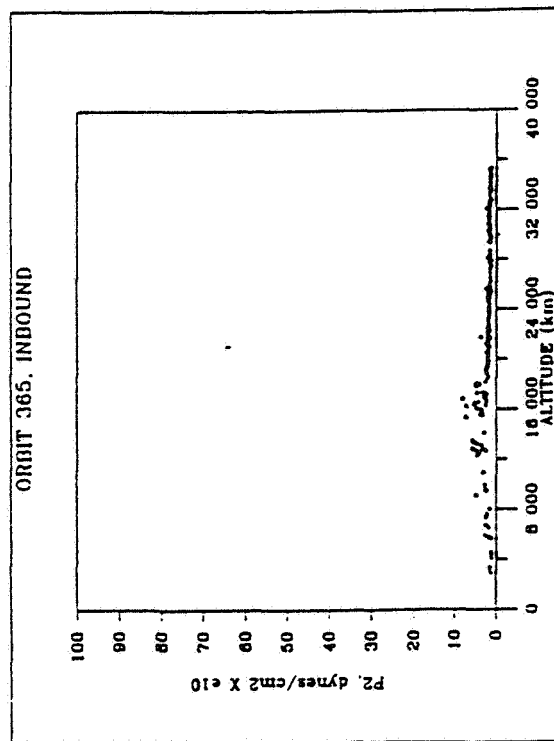
Figure 4.1.2.4 ORPA Plot of Bow Shock Crossing Orbit 334 Inbound
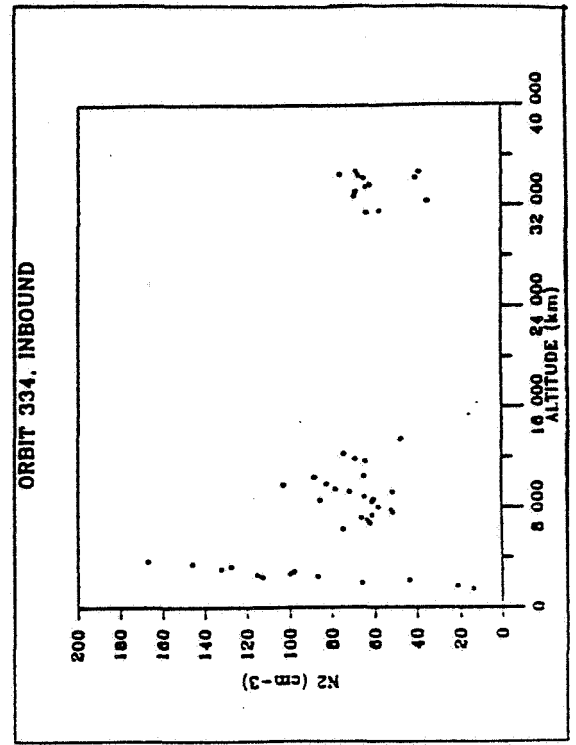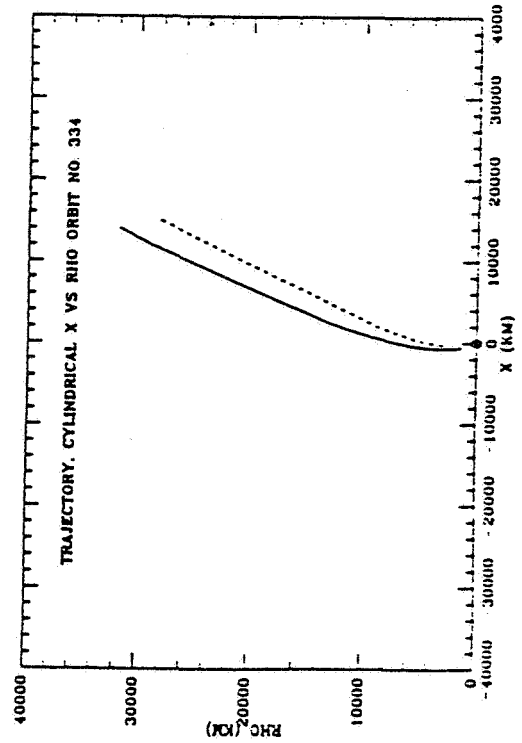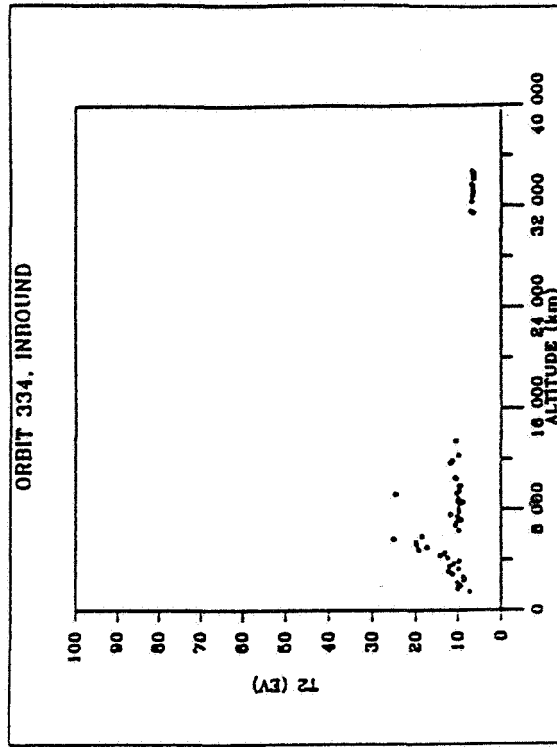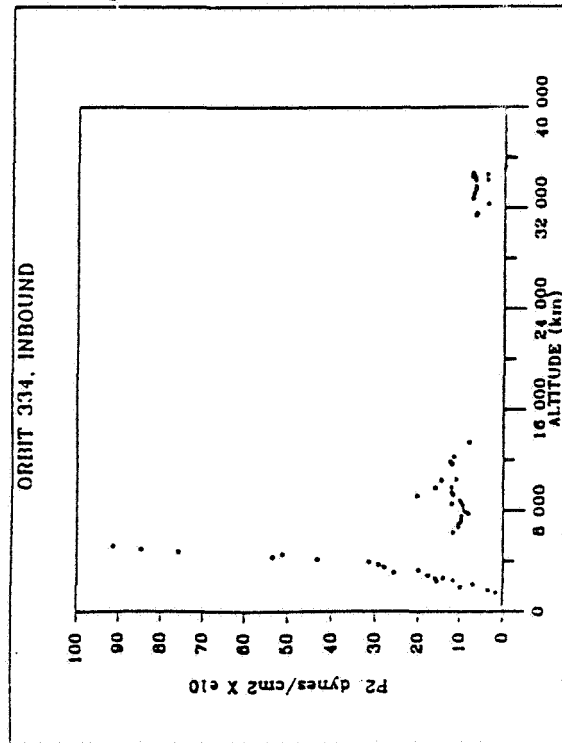
Figure 4.1.2.5   The Orbit of PVO as viewed perpendicular to the orbit plane. Periapsis — solid dot, apoapsis — solid square. X's are at 1 hour intervals before and after periapsis. The arrow denotes the direction of spacecraft.
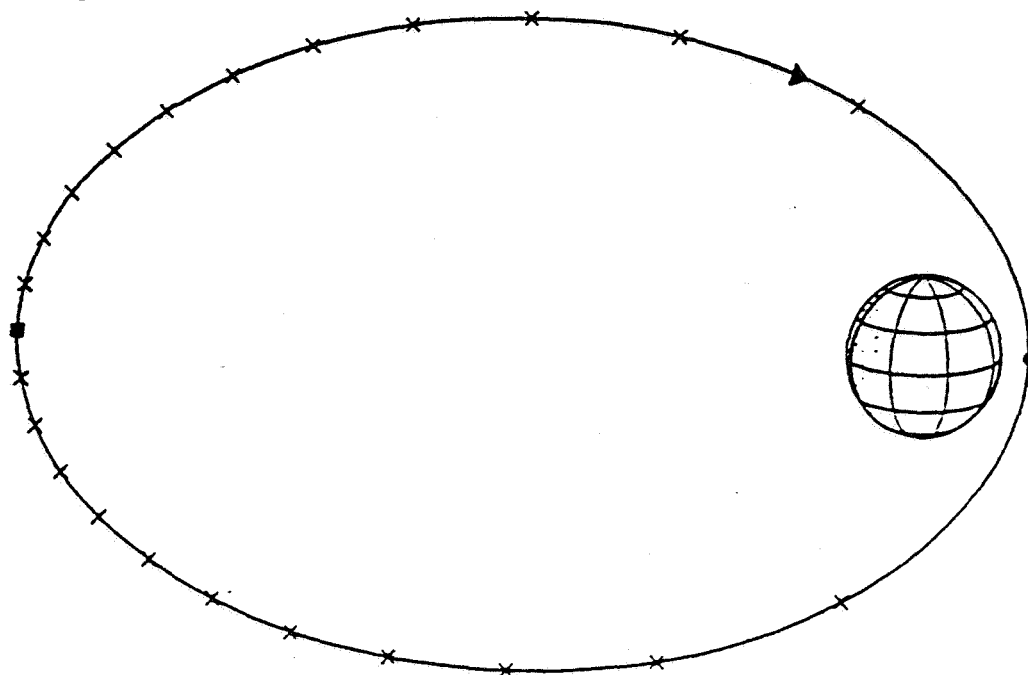
The orbit of PVO as viewed from over the north pole of Venus to show the latitude covered by the near polar inclination of 74.4 degrees.
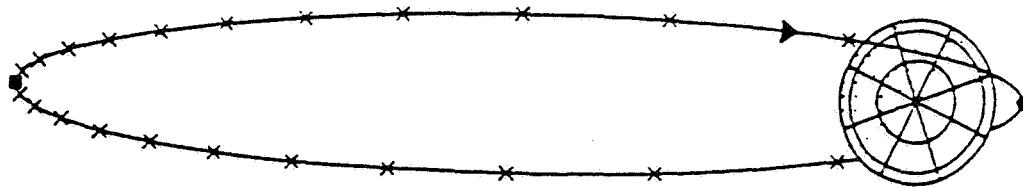
DENOTES DARK SIDE

Source: Colin (1989)

Figure 4.1.2.6 Diagram of the Solar Wind-Venus Interaction

Shows:
- Position of the Spacecraft Crossing of Bow Shock Relative to the Planet-Sun Direction
- Magnetic Field Pile Up on the Day-Side Hemisphere of Venus
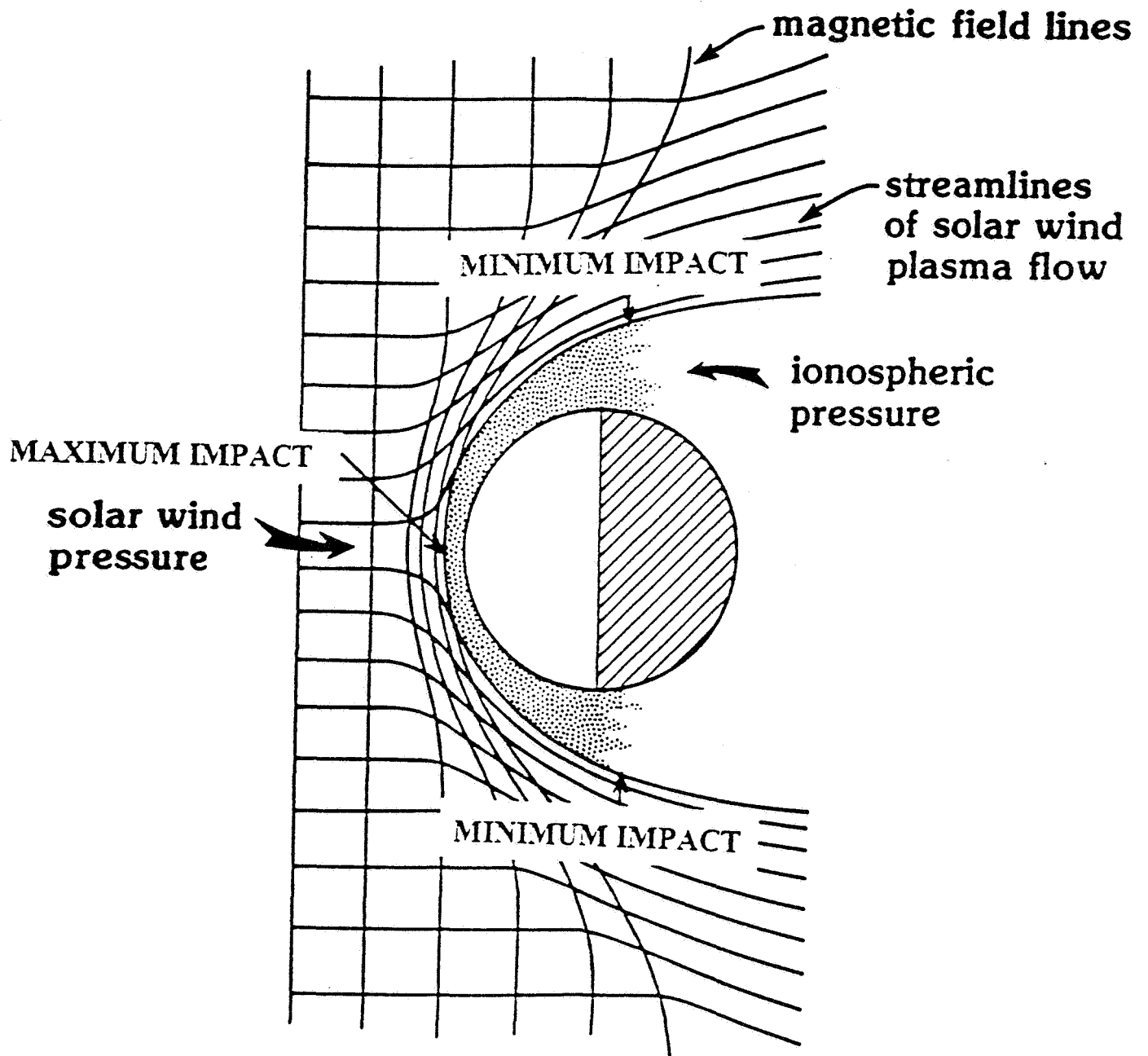
Source: Colin (1989)

4.2 M_{spr} vs M_{def} Comparison

4.2.1 Spreiter Model

Spreiter and his coworkers have derived a model to describe the gas dynamics of the bow

shock formation (1966). They developed a mathematical expression that relates the plasma and

field parameters on either side of the bow shock. This expression has been derived under the

assumption that the magnetic field induced by the solar wind itself was parallel to the flow, i.e.,

$v /\!/ B$. Although this parallel flow condition does not always hold to be true, this assumption

simplifies the mathematical derivation allowing Spreiter and his coworkers to apply their gas

dynamic model to the solar wind-planet interaction.

Their findings were that the ratio of free streaming density, ρ_∞, to the density just behind

the bow shock, ρ_b, could be expressed as:

$$\rho_\infty/\rho_\beta = [(\gamma - 1) M_\infty{}^2 + 2] / [(\gamma + 1) M_\infty{}^2] \qquad (\gamma = \text{ratio of specific heats;}$$
$$M_\infty = \text{upstream Mach number })$$

A similar one has been developed for the corresponding temperatures. They have developed

these gas dynamic equations, initially, by applying them to the case of the solar wind-earth

interaction. The solar wind interaction with the upper ionosphere of the earth is similar to the

one for the solar wind-Venus interaction, in the extent that the terrestrial obstacle is spherical and

the shock boundary is paraboloidal. However, as stated previously, the earth has a strong

magnetic field that shields the terrestrial ionosphere/atmosphere from the solar wind. Combining

this solar wind shield-off together with the assumption of parallel flow, they assume no entrance

of the magnetic field into the picture. (Since the case of relative movement we have $E = - v \times B$,

if the solar wind velocity and the interplanetary magnetic field are parallel, then the $E = - v \times B$

will be **0**, allowing neglect of electromagnetic influence to be justifiable.) This absence of magnetic field influence partially justifies their use of only fluid equations. (i.e. use of only hydrodynamic equations instead of magnetohydrodynamic equations, which would be more appropriate to describe our system which involves the magnetic-field influence.)

This model contains another simplification; namely, the assumption of a collision-dominated medium to be the interacting medium of the solar wind.. Unless modified appropriately, this assumption is not wholly applicable to our study which examines the nature of the solar wind, which is a collisionless plasma. This assumption on the nature of medium along with the assumption on neglect of no magnetic field force, the Spreiter model should be incomplete when applied to the Venus-solar wind interaction. In order for the Spreiter model to describe the solar wind interaction with a planetary obstacle like Venus more fully, a modification is needed that allows for the effects due to a collisionless plasma and mass loading. Nevertheless, the Spreiter model seems to work to a degree. Thus, the logical step for us to take then is to test the Spreiter model against the actual value of Mach number (the parameter involved in the Spreiter model) computed on the basis of the measured shock jump. This comparison should give us an idea of what scope of modification is necessary in order for the Spreiter model to become more complete. We suspect that their simplifying assumptions will become critical pivotal factors, when actual data has been compared to the values derived from using their model and we expected this to be the case for the PVO Venus data. Throughout this research, we will assume the atmosphere around Venus to be a monatomic gas. Hence, a value for the ratio of specific heats, $\gamma = 5/3$ is used.

- **Mach Number from the Spreiter Model: M_{spr}**

Mass density, ρ, in the Spreiter model is applicable specifically for a neutral proton-electron gas. Since our ORPA electron data is much more reliable and useful than the OPA proton data, we try to transform the Spreiter model into the form that substitutes the proton mass density with the electron number density. According to Tatraliyay and his coworkers (1992), we can safely make an assumption that the number of helium atoms counted from the PVO data would be negligible due to the overpowering proton abundance (the actual helium contribution might increase the density by 1-10%, which would not significantly influence the results.). The subscripts ∞ and b refer to upstream and downstream components, respectively, of the flow either side of the bow shock. The ratio of the mass density can be written as,

$$\rho_\infty/\rho_b = n_\infty \cdot m_\infty / n_b \cdot m_b = n_\infty / n_b \quad \text{(since mass density, } \rho = n \cdot m \text{ and } m_\infty = m_b,$$
$$\text{the masses cancel out)}$$

resulting in,

$$n_\infty / n_b = [\,(\gamma - 1)\, M_\infty^{\,2} + 2\,] / [\,(\gamma + 1)\, M_\infty^{\,2}\,]$$

We now solve the above equation for M_∞,

$$n_\infty\,(\gamma + 1)\, M_\infty^{\,2} - n_b\,(\gamma - 1)\, M_\infty^{\,2} = 2n_b$$

$$M_\infty^{\,2}[\, n_\infty\,(\gamma + 1)\, - n_b\,(\gamma - 1)\,] = 2n_b$$

$$M_\infty = [\, 2n_b\, / \,[n_\infty\,(\gamma + 1)\, - n_b\,(\gamma - 1)]\,]^{1/2}$$

We will express this Mach number as M_{spr}.

• **Mach Number from the PVO Data:** M_{def}

The standard procedure to calculate the mach number is to use its exact definition: the ratio of velocity of the object to the speed of the sound,

$M_{def} = v_{solar\ wind} / c_{sound}$.

The speed of sound may be obtained as,

$$c_s = (\gamma p / \rho)^{1/2} = [\ \gamma nk(T_e + T_p) / n(m_e + m_p)\ ]^{1/2}$$

$$(\text{pressure: } p = \Sigma nkT = nk(T_e + T_p))$$

Again, using reasonable approximations, we want to transform the equation above in a way that the ORPA electron data is to be employed.

$$\text{Since } m_e << m_p, \quad m_e + m_p = m_p. \qquad (1)$$

Due to the proton temperature variation, we have to be careful when approximating the temperature values. Instead of taking a rough average, we have decided to retain two cases for our temperature values: T_p maximum possible and minimum possible,. By doing so, we will be able to discuss the whole range of pressures at the solar wind. The electron temperature, T_e, in the interplanetary medium typically ranges from 100,000 to 200,000 °K. The proton temperature, T_p, on the other hand, ranges from about 20,000 °K to 200,000, i.e., 0.2 to 1.0 of Te. This information allows us to make a simplifying assumption: at T_e max, $T_e = T_p$ which leads to $T_e + T_p = 2T_e$; at T_e min, $T_e + T_p = 1.2\ T_e$. Therefore, our T_e range used for this study becomes

$$1.2\ T_e \le (T_e + T_p) \le 2\ T_e. \qquad (2)$$

Combining conditions (1) and (2), and canceling n's, we have,

$$c_s = [\ \gamma k(T_e + T_p) / m_p\ ]^{1/2} = [\ 2\gamma kT_e / m_p\ ]^{1/2} (\text{max}) \quad \text{or} \quad [\ 1.2\gamma kT_e / m_p\ ]^{1/2} (\text{min})$$

Putting this expression back into the Mach number equation, we get

$$M_{def} = v_s \left(2\gamma k T_e / m_p \right)^{-1/2} \text{(max)} \quad \text{or} \quad v_s \left(1.2\gamma k T_e / m_p \right)^{-1/2} \text{(min)}.$$

This Mach number is to be obtained from the ORPA data. We will express this Mach number as M_{def}.

4.2.2 Collecting Parameter Values for Comparison

We need the following variable values to perform the comparison of M_{spr} and M_{def}.

M_{def} --- v_s, T_e with constants: (γ, k, m_p)

M_{spr} --- n_b, n_∞ with constants: (γ)

We took the random numbers of data from orbits 1-825. For each of these orbits, there could be two crossings of the bow shock by the spacecraft on the day-side hemisphere of the planet (see Figure 4.1.2.5). First of all, T_e, n_b and n_∞ are obtained from the ORPA electron data. Figure 4.2.2.1 shows the method we used in determining the parameter values from each orbit. T_e and n_∞ are the average values of the horizontal steady line in the ORPA plot of temperature and density before the spacecraft crosses the bow shock. The density, n_b, on the other hand, is the point where the approximate linear curve, fitted against the gradual decline in the parameter intersects the line parallel to the vertical axis that touches the edge of the shock jump. Also, it needs to be noted that we converted the unit of T_e from electron volts in ORPA plot into degrees Kelvin to apply the values into the equation.

$$T \, (^\circ K) = [(1.60 \times 10^{-19} \text{ Joules}) / (1.38 \times 10^{-23} \text{ Joules})][^\circ K/ev] \, T \, (ev).$$

Second, the solar wind velocity data was obtained from the OPA data. (Although the proton density data from OPA is considered somewhat unreliable and temperature data not at all useful, its velocity data is safe.) As seen from the Figure 4.2.2.2, the solar wind velocity is a

Figure 4.2.2.1   Measurement of n_s, n_b and T_s from the ORPA Plot of Bow Shock Crossing Orbit 320 Inbound

ORBIT 320. INBOUND

ORBIT 320. INBOUND
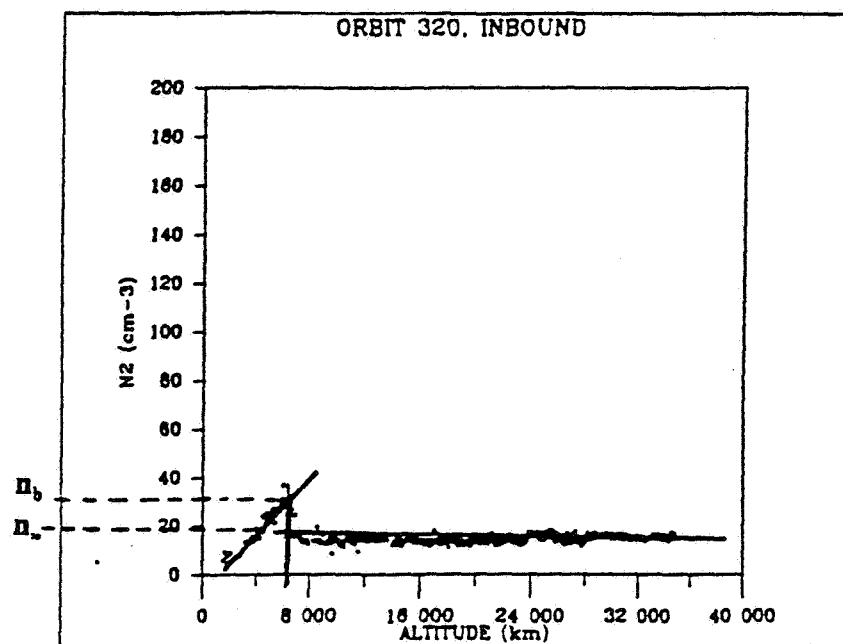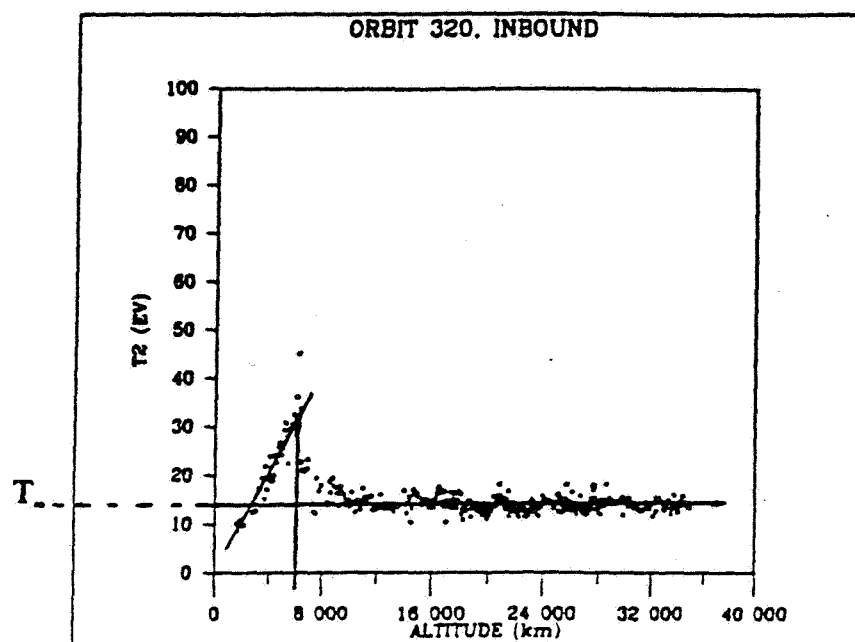
Figure 4.2.2.2   OPA Plot of Proton Velocity
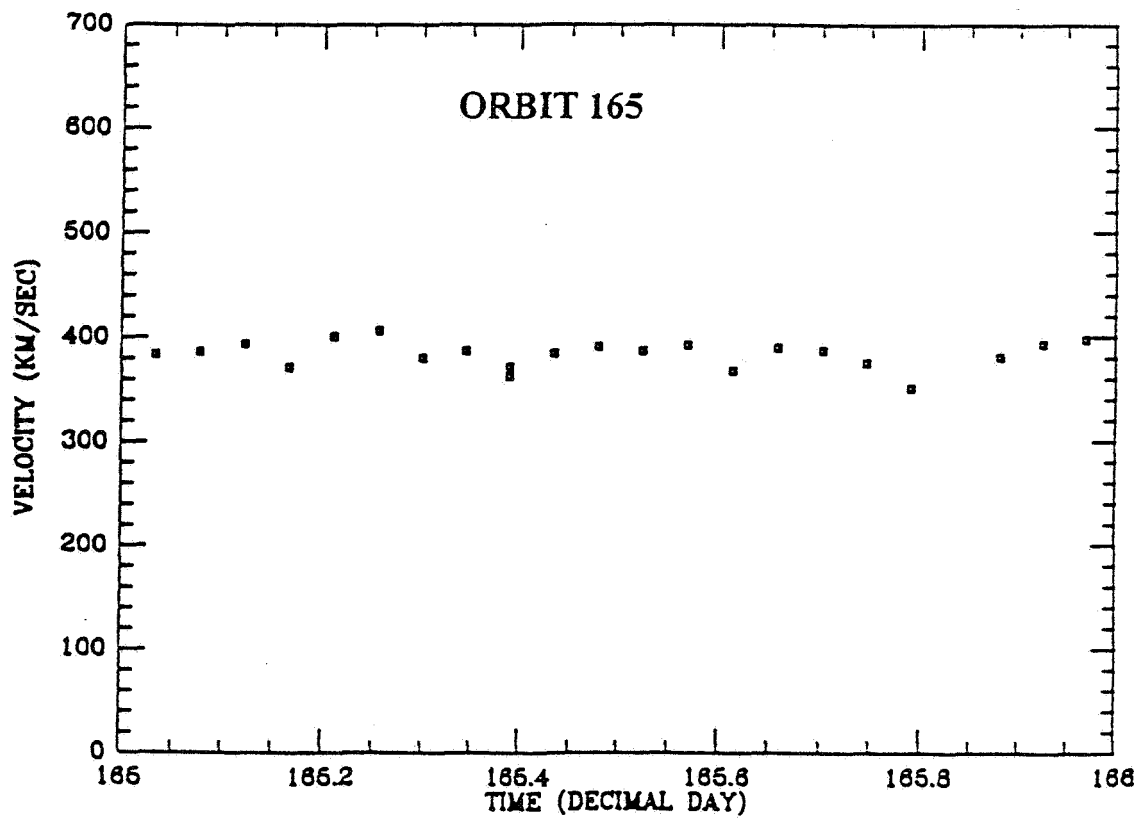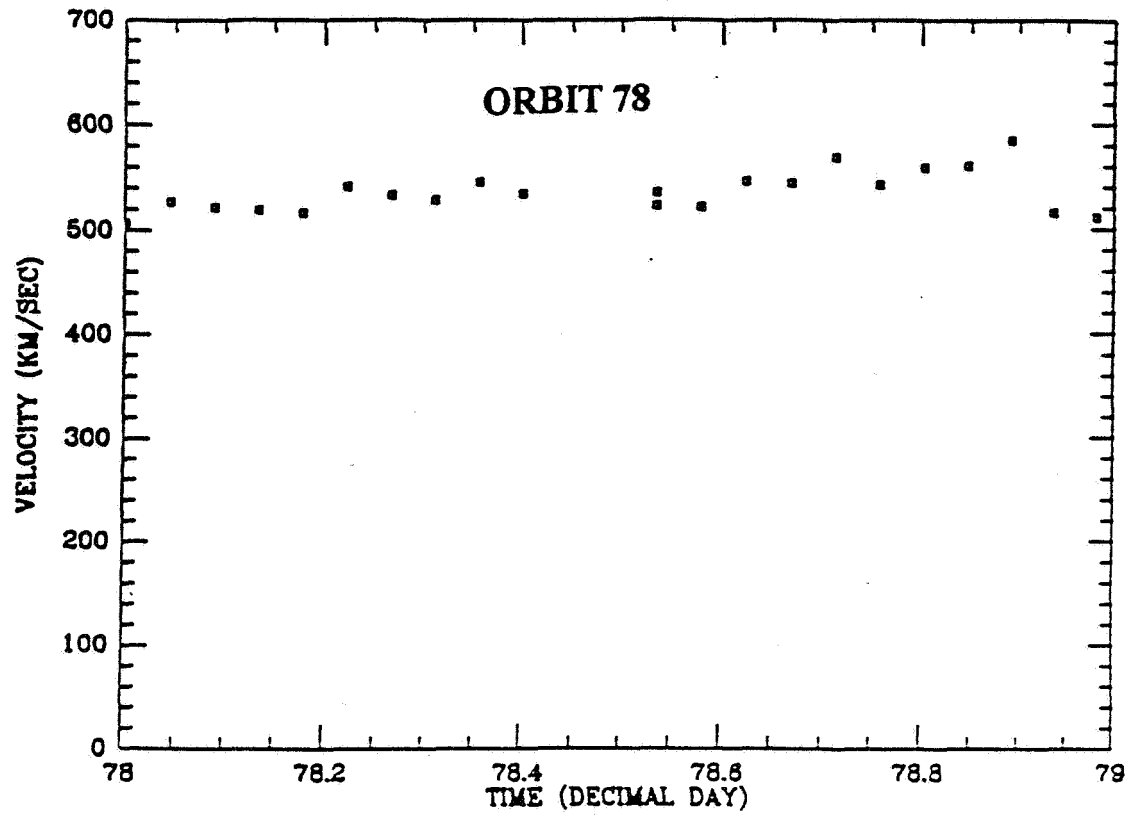
rather stable parameter. In some orbits, they become almost a straight horizontal line with so small of a fluctuations in its 24 hrs. period, in which the spacecraft was set to complete for each orbital motion. Although the time resolution of the OPA data is still quite poor, this stability of the solar wind velocity allows us to use its average value as the velocity in the estimation of M_{def}.

4.2.3   Calculation and Comparison of M_{spr} & M_{def}

Next step is to enter all the values obtained into the equations below:

$$M_{spr} = [\ 2n_b\ /\ [n_-\ (\gamma + 1)\ -\ n_b\ (\gamma - 1)]\ ]^{1/2}$$

$$M_{def} = v_s\ [\ (1.2 \sim 2)\ \gamma kT_e\ /\ m_p\ ]^{-1/2}$$

The Table 4.2.3.1 contains the results from the computation of M_{spr} and M_{def}, for each randomly chosen orbit. We divided the M_{def} columns into two which correspond with the two extreme cases of the electron- proton temperature relationships. Also, we calculated each Mach number for both inbound and outbound measurements. Although, the values from these two measurements from one orbit differed slightly, their result came out to be quite similar. Thus, we only plotted the M_{spr}-M_{def} comparison graph only for the inbound, assuming the result from the outbound would be similar. When we see the Figure 4.2.3.1 which shows the M_{spr} plotted along with M_{def}, we noticed, that except the two cases out of the thirty cases (orbit 40 and 90) we calculated, M_{spr} was smaller than M_{def}. Beside the two abnormal points,, the relationship, $M_{spr} <$ M_{def}, was consistent. When we take the plasma parameter values under the condition of $T_e = T_p$, the average value of M_{spr} was 2.71 with its maximum 4.27 (excluding the two abnormal cases) and its minimum 1.14. Similarly, the average value of M_{def}, on the other hand, was 6.93 and its

Table 4.2.3.1 Computed Results of M_{spr} and M_{def}

Orbit #	T(infinity) (ev) inbound	(ev) outbound	n(infinity) (/cm3) inbound	(/cm3) outbound	n(behind) (/cm3) inbound	(/cm3) outbound	velocity (km/sec)	M(spr) inbound	M(spr) outbound	M(def) inbound	(Te=Tp) outbound	M(del) inbound	(Te>>Tp) outbound	Note: Mspr?
1	8.524	9.817	12.780	13.144	38.107	36.084	491.9	2.9654	2.5629	9.4306	8.7877	13.3401	12.3856	v
2	8.590	9.695	12.183	11.427	36.084	31.115	450.8	2.9269	2.5300	8.6094	8.1039	12.1784	11.4220	v
4	14.373	15.110	8.359	7.873	22.174	20.009	391.3	2.4311	2.2870	5.7773	5.6346	8.1722	7.9416	v
11	11.150	10.019	38.796	29.845	52.562	121.702	481.8	1.2396	ERR	8.0764	8.5200	11.4244	12.0084	v
12	6.931	8.413	13.490	9.775	38.284	26.874	400.2	2.7078	2.5688	8.5087	7.7230	12.0360	10.8851	v
19	9.823	10.430	9.871	10.530	24.433	24.012	619.3	2.2074	1.9949	11.0603	10.7336	15.6453	15.1283	v
25		17.811		30.264		96.064	415.7	ERR	3.3980	ERR	5.5134	ERR	7.7708	v
30	10.761	11.016	9.699	12.375	33.307	22.638	580.5	4.2712	1.5902	9.9052	9.7899	14.0113	13.7981	v
35	5.783	9.092	13.064	11.982	21.294	20.520	421.5	1.4365	1.4988	9.8109	7.8245	13.8779	11.0280	v
40	14.182		32.924		125.707		298.0	7.9662	ERR	4.4293	ERR	6.2654	ERR	^
49	13.491		20.075		40.133		446.7	1.7315	ERR	6.8074	ERR	9.6294	ERR	v
57	13.542	13.428	21.109	15.184	29.807	40.782	493.1	1.2795	2.4770	7.5003	7.5321	10.6096	10.6160	v
66	17.571	16.419	26.190	27.001	58.775	69.064	337.0	1.9585	2.3073	4.5001	4.6552	6.3655	6.5613	v
73	14.530	15.389	23.652	21.100	66.160	50.487	381.5	2.6424	2.1138	5.6021	5.4435	7.9244	7.6722	v
78	13.275	14.704	24.433	22.753	71.276	53.595	543.4	2.8442	2.0734	8.3481	7.9321	11.8088	11.1798	v
90	15.912		13.911		52.845		394.2	7.5523	ERR	5.5315	ERR	7.8245	ERR	<>
110	10.245		8.560		22.365		569.8	2.3777	ERR	9.9644	ERR	14.0952	ERR	v
115	62.489		13.622		30.917		322.0	1.9840	ERR	2.2800	ERR	3.2252	ERR	v
125	10.122		24.756		32.145		350.8	1.2008	ERR	6.1718	ERR	8.7303	ERR	v
130	13.977		23.895		76.119		346.2	3.4278	ERR	5.1833	ERR	7.3320	ERR	v
135	13.845	14.950	14.020	11.022	28.703	39.467	435.0	1.7737	5.0697	6.5438	6.2973	9.2565	8.8756	v
150	17.470		22.400		42.598		352.0	1.6491	ERR	4.7139	ERR	6.6681	ERR	v
180	18.044	15.817	13.781	18.301	44.421	60.924	419.1	3.5311	3.8119	5.5225	5.8985	7.8119	8.3135	v
185	17.100	17.720	17.592	18.714	28.267	23.965	388.7	1.4193	1.1886	5.2614	5.1686	7.4425	7.2847	v
225		9.302		6.966		19.319	551.0	ERR	2.6053	ERR	10.1123	ERR	14.2526	v
230	13.758	15.114	27.677	20.230	90.726	70.002	351.7	3.6936	4.3908	5.3074	5.0637	7.5076	7.1370	v
235	17.974	17.975	28.344	30.903	34.388	82.868	402.8	1.1429	2.4709	5.3181	5.3179	7.5227	7.4952	v
240	11.057	13.932	17.835	13.378	58.474	30.602	459.1	3.6954	2.0022	7.7281	6.8847	10.9318	9.7036	v
241	10.244		10.176		13.593		529.2	1.2265	ERR	9.2549	ERR	13.0015	ERR	v
242	15.725	45.919	11.239	39.965	51.531	53.808	493.8	ERR	1.2338	6.9701	4.0789	9.8596	5.7489	v

Figure 4.2.3.1 Comparison of M_{spr} and M_{def}
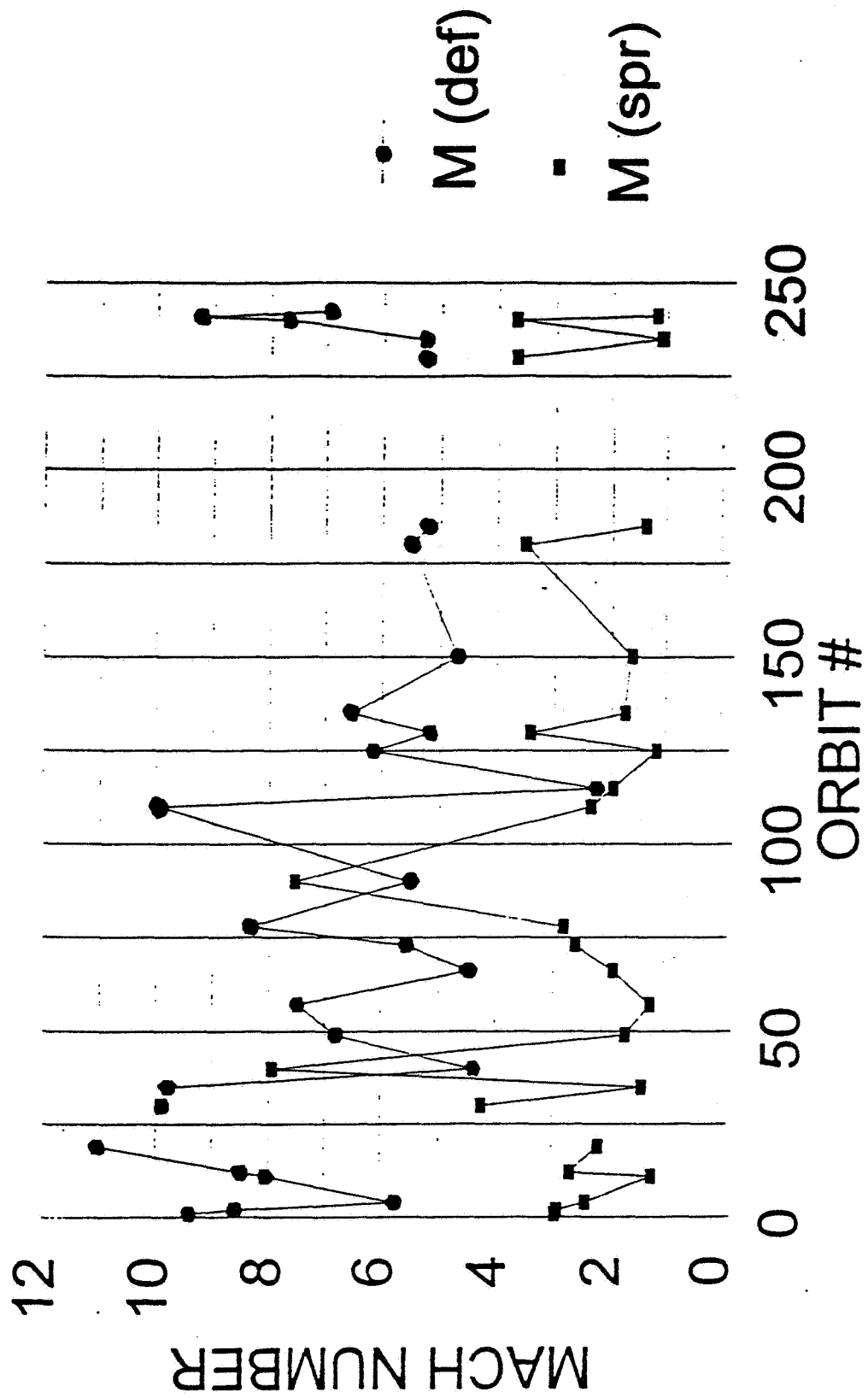
minimum 2.28 and its maximum 11.06. We noticed that M_{spr} does not bounce around as much as M_{def}. This could be due to our lack of knowledge of exact proton temperature, since we substituted the electron temperature which shows a considerable variation.

As noted above, the Mach number derived for orbit 40 and 90 showed abnormal behavior compared to the rest of the Spreiter Mach number data: M_{spr} (#40) = 7.97 and M_{spr} (#90) = 7.55. As we studied the original ORPA plots of plasma parameter versus the spacecraft altitude, we found that the orbit #90 had a relatively low electron temperature with a small jump (see Figure 4.2.3.2) and that the orbit #40 had an extremely high density jump (Figure 4.2.3.3). These abnormal characteristics the original plasma parameter showed in both orbits might have led to the contrasting result to the general $M_{spr} < M_{def}$ relationship. We also noticed that the value of the M_{def} becomes closer to M_{spr} in these abnormal situations, when we assume the proton temperature to be considerably smaller than the electron temperature, i.e., $T_e \gg T_p$, instead of $T_e = T_p$ condition. For example, in the case of the orbit # 40, $M_{def} (T_e \gg T_p) = 6.26$ whereas $M_{def} (T_e = T_p) = 4.43$ widens its gap against the $M_{def} = 7.97$. Again, our uncertainty in the proton temperature may be effecting the result in these abnormal situations. It is also possible that the magnitude and the direction of the interplanetary magnetic field produced an abnormally strong type of interaction.

4.2.4 The Possible Explanations to the M_{spr}-M_{def} Variance

After carefully examining the result of M_{spr}-M_{def} comparison, we believe that we have verified that the Spreiter model is incomplete as far as its predictability of the bow shock formation for planets similar to Venus. M_{spr} did not agree well with M_{def} -- M_{spr} was generally

B-39

Figure 4.2.3.2 ORPA Plot of Bow Shock Crossing Orbit 90 Inbound

ORBIT 90, INBOUND

ORBIT 90, INBOUND

ORBIT 90, INBOUND

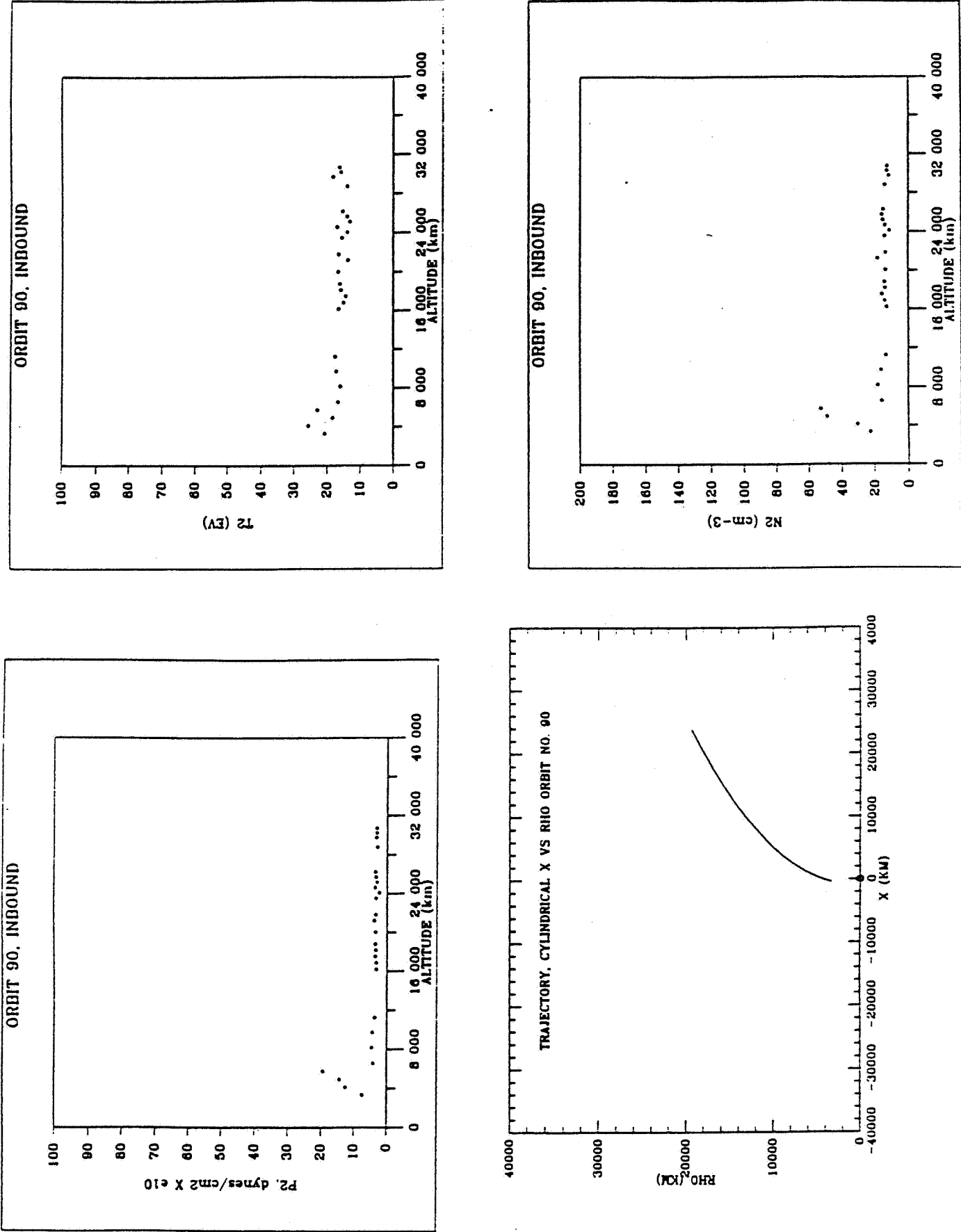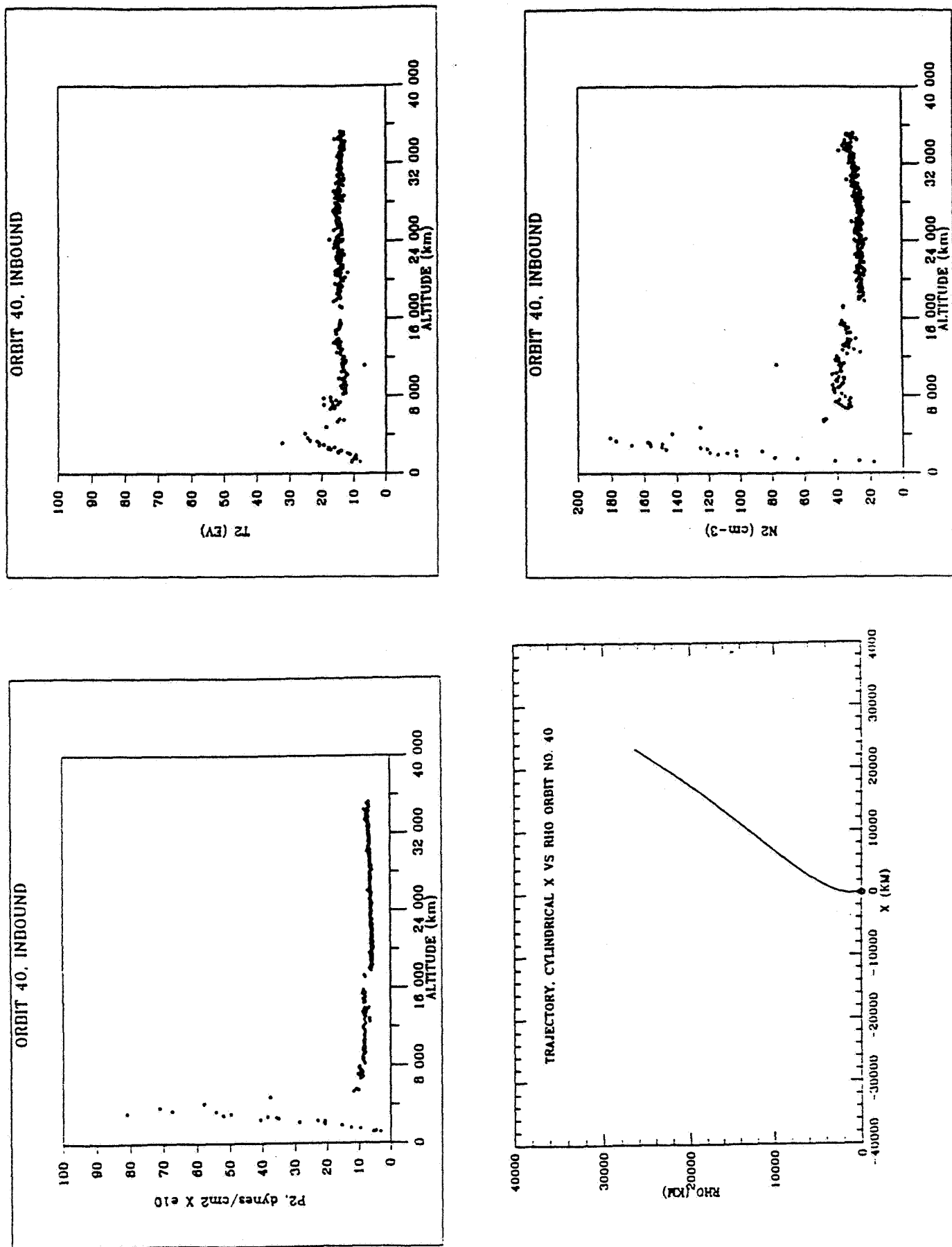TRAJECTORY, CYLINDRICAL X VS RHO ORBIT NO. 90

Figure 4.2.3.3 ORPA Plot of Bow Shock Crossing Orbit 40 Inbound

found to be smaller than M_{def} by the average ratio of about 1 to 2.6, respectively, which was a big difference, even though they both were describing the same phenomenon. Thus, we then searched for the possible explanations to why the referred Mach number derived using the Spreiter model differed so much from the actual Mach number computed on the basis of its definition.

We suspected the most crucial vulnerability of the Spreiter model to lie in its initial assumption that neglects its magnetic field influence on the solar wind plasma. The base of the Spreiter model came from its application on earth, which has a definitely different magnetic field than that of Venus. Let us discuss the differences in the nature of the solar wind interaction with both planets, earth and Venus, and simultaneously refer back to the Spreiter model feasibility. By doing so, we may see what kinds of modification the Spreiter model needs in order for it to be applicable to other planetary obstacles with different planetary magnetic fields.

The terminology, "hard" and "soft" are sometimes used in the field of plasma physics to classify the solar wind obstacles depending on how rigidly each planet can shield off the solar wind entrance into its ionosphere region. The Spreiter model has been created under the restriction that the solar wind is interacting with a "hard" obstacle, such as the planetary magnetic field of the earth. That is, the earth is considered to be a "hard" obstacle because of its strong magnetic field. If the solar wind is able to interact with the ionosphere and upper atmosphere of a planet, the obstacle presented by the planet will likely be "soft" because of mass loading (discussed previously) and other factors. As mentioned before, Venus' magnetic field is almost negligible or undetectable, thus, Venus is considered to be a "soft" obstacle by allowing the solar wind to interact directly with its atmosphere in its ionopause region. The Venus' bow shock and

magnetosheath are located much closer to the planet than that of the earth. The word, "soft" seems appropriate, since the Venus is like a "soft cushion" that is unable to resist the external impact on its surface. On the other hand, the earth and its strong magnetic field appear hard like "concrete," guarding off the impact of the solar wind, allowing very small influence by the intruder, the solar wind, in its ionosphere.

When the "soft" obstacle lets the solar wind into its ionosphere, various magnetohydrodynamics reaction may take place. As mentioned earlier, one such interaction involves the charge exchange between the solar wind protons and the atmospheric neutral oxygen ions. The charge exchange results in the pick up of these ions by the solar wind electric field ($E = -v \times B$) ala $E \times B$ drift and eventually to a mass loading effect. The slowing down caused by the mass loading of upstream plasma near the bow shock region causes formation of the shock jump, which is usually smaller than that due to a strong planetary magnetic field.

It seems reasonable to assert, therefore, that the Spreiter model becomes inapplicable when the obstacle is a "soft" obstacle. The more dominant the magnetic field influence is allowed to become, due to the inability of the planet's defense against such intervention, the more complex its influences become on the plasma interaction around the planetary obstacle. Since the Spreiter model does not take the magnetic field influence into account, the softer the obstacle becomes, the more the model appears to show its vulnerability of not being able to respond to all of the MHD reactions taking place upstream and in the vicinity of the bow shock.

4.3 Pick-Up Ion Fraction

4.3.1 Bow Shock Comet Model for Ion Pick-Up

One of the notable MHD reaction that may be taking place in the solar wind-Venus interaction is that of a mass loading effect. Mass loading effect is less likely to occur on the "hard" obstacle such as earth because the planetary magnetic field prevents the solar wind from getting close enough to the atmosphere/ionosphere. As noted previously, the discrepancies we have observed when comparing the plasma parameters, in the forms of M_{spr} and M_{def}, may be due to the Spreiter model's inability to include the MHD effect such as mass loading in its expression. However, we are not sure to what extent this mass loading effect influences or causes the bow shock formation. Hence, the next logical step is to try to evaluate the significance of this mass loading effect. In order to measure the significance of such an effect, we may estimate the amount of ions that get picked up as the solar wind interacts with the planet's ionosphere. The amount of ion pick up occurring should be directly correlated to the relational impact of the mass loading on the bow shock formation.

There is a model developed by Cloutier (1982) which describes the fractional ratio of ion pick up taking place during the solar wind-comet interaction. This model has been developed as part of the study of cometary bow shocks. A comet is another obstacle that interacts with the solar wind. Although there are similarities, the comet also differs from the earth and Venus in various ways. A comet has an extremely small nucleus, nevertheless, at 1 A.U. of the sun the virtual absence of gravity allows its atmosphere to be very large, much larger than that of earth or

Venus. Because a comet does not have a magnetic field, but its atmosphere is so large, it is considered to be "extremely soft." Venus is a similar obstacle to a comet in the context that it is incapable of shielding off the solar wind from the ionosphere, but because of its strong gravity, the shock interaction is much closer to the planet. The comet's bow shock formation is almost exclusively due to mass loading pick up, whereas that at Venus must also be due in part to magnetic field pile up. Furthermore, the use of Mach number in the equation used in Cloutier's model is another aspect that makes this model a good candidate to be applied in our study. Hence, it seems logical to consider the Cloutier model as another extreme to apply to the PVO data to help better understand some of the complexities of the Venus bow shock formation.

Before introducing the model, we need to understand the movement of the ion when created upstream of the nucleus of a comet. As similar to the case of Venus, the mass loading occurs near the bow shock. This mass loading takes place due to the ions created upstream in the flow of the solar wind by whatever process that involves the ionization. The ion finds itself in the electric field in the instant it becomes an ion, which is expressed as $E = -v \times B$ accordingly with the Faraday effect for the geometry below:
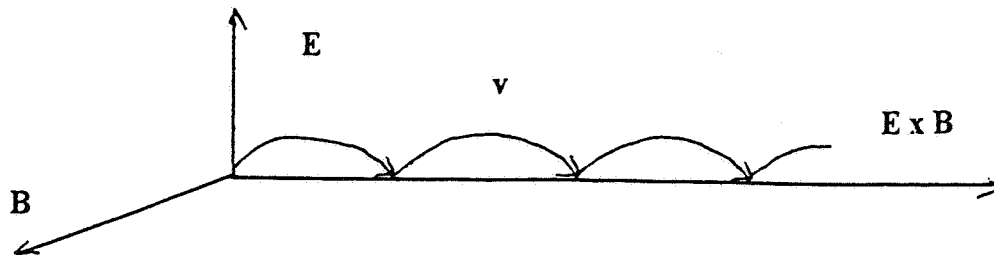
Then, the particle starts its drifting motion (as shown in Figure 4.3.1.1) in the direction of the flow with a velocity given by v_D. The drifting motion of a particle under magnetic field influence is expressed as

$$v_D = E \times B / B^2$$

Figure 4.3.1.1 Drift Motion of Pick Up Ions Due to the Solar Wind-Venus Interaction

Source: Colin (1989)
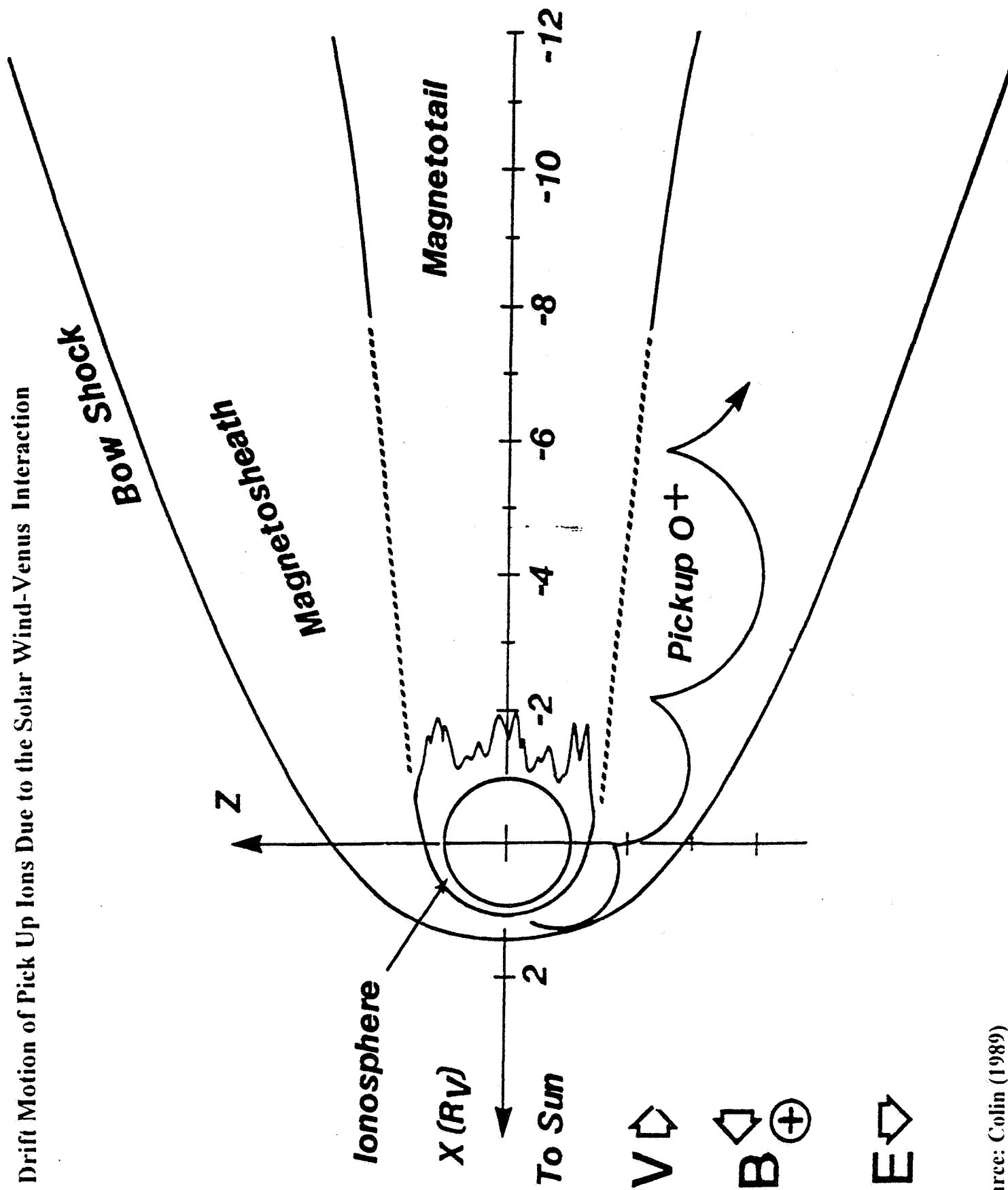
which ends up with the solar wind velocity, **v**,

$$\mathbf{v_D} = \mathbf{E} \times \mathbf{B} / B^2 = \mathbf{E} \times \mathbf{B} / B^2 = -(\mathbf{v} \times \mathbf{B}) \times \mathbf{B} / B^2$$

$$= \mathbf{B} \times (\mathbf{v} \times \mathbf{B}) / B^2 = \mathbf{v}\,\mathbf{B} \cdot \mathbf{B} / B^2 - \mathbf{B}\,(\mathbf{v} \cdot \mathbf{B}) / B^2$$

$$= \mathbf{v}$$

The fact that, $\mathbf{v_D} = \mathbf{v}$, shows the conservation laws of motion being held within the plasma during the interaction between the solar wind and the comet, which will be used in Cloutier's model discussed later. Note that when O^+ is formed, it has a velocity of only several kilometers per second. The action of $\mathbf{E} \times \mathbf{B} / B^2$ to bring O^+ up to solar wind velocities must slow down the solar wind.

Wallis (1973) has shown that the bow shock formation is linked to the condition in which the modified mass flux p'v' satisfies the equation:

$$\rho' v' = \rho_s v_s \, (\gamma^2 / \gamma^2 - 1)$$

where γ is the ratio of specific heats (used also in Spreiter model), ρ_s is the upstream undisturbed solar wind mass density, and v_s is the solar wind velocity. Wallis transforms this model into a form in which the ion pick up fraction is calculatable. The modified mass flux, $\rho'v'$, is the resultant flux after the additional flux, ρv, has been added due to the created ions during the mass loading process as shown in the diagram below.

```
        ---------------->                        ---------------->
      ρ s V s              ⇑                  ρ' v'
                   S = ρ v added
```
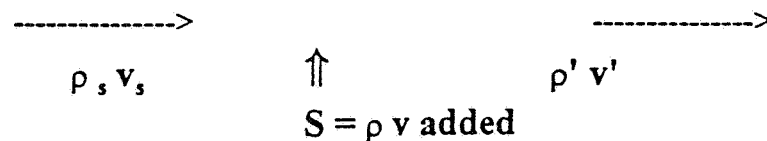
However, he oversimplifies the phenomenon by only applying the conservation of momentum flux. Years later, another plasma physicist, Cloutier made improvements on the Wallis' model

B-47

by adding the mass flux and the energy flux into the picture (the Wallis' model had only included the momentum flux). Thus, the number of the needed flux equations become three and they are expressed as:

Mass $\qquad$ $\rho_s v_s + S = \rho' v'$ $\hfill$ (3)

Momentum $\qquad$ $\rho' v'^2 + \rho' = \rho_s v_s^2 + \rho_s$ $\hfill$ (4)

Energy $\qquad$ $[1/2\, \rho' v'^2 + (\gamma/(\gamma-1))\, \rho']\, v' = [1/2\, \rho'\, v'^2 + (\gamma/(\gamma-1))\, \rho_s]\, v'$ $\hfill$ (5)

The variable η is employed to simplify the process of solving the equations and also to perform the derivation in terms of the ratio of the velocities,

$$\eta = v_s / v'.$$

Combining the equation (3), (4) and (5), we obtain the equation for η,

$$\eta = 1/2\, \{(1+\eta_o) +/- [(1-\eta_o)^2 - 4\,\sigma\,\eta_o]^{1/2}\}$$

where

$$\eta_o = [(\gamma+1)\, M^2] / [2 + (\gamma-1)]$$

$$M^2 = [v_s / (\gamma\, \rho_s / \rho_s)^{1/2}]^2 = \rho_s v_s^2 / \gamma\, \rho_s$$

$$\sigma = S / \rho_s v_s$$

Here, we face the possibility of η becoming an imaginary number. The imaginary number in the physical expression indicates that the system is in an unstable condition, hence, the system is likely to go through a non-smooth transition. Thus, if η is imaginary, we have a good possibility of having a jump in the parameters, which leads to the formation of the shock. The satisfaction of the condition, $4\,\sigma\,\eta_o \le (1-\eta_o)^2$, is necessary for the shock, i.e., a shock forms if

$$\sigma > (1-\eta_o)^2 / 4\,\eta_o. \hfill (6)$$

The right-hand side of (6) will turn out to be, according to the Cloutier's model, the threshold

point for the shock formation. Hence, we call it

$$\sigma_{max} = (1 - \eta_o)^2 / 4\eta_o.$$

This model enables us to calculate the pick up ion fraction, α, which is related to the ratio

of mass density ρ'/ρ_s obtained through the manipulation of the equations introduced above.

4.3.2   Calculation of Pick-Up Ion Fraction

Although the typical Mach number, $M = 2$, for the solar wind-comet interaction is

usually used for the calculation of ion pick up fraction for the Cloutier model, we will use the

average Mach number we obtained using the Spreiter model, to estimate the ion pick up fraction

in the case of Venus. We will first take the average M_{spr} of 2.71 with the ratio of specific heats of

5/3.

Thus, for $M = 2.71$ and $\gamma = 5/3$,

$$\eta_o \qquad = [(\gamma + 1) M^2] / [2 + (\gamma - 1)] = 2.8399$$

thus $\quad \sigma_{max} \qquad = (1 - \eta_o)^2 / 4 \eta_o = 0.2980$

and $\quad \eta \qquad = v_s / v' = 1/2 \{(1 + \eta_o) +/- [(1 - \eta_o)^2 - 4 \sigma \eta_o]^{1/2}\} = 1.9228.$ (7)

Using $\sigma = S / \rho_s v_s$ to replace flux S,

$$\rho' v' \qquad = \rho_s v_s + S \implies \rho' v' = \rho_s v_s + \sigma \rho_s v_s = \rho_s v_s (1 + \sigma)$$

Hence,

$$\rho' v' \qquad = \rho_s v_s (1 + 0.2980) = 1.2980 \ \rho_s v_s \qquad \qquad (\text{i.e., } 0.2980 \ \rho_s v_s \text{ added})$$
$$\rho' / \rho_s = 1.2980 \ v' / v_s$$

$$= (1.2980) (1.9228) \qquad \text{(since } \eta = v_s / v' \text{ from (7))}$$

$$= 2.4956 \qquad\qquad (8)$$

Putting the mass density equation in terms of the ion pick up fraction value, α, $(0 < \alpha < 1)$,

$$\rho' \qquad = n \left[16\,\alpha + (1 - \alpha) \right] m_p \qquad (9) \qquad (16 m_p \text{ for mass of oxygen})$$

$$\rho_s \qquad = n\,m_p \qquad\qquad\qquad (10)$$

By equating the ratio of mass density before and after the flux addition, we obtain an equal form of mass density ratio as (8), hence,

$$\rho' / \rho_s \qquad = \left[n \left\{ (16\,\alpha + (1 - \alpha)) \right\} m_p \right] / \ n\,m_p$$

$$= 16\,\alpha + (1 - \alpha)$$

$$= 2.4956$$

From the relationship above we compute α,

$$16\,\alpha + (1 - \alpha) \quad = \ 2.4956$$

$$\alpha \quad = \ 0.09971$$

Finally, we obtained the value for the pick up fraction of 16 mp ions (oxygen ions) using the average Mach number from the Spreiter model.

$$\alpha_{ave} \quad = \ 9.97 \ \%$$

Similarly, we computed two other ion pick up fraction values to determine the range of α by

taking the minimum and maximum M_{spr} values resulting in values, respectively of

$$\alpha = \ 0.798 \ \% \quad \text{and} \quad 23.63 \ \%.$$

From the fractional values obtained above, we can discuss the significance of the pick up

of oxygen ion (O^-) taking place near Venus ionosphere. The occurring fraction of 9.97 % is

relatively high. Almost one out of ten solar wind ions coming in will give its charge away to the

neutral oxygen atoms that flowed outwardly from the Venus atmosphere. Hence, we argue that

the ion pick up is a factor significant enough to be included into the bow shock formation

models. Although applying the comet model to the Venus problem is oversimplifying the

physics, we suggest that this result is meaningful. It provided us the idea about the importance of

MHD influences in the bow shock forming medium, particularly of the ion pick up which is the major cause of the mass loading of the solar wind.

We also noticed the wide range the fractional value, α, lies in, i.e.,

$$\alpha_{max}/\alpha_{min} = (23.63\ \%)\ /\ (0.798\ \%) = 29.6 \approx 30$$

While $(M_{spr}\ max)\ /\ (M_{spr}\ min) = 3.6)$. This shows that the α is very sensitive to the change in the Mach number. At the same time, we know that the inferred α must be strongly connected to the nature of the interplanetary magnetic field embedded in the solar wind, since its piling up at the ionopause could modify the amount of charge exchange that takes place. It seems logical, therefore, to expect a relationship between the Mach number and the strength and orientation of magnetic field, and also that such a relationship would vary as the α value fluctuates. We suspect that the high variation in the rate of ion pick up occurring is likely due to the magnetic field variation and also to the changing solar activities.

Two conditions, one from the magnetic field variation and the other from the changing solar activities, seemed to possibly influence the resulting ion pick up fraction. Let us discuss the influence from these two factors: the direction of magnetic field and the solar activity cycle.

If the interplanetary magnetic field is perpendicular to the path of the solar wind, the highly conducting state of the Venus ionosphere could lead to a pile up of the interplanetary magnetic field on the day-side hemisphere of the planet.(see Figure 4.1.2.6) The magnetic field pile up could lead to the creation of a "hard" obstacle out of a "soft" obstacle, since the piled up magnetic field can behave as a shield against the solar wind intervention into the ionosphere of Venus. If the magnetic field achieves such a condition, the solar wind must deflect away from the planetary obstacle, and mass loading due to ion pick up is less likely to occur under such

conditions.

The other case is solar cycle influence on the ion pick up. When the sun is active and producing intense UV radiations, this could cause more ionization of oxygen atoms upstream of the planet's ionosphere/atmosphere, and increase the amount of mass loading. (See Figure 4.3.2.1 which shows the solar cycle effect on Venus' bow shock.) However, at such times the interplanetary magnetic field may be stronger. It is not clear which of these two competing factors are more important.

Figure 4.3.2.1   Solar Cycle Effects on Venus' Bow Shock
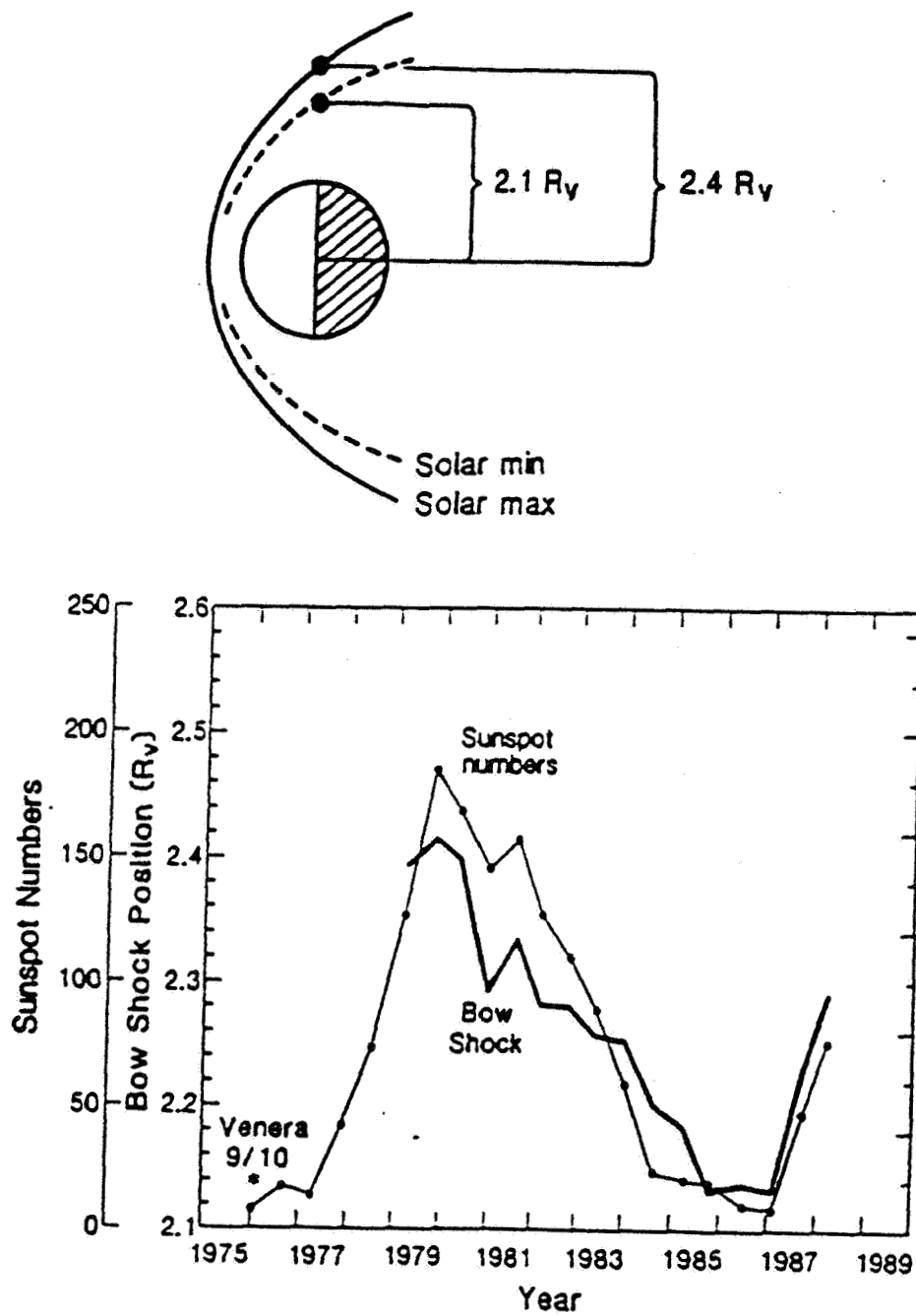
Source: Colin (1989)

. Conclusion and Summary

. By utilizing plots of the bow shock jump using the ORPA electron data, we have tried to test the feasibility of Spreiter's gas dynamic model which attempts to describe the nature of the bow shock formation. The comparison between the inferred mach number using the Spreiter model and the experimental data from its definition showed the relationship of $M_{spr} < M_{def}$ to be true most of the time. The Mach number calculated using the Spreiter model had its average of 2.71 and ranged from 1.14 to 4.27 (excluding two abnormal events), whereas the Mach number from its definition had its average of 6.93 and ranged from 2.28 to 11.06 .

We argue that the reason behind such a disagreement between the two values is the oversimplification on the initial assumption the Spreiter model makes. The Spreiter model was initially developed for a "hard" obstacle such as the earth. The earth has a strong magnetic field that can shield the solar wind from the planet's ionosphere/atmosphere. However, for the case of Venus, there is no planetary magnetic field, and, therefore, the solar wind freely enters into its ionosphere and starts to interact with the neutral atoms flowing upstream of the planet. This solar wind's entrance into outer atmosphere of the planet creates various complexities when one attempts to predict the bow shock formation, which the Spreiter model is not able to do in the case of Venus.

One of the complexities the solar wind-Venus interaction faces and Spreiter fails to include in his model is that of the mass loading phenomenon. Mass loading at the solar wind-planet interaction points slows down the plasma flow in the region. We tried to estimate the impact this has on the plasma parameter fluctuation and, consequently, to the bow shock

formation. We used Cloutier's model developed for the solar wind-comet interaction which include the expressions which allows us to calculate the ion pickup fraction, which is directly related to the mass loading. We reasoned that if the ion pick up fraction is great, then mass loading factor is significant enough to be included into the basic assumption which the predictive model on bow shock formation would be based on.

The results from such a computation using the Cloutier's model was that the fraction of 16 m_p ions (oxygen ions), that were picked up had its average of 9.95% and ranged from 0.78% to 23.63%. We argue that these fractional values are significant enough, and therefore mass loading effects should be considered when constructing a model for bow shock formation, particularly, for the planetary obstacles that are "soft," i.e., that are vulnerable to the solar wind intervention into the planet's ionosphere region. However, this result takes only charge exchange and mass loading into account, neglecting the effect of interplanetary magnetic field pile up in the day-side ionosphere of Venus. This is clearly needed in order to more accurately estimate the amount of charge exchange production and subsequent pick up of O÷.

Clearly, there are various complex MHD actions taking place in the bow shock forming region. We showed our concerns on the neglect of these significant factors in the already-existing bow shock models. However, we also faced the difficulty in modifying these plasma dynamics models due to its overwhelming complexity and were forced to neglect important factors such as the direction of magnetic field and solar activities. However, this research confirms the need for a continuation of careful investigations on this uniquely complex solar wind-Venus interaction, possibly employing the OPA-ORPA data available from the PVO mission which still may offer us the various uncovered truths about the complex nature of

plasma. Moreover, this study also should draw the attention of future researches in that a model with the various MHD factors involved needs to be developed in order for us to further our understanding on the curious phenomenon of bow shock formation and the complex nature of plasma dynamics occurring at Venus.

We will close with the following quote from *Ten Years of Discovery*, the publication completed by the members of PVO mission team, since it seemed to echo with this Venus bow shock study and many other scientific efforts all over the world trying to understand the complexity of the universe.

"...Pioneer Venus discoveries have to a large degree answered the simple questions about the Venus ionosphere that were posed before encounter. But, in the process of answering he simple questions, the PVO investigators have become aware that Venus is much more complicated than our early questions implied. Thus 10 years later we sill have many questions, and the answers to our original questions have been incomplete in many cases. They were the right initial questions, of course, but nature is always more complex than one imagines from a position of ignorance. Our direct contact with this new world has brought with it many surprises and a new set of question; questions concerned not so much with what the Venus ionosphere is like, but what causes it to be that way. . . ."

Works Cited

Guidance and assistance from Dr. Douglas Jones, BYU Physics and Astronomy Department

Cloutier, P.A., et al., "Physics of the Interaction of the Solar Wind with the Ionosphere of Venus: Flow/Field Models," *Venus*, edited by Wilkening, The University of Arizona Press, 1982

Colin, Lawrence, ed. "Pioneer Venus Orbiter - Ten Years of Discovery." Unpublished Report, 1989.

Dessler, A.J. "Solar Wind and Interplanetary Magnetic Field." *Review of Geophysics*, 5, 1-42, 1967.

Egeland, A., O. Holeter, and A. Omholt, ed. *Cosmical Geophysics.* Universitetsforlaget, Oslo, 1973.

Gifford, Dawn. "Comparison of ORPA Suprathermal Electron and OPA Solar Wind Proton Data from the Pioneer Venus Orbiter." Unpublished Report, 1993.

Knudsen, W.C., J. Bakke, K. Spenner and V. Novak. "Retarding Potential Analyzer for the Pioneer-Venus Orbiter Mission." *Space Science Instrumentation* 4, 351-372, D. Reidel Publishing Company, Dordrecht, Holland. 1979.

Levine, Joel S. "Planetary Atmospheres," *Encyclopedia of Physical Science and Technology*, 12, 729-757, American Press, Inc. 1992

Lui, A. T. Y., "Road Map to Magnetotail Domains," *Magnetotail Physics*, edited by A. T. Y. Lui, John Hopkins University Press, Baltimore, 3, 1987

Mihalov, J. D., C.T. Russell, W. C. Knudsen, and F. L. Scarf, "Pioneer Venus and Near-Earth Observation of Interplanetary Shocks." *Journal of Geophysical Research*, 92, A4, 3385-3391, American Geophysical Union, 1987.

Mihalov, J.D., J.R. Spreiter and S. S. Stahara, "Comparison of Gas Dynamic Model with Steady Solar Wind Flow around Venus." *Journal of Geophysical Research*, 87, A12, 10,363-10,371, American Geophysical Union, 1982.

Ratcliffe, J.A. *An Introduction to the ionosphere and magnetosphere*, University Press, Cambridge, 1972.

Spreiter, John R. and S. S. Stahara. "Solar Wind Flow Past Venus: Theory and Comparisons." *Journal of Geophysical Research*, 85, 7715-7738, American Geophysical Union, 1980.

Spreiter, John R. and S. S. Stahara. "Computer Modeling of Solar Wind Interaction with Venus and Mars." *Venus and Mars: Atmospheres, Ionospheres, and Solar Wind Interactions, Geophysical Monograph*, 66, 345-383, American Geophysical Union, 1992

Spreiter, John R., Summers and Alksne, *Planetary Space Science*, 14, 223-253, 1966

Tatrallyay, M., C.T. Russell, J.D. Mihalov and A. Barnes. "Factors Controlling the Location of the Venus Bow Shock." *Journal of Geophysical Research*, 88, A7, 5613-5621, American Geophysical Union, 1983.

Wallis M. K., "Weakly-Shocked Flows of the Solar Wind Plasma through Atmospheres of Comets and Planets" *Planetary Space Science*, 21, 1647-1660, 1973